



Mr. Nuttapon Jirakittiwut

A Dissertation Submitted in Partial Fulfillment of the Requirements  
for the Degree of Doctor of Philosophy in Chemistry

Department of Chemistry

FACULTY OF SCIENCE

Chulalongkorn University

Academic Year 2021

Copyright of Chulalongkorn University



จุฬาลงกรณ์มหาวิทยาลัย  
**CHULALONGKORN UNIVERSITY**

การตรึงกระดาษด้วยพีเอ็นเอสำหรับการตรวจวัดพีซีอาร์แอมพลิคอน



วิทยานิพนธ์นี้เป็นส่วนหนึ่งของการศึกษาตามหลักสูตรปริญญาวิทยาศาสตรดุษฎีบัณฑิต  
สาขาวิชาเคมี ภาควิชาเคมี  
คณะวิทยาศาสตร์ จุฬาลงกรณ์มหาวิทยาลัย  
ปีการศึกษา 2564  
ลิขสิทธิ์ของจุฬาลงกรณ์มหาวิทยาลัย



ณัฐพล จิระกิตติวุฒิ : การตรึงกระดาษด้วยพีเอ็นเอสำหรับการตรวจวัดพีซีอาร์แอมพลีคอน . ( PNA-IMMOBILIZED PAPER FOR DETECTION OF PCR AMPLICONS) อ.ที่  
 ปรึกษาหลัก : ศ. ดร.ธีรยุทธ วิไลวัลย์, อ.ที่ปรึกษาร่วม : รศ. ดร.ธนัชฐ์ ปราณินทร์รัตน์

การตรวจวัดดีเอ็นเอมีความสำคัญอย่างมากต่อโจทย์ที่หลากหลายจึงทำให้มีการวิจัยและพัฒนาอุปกรณ์ตรวจวัดดีเอ็นเอเพิ่มขึ้นอย่างต่อเนื่อง ในงานนี้จะเน้นการพัฒนาอุปกรณ์ตรวจวัดดีเอ็นเอที่ใช้กระดาษเป็นฐานและใช้ไพร์โรลิดินิลพีเอ็นเอ (pyrrolidinyl peptide nucleic acid, PNA) มาเป็นโพรบ อุปกรณ์ตรวจวัดดีเอ็นเอนี้ถูกออกแบบให้มีพีเอ็นเอโพรบหลายชนิดอยู่บนอุปกรณ์ชิ้นเดียวกันเป็นระบบตรวจสอบภายในเพื่อเพิ่มความถูกต้องในการอ่านและแปลผล จากนั้นจึงนำกระดาษที่ตรึงด้วยไพร์โรลิดินิลพีเอ็นเอโพรบนี้ไปใช้ในการตรวจวัดดีเอ็นเอ ตามด้วยการตรวจวัดดีเอ็นเอที่จับยึดกับไพร์โรลิดินิลพีเอ็นเอโพรบที่ถูกตรึงอยู่บนกระดาษโดยการสร้างสัญญาณสีจากปฏิกิริยาที่เร่งโดยเอนไซม์ ในงานนี้ได้นำอุปกรณ์ตรวจวัดดีเอ็นเอที่พัฒนาขึ้นไปใช้สำหรับการวินิจฉัยโรคธาลัสซีเมียชนิดฮีโมโกลบินอี (hemoglobin E, HbE) และการตรวจหาการปนเปื้อนของเชื้อ *Bacillus cereus* ในข้าว จากผลการทดลองพบว่าอุปกรณ์ตรวจวัดดีเอ็นเอที่พัฒนาขึ้นสามารถนำไปตรวจวัดยีนกลายพันธุ์ที่ทำให้เกิดโรคธาลัสซีเมียชนิด HbE อย่างจำเพาะเจาะจง ซึ่งมีขีดจำกัดของการตรวจวัดอยู่ที่ 0.1 ng ของปริมาณดีเอ็นเอตั้งต้น สำหรับการตรวจวัดเชื้อ *B. cereus* พบว่าอุปกรณ์ตรวจวัดดีเอ็นเอที่พัฒนาขึ้นแสดงความจำเพาะต่อเชื้อ *B. cereus* เท่านั้น โดยมีขีดจำกัดของการตรวจวัดอยู่ในระดับที่ต่ำ ด้วยความจำเพาะเจาะจงที่สูงของไพร์โรลิดินิลพีเอ็นเอโพรบทำให้ระบบตรวจวัดที่พัฒนาขึ้นสามารถทำที่อุณหภูมิห้องได้โดยไม่จำเป็นต้องอาศัยเครื่องมือเพื่อควบคุมอุณหภูมิ ซึ่งตอบรับกับคุณลักษณะของอุปกรณ์ตรวจวัดที่เป็นที่ต้องการในปัจจุบัน

สาขาวิชา เคมี  
 ปีการศึกษา 2564

ลายมือชื่อนิสิต .....  
 ลายมือชื่อ อ.ที่ปรึกษาหลัก .....  
 ลายมือชื่อ อ.ที่ปรึกษาร่วม .....

# # 5972814623 : MAJOR CHEMISTRY

KEYWORD: paper-based sensor, DNA detection, peptide nucleic acid, PNA,  
thalassemia diagnosis, foodborne pathogen detection, pyrrolidinyl  
PNA

Nuttapon Jirakittiwut : PNA-IMMOBILIZED PAPER FOR DETECTION OF PCR  
AMPLICONS. Advisor: Prof. Dr. TIRAYUT VILAVAN Co-advisor: Assoc. Prof.  
Dr. THANIT PRANEENARARAT

DNA detection is very important in diverse fields leading to a continuous increase in the research and development of various DNA sensors. This study focuses on the development of a paper-based DNA sensor by using pyrrolidinyl PNA as a recognition probe. The PNA-immobilized DNA sensor was designed to contain several PNA probes in the same device as a self-check system to increase the accuracy and facilitate the data collection and interpretation. The PNA-immobilized paper was then utilized for the detection of the DNA target, followed by the visualization of the captured target DNA via an enzyme-catalyzed colorimetric reaction. In this work, the developed DNA sensor was applied in the diagnosis of HbE which is a common form of thalassemia, and the identification of *Bacillus cereus* contamination in rice samples. The results showed that the developed sensor can be successfully used for highly specific detection of the mutated gene responsible for HbE thalassemia with a detection limit of 0.1 ng DNA template. For the detection of *B. cereus*, the sensor showed very high specificity for *B. cereus* among several related bacteria species with a low detection limit. Due to the excellent specificity of the pyrrolidinyl PNA probe, the DNA detection can be performed at ambient temperature without the requirement of a sophisticated temperature controlling system.

Field of Study: Chemistry

Academic Year: 2021

Student's Signature .....

Advisor's Signature .....

Co-advisor's Signature .....

## ACKNOWLEDGEMENTS

Firstly, I would like to express my sincere gratitude to my advisor Prof. Dr. Tirayut Vilaivan and my co-advisor Assoc. Prof. Dr. Thanit Praneenararat for the continuous support of my Ph.D study and related research, for their patience, motivation, and immense knowledge. Their guidance helped me in all the time of research and writing of this thesis. Besides my advisor, I really appreciate my colleague, Thongperm Munkongdee, for her training and knowledge. I also offer my heartfelt thanks to Assoc. Prof. Rungaroon Waditee-Sirisattha for her generosity and support. Moreover, I would like to thank the rest of my thesis committee: Professor Dr. Voravee Hoven, Professor Dr. Orawon Chailapakul, Professor Dr. Vudhichai Parasuk and Dr. Orapan Sripichai, for their insightful comments and encouragement, but also for the hard question which incited me to widen my research from various perspectives. My sincere thanks also go to Science Achievement Scholarship of Thailand and Distinguished Research Professor Grant for an opportunity to study in PhD program. This work was supported by the research grant from Center of Excellence on Medical Biotechnology (HbE part) and the Thailand Research Fund (B. cereus part). Without their precious support it would not be possible to conduct this research. I thank members of TV, TP, and TRC groups for the stimulating discussions, for the safety manners we were reminding together, and for all the fun we have had in the last five years. Last but not the least, I would like to thank my family: my parents and sister for supporting me spiritually throughout writing this thesis and my life in general.

Nuttapon Jirakittiwut

## TABLE OF CONTENTS

	Page
ABSTRACT (THAI).....	iii
ABSTRACT (ENGLISH).....	iv
ACKNOWLEDGEMENTS.....	v
TABLE OF CONTENTS.....	vi
LIST OF FIGURES.....	9
LIST OF SCHEMES.....	13
LIST OF TABLES.....	1
CHAPTER I INTRODUCTION.....	2
1.1 Paper-based DNA sensor.....	2
1.2 Peptide nucleic acid (PNA).....	6
1.2.1 History of peptide nucleic acid and its property.....	6
1.2.2 Recent development of conformationally constrained PNAs and their attractive features.....	8
1.3 Paper-based analytical device employing PNA as a probe.....	9
1.4 Impactful applications of the use of DNA sensors based on pyrrolidinyl PNA..	15
1.5 Rationale and objective of this work.....	19
CHAPTER II EXPERIMENTAL SECTION.....	21
2.1 Materials.....	21
2.2 Synthesis of pyrrolidinyl PNA.....	21
2.2.1 Pyrrolidinyl PNA monomer synthesis.....	21
2.2.2 Solid phase peptide synthesis.....	22



2.3 Preparation of DNA samples.....	24
2.3.1 for HbE detection .....	24
2.3.2 for <i>B. cereus</i> detection from isolated bacteria .....	25
2.3.3 for <i>B. cereus</i> detection from spiked rice samples.....	26
2.4 Preparation of the pyrrolidinyl PNA-immobilized paper sensor .....	26
2.5 DNA detection method .....	27
2.6 Image analysis by Scion Image software.....	29
CHAPTER III RESULTS AND DISCUSSION.....	31
3.1 Synthesis and characterization of pyrrolidinyl PNA oligomers .....	31
3.2 Sensor fabrication and DNA detection process.....	32
3.3 Optimization of the DNA detection method .....	35
3.3.1 Design of the sequences of PNA probes and DNA primers for HbE detection .....	36
3.3.2 Effect of temperature.....	37
3.3.3 Effect of salt concentration.....	38
3.4 The performance of pyrrolidinyl PNA-immobilized sensor in thalassemia diagnosis .....	39
3.4.1 Specificity .....	39
3.4.2 Limit of detection.....	41
3.4.3 The validation of the method with real samples.....	41
3.4.4 Repeatability.....	48
3.4.5 Shelf life .....	49
3.5 The performance of the PNA-immobilized sensor for pathogen detection .....	50
3.5.1 Genomic analysis of suitable gene candidates for species identification	50

3.5.2 Design of the sensor .....	52
3.5.3 Specificity .....	53
3.5.4 Limit of detection.....	55
3.5.5 The performance evaluation in real samples .....	57
3.5.6 The concept of smartphone application .....	59
CHAPTER IV CONCLUSION.....	61
REFERENCES .....	63
Optimization of the DNA detection method by using the divinyl sulfone (DVS) method for PNA immobilization.....	73
Preparation of PNA-immobilized paper by using DVS.....	73
The effect of spacer between paper surface and PNA probe .....	75
The effect of type of pyrrolidiny PNA.....	77
Gel electrophoresis of DNA samples used in the thalassemia diagnosis.....	79
The effect of Ca <sup>2+</sup> ion in CMC coating.....	79
Gel electrophoresis results and data of PCR sequences used in the detection of <i>B. cereus</i> .....	84
Characterization of pyrrolidiny PNA.....	87
Thermal denaturation experiments .....	92
VITA.....	93

## LIST OF FIGURES

<b>Figure 1.1</b> a) Schematic illustration of the principle of dot-blot assay. b) Example of the result from the detection of $\beta$ -globin gene.....	3
<b>Figure 1.2</b> a) Schematic illustration of the principle of reverse dot-blot assay shows that two probes with different sequences are used to detect target DNA at the different position of DNA sequence. b) Example of the result from the detection of $\beta$ -thalassemia mutations.....	4
<b>Figure 1.3</b> a) Schematic illustration of the principle of DNA detection on lateral flow test strip b) Image result from the detection of negative control (left) and target DNA (right). .....	5
<b>Figure 1.4</b> a) Schematic representation of fluorescence detection through competitive hybridization between fluorophore-labeled probe, quencher probe and DNA target. b) Origami paper analytical device with three components in each layer. ....	6
<b>Figure 1.5</b> a) Repeating units in the structure of DNA and aegPNA. b) an aegPNA-DNA duplex in the antiparallel mode, showing the base pairing according to the Watson-Crick base-pairing rules.....	7
<b>Figure 1.6</b> a) acpcPNA and <i>epi</i> -acpcPNA structure. b) Antiparallel hybrid of pyrrolidinyl PNA and DNA.....	9
<b>Figure 1.7</b> Schematic representation of oligonucleotide-templated selenocystine–selenoester ligation reaction using in lateral flow test of target RNA.....	10
<b>Figure 1.8</b> a) Schematic representation of enzymatic amplified colorimetric detection of DNA following Dot blot hybridization using filter paper functionalized with positively charged polymer brushes and the peptide nucleic acid probe. b) Representative images of the test results demonstrating the specificity and efficiency of b-PNA SLE2.....	11
<b>Figure 1.9</b> Fabrication of DNA sensor using DVS activation to immobilize pyrrolidinyl PNA onto paper and DNA detection with cationic dye .....	12

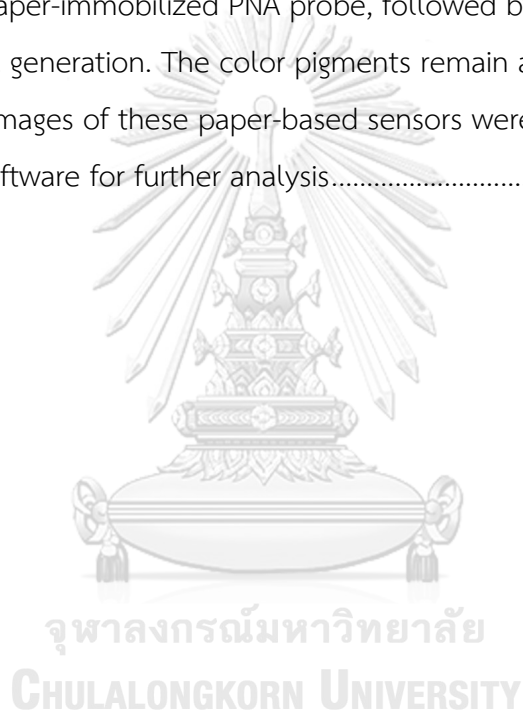
<b>Figure 1.10</b> a) The paper-based colorimetric assay for DNA detection based on pyrrolidinyl PNA-induced nanoparticle aggregation. b) Photograph of visual color changes obtained from detection of MERS-CoV, MTB, and HPV in the presence of complementary DNA. ....	13
<b>Figure 1.11</b> a) The concept of the pyrrolidinyl PNA-induced nanoparticle aggregation in the present and absent of DNA target. b) The graph of $\Delta$ intensity of complementary (c-DNA), single-base mismatched (Mis/1b-DNA), two-base mismatched (Mis/2b-DNA), and non-complementary DNA (NC-DNA). ....	14
<b>Figure 1.12</b> The principle of the fluorescence-based detection of target DNA using the acpcPNA-immobilized paper-based sensor and ssDNA-specific fluorescence dye. ....	15
<b>Figure 2.1</b> Structures of pyrrolidinyl PNA monomers and ACPC spacer used in solid phase peptide synthesis of acpcPNA and <i>epi</i> -acpcPNA. ....	22
<b>Figure 2.2</b> a) Sequence of primers, namely China1 and China2. b) Sequence of PCR amplicon from $\beta$ -globin gene (grey highlight: primer sequences, red alphabets: detection region and a red alphabet with underline: a position of mutated base). ....	25
<b>Figure 2.3</b> Image analysis by using Scion Image software consists of 3 steps: a) area selection, b) plot profile creation, and c) peak area measurement. ....	30
<b>Figure 3.1</b> a) Layout of PNA-immobilized paper for the detection of HbE mutation and b) three expected patterns of the results from DNA detection of normal, HbE heterozygous and HbE homozygous genotypes. N probe = normal probe. ....	36
<b>Figure 3.2</b> a) Position of PCR product on $\beta$ -globin gene. b) Sequence of PCR amplicon from $\beta$ -globin gene (grey highlight: primer sequences, red alphabets: detection region and a red alphabet with underline: a position of mutated base). ....	37
<b>Figure 3.3</b> The effect of temperature to the performance of the paper-based DNA sensor. ....	38
<b>Figure 3.4</b> The effect of salt concentration to the performance of paper-based DNA sensor. ....	39

<b>Figure 3.5</b> The results from the DNA detection of each genotypes including normal, HbE heterozygous and HbE homozygous genotypes providing different spot patterns...	40
<b>Figure 3.6</b> Limit of detection of the paper-based DNA sensor for HbE detection (top row – normal genotype; bottom row – HbE homozygous genotype). The amount of DNA presented the amounts of the template used for subsequent amplifications. ....	41
<b>Figure 3.7</b> A scanned image of 100 paper-based sensor that were tested against 100 real samples. ....	42
<b>Figure 3.8</b> Plots of intensity ratios with suggested optimized ratios as obtained from the generation of ROC curves between a) normal vs HbE heterozygous genotypes and b) HbE heterozygous vs HbE homozygous genotypes. It should be noted that normal samples with intensity ratios above 35 were not shown for the sake of clarity at the cutoff area.....	44
<b>Figure 3.9</b> Box plots showing median, IQR, and outliers of ratios from each genotype data set with a) the total view of all data, b) the borderline between normal and HbE heterozygous genotypes, and c) the borderline between HbE heterozygous and HbE homozygous genotypes. ....	45
<b>Figure 3.10</b> ROC curves of the discrimination between a) normal vs HbE heterozygous genotypes, and b) HbE heterozygous vs HbE homozygous genotypes .....	48
<b>Figure 3.11</b> Reproducibility test on two genotypes (a – normal; b – HbE homozygous). Each genotype was evaluated by testing three samples for three repetitions. ....	49
<b>Figure 3.12</b> The effect of storage periods on the performance of the sensor.....	50
<b>Figure 3.13</b> Putative sequences of the amplicons from the gene A) <i>groEL</i> , B) <i>motB</i> and C) <i>16s rRNA</i> (grey highlight: primer sequences and red alphabets: detection region). ....	52
<b>Figure 3.14</b> a) Schematic layout of the paper-based sensor showing the locations and the sequences of the PNA probes used in this study, along with b) the list of all possible outcomes of the sensor.....	53

- Figure 3.15** Species specificity of the sensor carrying three immobilized PNA probes, namely GroEL, 16s, and MotB with DNA samples from amplification with a) *groEL* primers, b) *motB* primers and c) *16s rRNA* primers. .... 55
- Figure 3.16** Limit of detection of the sensor carrying three immobilized PNA probes, namely GroEL, 16s, and MotB with DNA samples from amplifications of varying amounts of genomic DNA template with a) *groEL* primers, b) *motB* primers and c) *16s rRNA* primers. .... 56
- Figure 3.17** A scanned image of paper-based sensors for the detection of *B. cereus* in 25 spiked rice samples. Neg = negative control, which is a rice sample subjected to the same experimental protocol but without bacteria inoculation. Pos = the positive control, which is a direct amplification from isolated bacteria solution (no rice matrix). 58
- Figure 3.18** Box plot illustrating a) the absolute intensities of signals from GroEL, 16s and MotB probes, and b) the intensity ratios of signals from GroEL and MotB probes, with 16s probe as a control, *i.e.*, the denominator of ratio calculations. Pos and Neg samples are defined in the previous figure..... 59
- Figure 3.19** The pictures that show a) PNA-immobilized paper sheet held in a cassette after DNA detection and b) the setup of the smartphone holder with a smartphone and a sensor cassette being in place..... 60

## LIST OF SCHEMES

<b>Scheme 2.1</b> Preparation of pyrrolidinyl PNA-immobilized paper.....	27
<b>Scheme 2.2</b> DNA detection method by using pyrrolidinyl PNA-immobilized paper-based sensor and visualization of DNA target through enzymatic amplification assay.....	29
<b>Scheme 3.1</b> A schematic representation of the working principle of the paper-based DNA sensor. The PCR-amplified biotinylated DNA sample was denatured and captured by the paper-immobilized PNA probe, followed by the immobilization of enzyme and signal generation. The color pigments remain adsorbed on the paper, and the scanned images of these paper-based sensors were converted to numerical data by imaging software for further analysis.....	35



## LIST OF TABLES

<b>Table 1.1</b> Selected diagnostic methods at the DNA level for the identification of thalassemia genotypes .....	17
<b>Table 3.1</b> Characterization data of PNA probes .....	32
<b>Table 3.2</b> Two sample <i>t</i> -tests between each pair of genotypes.....	46
<b>Table 3.3</b> Two sample F-tests between each pair of genotypes.....	46
<b>Table 3.4</b> Effect of the cutoff ratios to the performance of the sensor in distinguishing between normal (34 samples) and HbE heterozygous genotypes (31 samples) .....	47
<b>Table 3.5</b> Effect of the cutoff ratios to the performance of the sensor in distinguishing between HbE homozygous (35 samples) and heterozygous genotypes (31 samples).....	47
<b>Table 3.6</b> Sequences of primers used in this study.....	51



# CHAPTER I

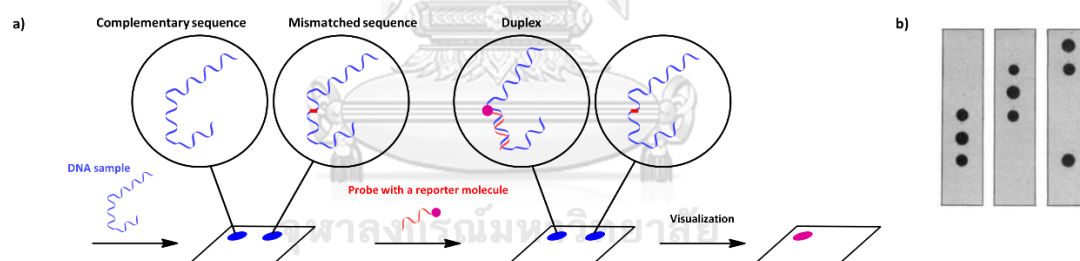
## INTRODUCTION

### 1.1 Paper-based DNA sensor

In recent years, paper-based analytical devices have been continuously developed and applied to many applications.<sup>1-3</sup> Paper is an economical, inexpensive, lightweight, and accessible material. As a base-material for analytical device, the major advantage of paper is its porosity that allows wicking of fluids. Additionally, paper is well-suited for various kinds of printing and chemical modification.<sup>4</sup> Furthermore, it can be folded into complex structures that allow facile control of the fluids flow and mixing. The so-called paper-based analytical devices (PADs) are highly suitable for point-of-care testing where simplicity, affordability, sensitivity, specificity, rapidity, and robustness are required. The DNA detection is very important in many applications such as forensic science, clinical diagnosis, food safety and microbial detection.<sup>5-13</sup> However, this usually requires expensive instruments and highly trained personnel, thus limiting its applications in limited-resource setting. Accordingly, paper-based DNA sensor is a promising tool for point-of-care testing, especially in remote area that has low resource and technology.

A classic example of DNA testing is the dot blot hybridization technique. It is based on the basic principle of nucleic acid hybridization assay where the DNA probe and target of interest bearing a sequence complementary to each other hybridize under the optimal condition of temperature and ionic strength.<sup>14-16</sup> In general, the target nucleic acid is first spotted onto a nylon membrane followed by hybridization with the probe labelled with a reporter molecule (**Figure 1.1a**). Next, the presence of the probe bound to the target DNA is visualized by a suitable technique depending on the nature of the reporter molecule attached to the probe.<sup>17</sup> For a radioactive reporter, the result was directly detected by autoradiography. However, there are major limitations such as short half-life of the radio isotope and serious health

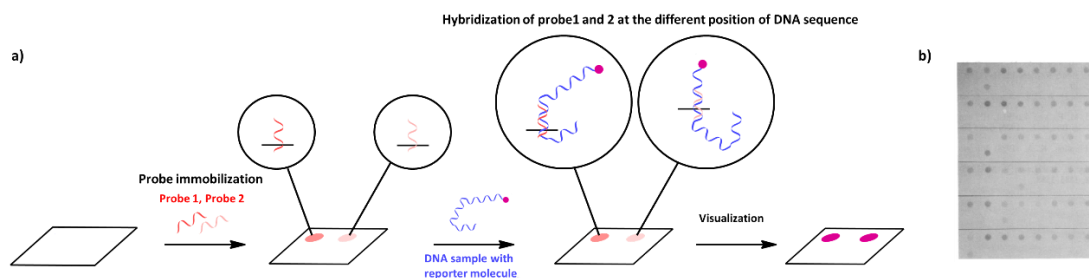
hazards. Nowadays, non-radioactive reporter molecules are more favorable. Several reporter systems take the advantage of the well-established biotin-streptavidin interaction, in which the reporter molecule is biotin attached to the nucleotide probe.<sup>17</sup> It can bind to streptavidin that is covalently conjugated with an enzyme such as alkaline phosphatase or horseradish peroxidase that can catalyze the formation of fluorescent or deeply-colored products. The successful hybridization between the probe and the target DNA is visualized by the signal generated by the enzyme which acts catalytically thus greatly enhance the signal compared to the directly-labeled probe.<sup>17-19</sup> This assay is simple to perform and the interpretation of results is straightforward.<sup>14, 16</sup> However, this method is not suitable for simultaneous detection of various mutations and polymorphisms in the same experiment. This is because each probe needs to be separately hybridized to the DNA sample that was previously spotted on the membrane. Thus, it is impractical for high-throughput testing.



**Figure 1.1** a) Schematic illustration of the principle of dot-blot assay. b) Example of the result from the detection of  $\beta$ -globin gene<sup>20</sup>

To overcome this limitation, the reverse dot-blot (RDB) technique was subsequently developed.<sup>16, 20</sup> According to this method, the probe is first attached onto the membrane (**Figure 1.2a**). The biotinylated target DNA obtained from PCR reaction with biotinylated primers was next hybridized with the immobilized probe on the membrane. Streptavidin-horseradish peroxidase or -alkaline phosphatase conjugate is subsequently added, and is captured by the biotin molecule on the DNA target. The signal is generated after addition of the chromogenic substrates that

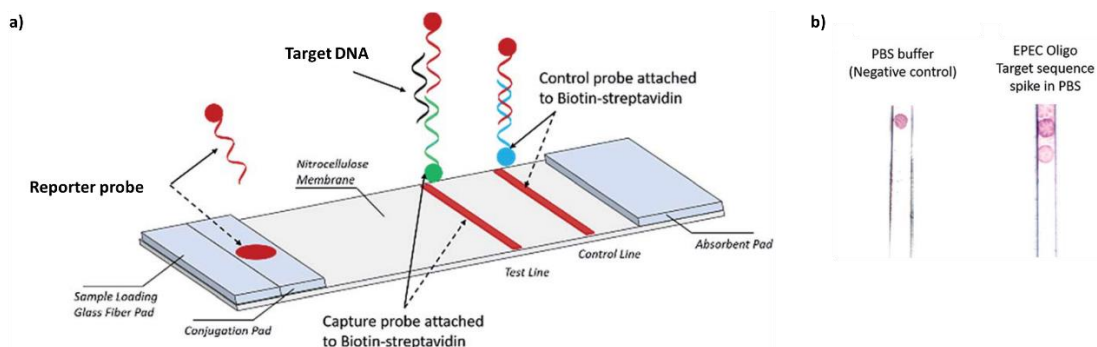
allows visualization as explained in the dot blot hybridization technique. Since multiple probes can be immobilized on the same membrane, the method enables simultaneous detection of various types of mutation.



**Figure 1.2** a) Schematic illustration of the principle of reverse dot-blot assay shows that two probes with different sequences are used to detect target DNA at the different position of DNA sequence. b) Example of the result from the detection of  $\beta$ -thalassemia mutations.<sup>20</sup>

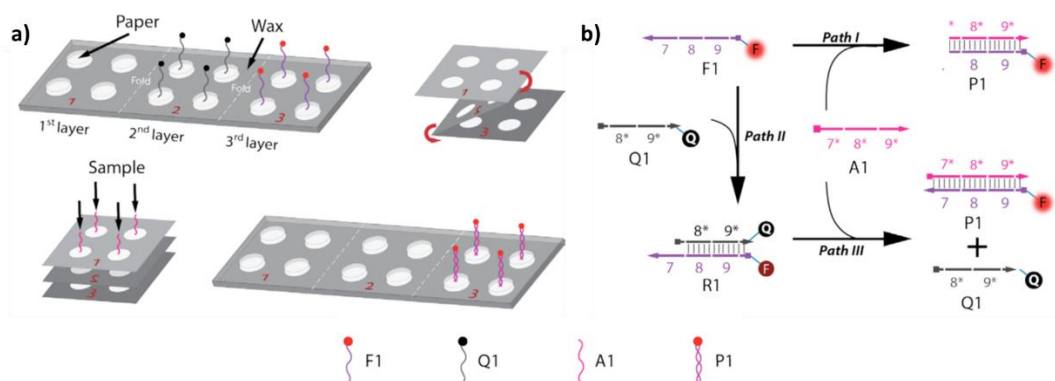
Another well-known assay format is the lateral flow assay. This assay is a useful point-of-care device that typically employs antibody-antigen interaction. Recently, the assay was applied for DNA detection by changing from antibody-antigen recognition to nucleic acid hybridization on the paper strip.<sup>4, 21</sup> The lateral flow strip generally consists of sample pad, conjugation pad, test line, control line and absorbent pad (**Figure 1.3a**). The test line carries a specific DNA probe that can capture the DNA target, and the gold nanoparticles reporter are functionalized with another DNA sequence that bind to a different region of the DNA target. The control line carries yet another DNA sequence that is complementary to the sequence present on the reporter probe. When the DNA sample was dropped onto the sample pad, it will migrate to absorbent pad by the capillary force. Once the sample reaches the conjugation pad, a complex of the DNA target and the DNA-functionalized reporter probe is formed. The complex and/or unhybridized reporter probe move along the paper strip and only the complex will be captured at the test line, while

the remaining reporter probe will be captured at the control line thus confirming that the device is working properly.<sup>22-25</sup>



**Figure 1.3** a) Schematic illustration of the principle of DNA detection on lateral flow test strip b) Image result from the detection of negative control (left) and target DNA (right).<sup>23</sup>

As mentioned above, the advantage of paper allows a variety of printing on the paper surface leading to wax printing technology. Wax-patterned technology enables the formation of microzone on a piece of paper similar to 96-multiwell plate.<sup>26</sup> With this format, the patterned paper can store the reagents without fluid dynamics in the hydrophilic zone. This and similar patterned paper-based devices have been extensively developed in the field of DNA detection. For example, fluorescence detection of DNA on origami-base paper analytical device was reported by Scida and coworker in 2013.<sup>27</sup> A wax-patterned paper was divided to 3 layers before folding (**Figure 1.4a**). A quencher probe and a fluorescence probe was dispensed in the second layer and the third layer respectively. After the paper was folded, the analyte was then added. In the presence of DNA target, the hybridization of the DNA target and the fluorescence probe occurred yielding the fluorescence signal (**Figure 1.4b**). In the absence of the DNA target, the quencher probe will bind to the fluorescence probe, resulting in the fluorescence quenching.



**Figure 1.4** a) Schematic representation of fluorescence detection through competitive hybridization between fluorophore-labeled probe, quencher probe and DNA target. b) Origami paper analytical device with three components in each layer.<sup>27</sup>

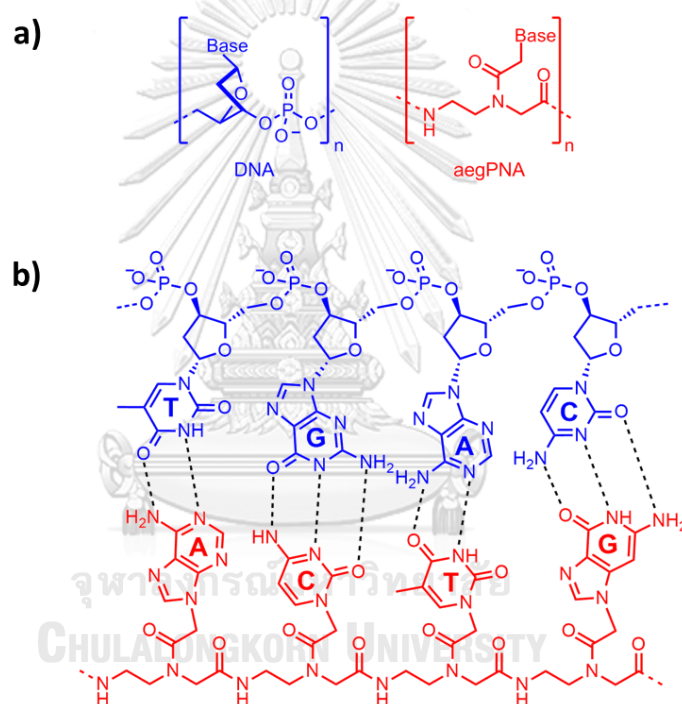
The examples as shown above indicates the utility of paper-based analytical device for the DNA detection. Nevertheless, the conventional DNA probe has a limitation of the specificity to the target sequence, especially the discrimination between complementary and the closely-related single-base mismatched sequences.<sup>22-24, 27</sup> In recent years, peptide nucleic acid or PNA which shows better discriminating power has been increasingly used as an alternative probe to replace the conventional oligonucleotide probes in many DNA sensors.

## 1.2 Peptide nucleic acid (PNA)

### 1.2.1 History of peptide nucleic acid and its property

PNA is a nucleic acid mimic that the sugar-phosphate backbone is replaced by a peptide backbone (**Figure 1.5a**). The first member of the PNA family, namely *N*-(2-aminoethyl)glycine PNA (aegPNA), was discovered by Nielsen and coworkers in 1991.<sup>28-30</sup> The backbone of aegPNA consists of *N*-(2-aminoethyl)glycine units that is uncharged as opposed to the negatively charged backbone of DNA. Despite the chemical functionalities of aegPNA is different from DNA, the intramolecular distance between consecutive nucleobases of aegPNA is similar to those of natural DNA.<sup>31</sup> Accordingly, aegPNA can bind to DNA following the Watson-Crick base pairing rules

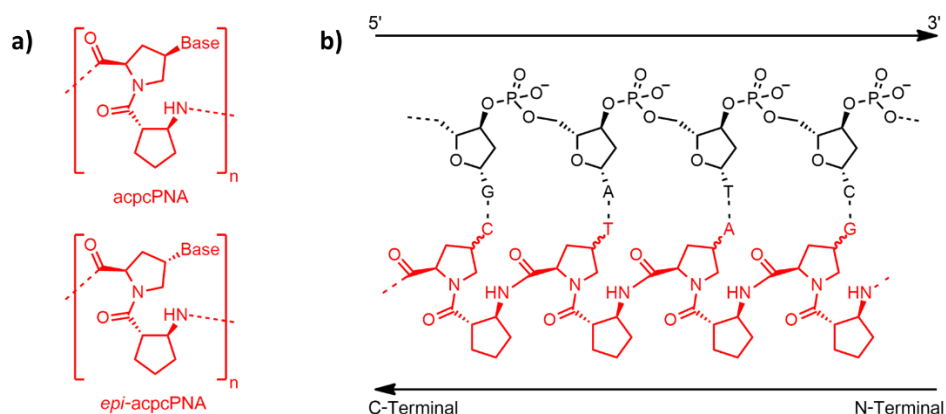
(Figure 1.5b). Due to the uncharged backbone of aegPNA, the absence of unfavorable electrostatic repulsion contributes to the higher thermal stability of aegPNA-DNA duplex than DNA-DNA duplex. The high stability of aegPNA-DNA duplex usually leads to a decrease of limit of detection in many DNA sensing applications.<sup>32, 33</sup> Another important feature of aegPNA is the ability to discriminate between complementary and single-base mismatch DNA with high specificity. Moreover, the chemical and biological stability of aegPNA is greater than that of DNA due to its unnatural peptide backbone.<sup>32, 34</sup> This results in a longer term storage at room temperature with better tolerance in samples containing proteinase and nuclease.



**Figure 1.5** a) Repeating units in the structure of DNA and aegPNA. b) an aegPNA-DNA duplex in the antiparallel mode, showing the base pairing according to the Watson-Crick base-pairing rules.

### 1.2.2 Recent development of conformationally constrained PNAs and their attractive features

During the past three decades, various analogues of PNA were continuously developed to further improve the properties of PNA such as enhanced binding affinity, solubility, etc. One of the most successful approach is the incorporation of conformational constraint into the PNA structure which can reduce the entropy change of the formation of PNA-DNA duplex. Based on this principle, pyrrolidinyl PNA consisting of nucleobase-modified proline and 2-amino-1-cyclopentanecarboxylic acid (**Figure 1.6a**), also known as acpcPNA, was introduced by Vilaivan and coworkers in 2005.<sup>35</sup> There are two stereoisomers of acpcPNA, acpcPNA with (2*R*,4*R*) configuration and *epi*-acpcPNA with (2*R*,4*S*) configuration, both of which bind to DNA with high affinity and specificity. Due to the rigid conformation, pyrrolidinyl PNA binds to DNA with higher thermal stability than aegPNA. Additionally, the great specificity towards DNA binding of pyrrolidinyl PNA is confirmed by a large decrease in thermal stability of mismatched hybrids compared to complementary hybrids. Interestingly, pyrrolidinyl PNA binds to DNA in only antiparallel direction (**Figure 1.6b**), whereas binding in both parallel and antiparallel directions were observed in aegPNA. The excellent performance of pyrrolidinyl PNA suggests it as a potential probe in many applications for DNA detection such as quartz crystal microbalance (QCM), surface plasmon resonance (SPR) and self-reporting fluorescence probe.<sup>35</sup> In this work, we aim to develop a paper-based colorimetric sensor for a rapid, in-field DNA detection by using pyrrolidinyl PNA as a probe.



**Figure 1.6** a) acpcPNA and *epi*-acpcPNA structure. b) Antiparallel hybrid of pyrrolidinyl PNA and DNA.

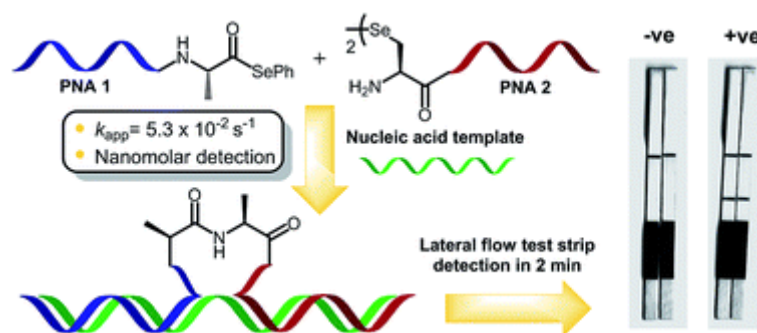
### 1.3 Paper-based analytical device employing PNA as a probe

As mentioned earlier, paper-based DNA sensor is an interesting topic for low-resource settings and remote area. Although great achievement in the DNA detection was achieved in various formats such as lateral flow assay, folded paper devices, and reverse dot blot assay, the specificity of standard DNA probes is a key limitation especially for single-base discrimination.<sup>22-24, 27, 36, 37</sup> In general, a strict temperature control is required to distinguish fully matched and single-base mismatch DNAs because of a small difference in their thermal stabilities (typically 10 °C or less). Therefore, the replacement of conventional DNA probe by pyrrolidinyl PNA or other PNA probes with greater performance in specificity has potential to improve the performance of DNA sensors. There are examples of paper-based colorimetric or fluorescent DNA sensors employing pyrrolidinyl PNA or aegPNA that provided a good result of discrimination ability, as shown below.

In 2018, a paper-based lateral flow assay was developed for the detection of RNA.<sup>38</sup> The detection method required a design of two PNA probes which are biotin-labelled selenocystine PNA probe (PNA 2) and fluorescein isothiocyanate (FITC)-labelled selenoester PNA probe (PNA 1). The selenocystine–selenoester peptide ligation of the PNA 1 and PNA 2 was performed employing target RNA as a template.

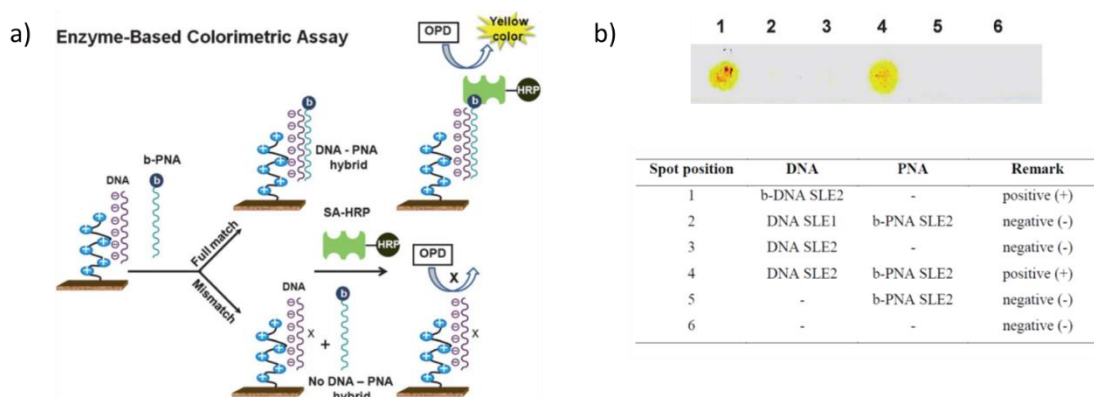


The fluorescent ligation product was captured by streptavidin in the test zone providing a detectable signal. The lowest detectable signal was observed at 0.33 nM of the target RNA. The sensor also showed the selectivity to complementary sequence over fully mismatched and partially mismatched sequences.



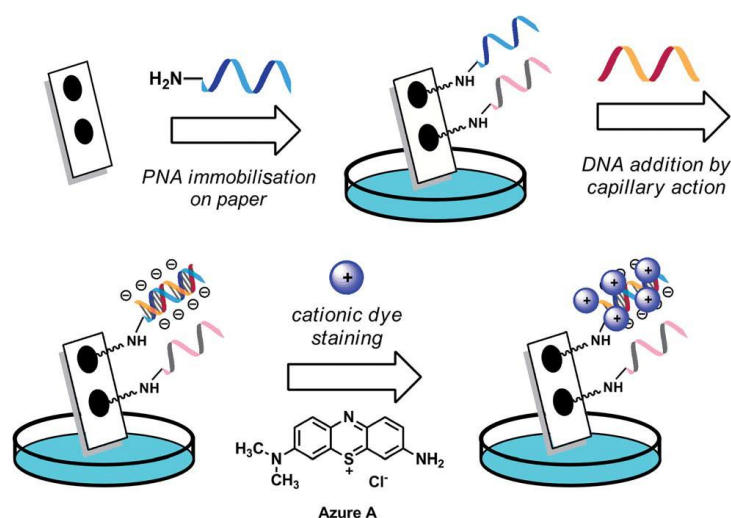
**Figure 1.7** Schematic representation of oligonucleotide-templated selenocysteine-selenoester ligation reaction using in lateral flow test of target RNA.<sup>38</sup>

In 2013, Laopa applied pyrrolidiny PNA as a reporter probe in a dot blot analysis.<sup>39</sup> The positively charged polymer (quaternized poly(dimethylamino)ethyl methacrylate) was grafted on a piece of filter paper to capture the negatively charged DNA target. After hybridization with a biotinylated pyrrolidiny PNA probe, the signal was obtained from enzymatically amplified reaction using streptavidin-horseradish peroxidase conjugate (**Figure 1.8a**). The limit of detection was around 10 fmol per spot with high specificity to allow single mismatch discrimination at ambient temperature (**Figure 1.8b**).



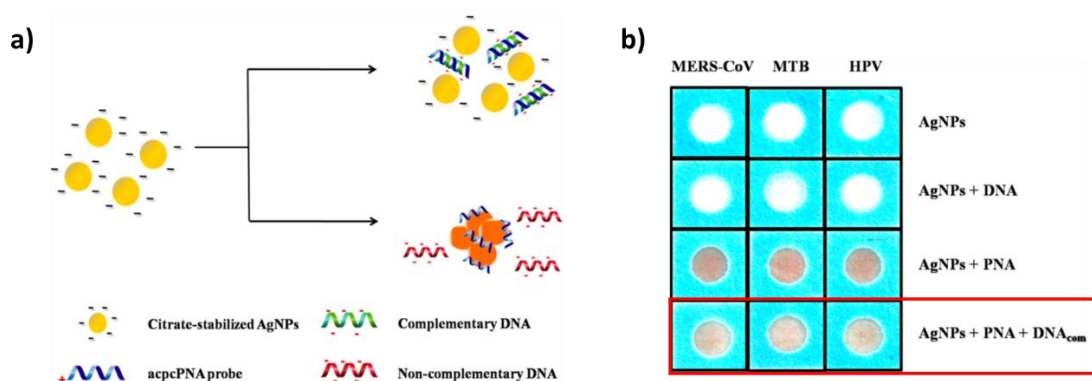
**Figure 1.8** a) Schematic representation of enzymatic amplified colorimetric detection of DNA following Dot blot hybridization using filter paper functionalized with positively charged polymer brushes and the peptide nucleic acid probe. b) Representative images of the test results demonstrating the specificity and efficiency of b-PNA SLE2<sup>39</sup>

In 2015, a paper-based analytical device was developed by immobilizing pyrrolidinyl PNA probe on the paper surface and associated with cationic dye for colorimetric detection.<sup>40</sup> The cellulose membrane was activated with divinyl sulfone prior to the immobilization of the pyrrolidinyl PNA probe. The DNA target was hybridized to the pyrrolidinyl PNA probe immobilized on the paper and was subsequently stained with a cationic dye (azure A) that binds to the DNA probe via electrostatic interaction to provide a blue spot (**Figure 1.9**). Good specificity was achieved in both double mismatch and single mismatch discriminations, while the detection limit is 3.3 pmol or 200 nM of DNA target per spot. Such paper-based sensor with immobilized pyrrolidinyl PNA probe showed a great promise in mismatch discrimination, although the detection limit was too high to allow the detection in real samples (unpublished results).



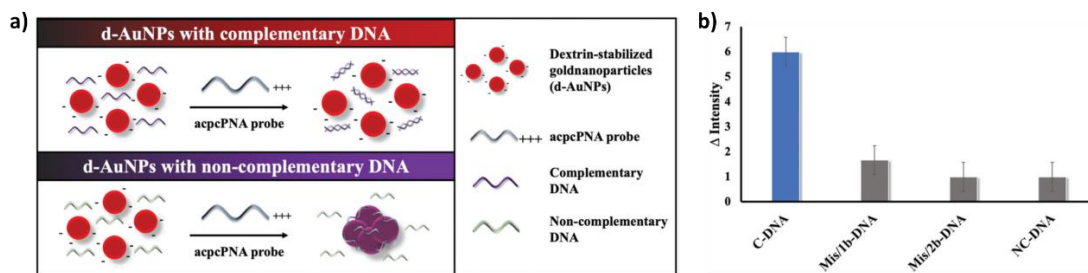
**Figure 1.9** Fabrication of DNA sensor using DVS activation to immobilize pyrrolidinyl PNA onto paper and DNA detection with cationic dye<sup>40</sup>

In 2017, the pyrrolidinyl PNA-induced nanoparticle aggregation was utilized for the DNA detection on paper-based sensor.<sup>41</sup> According to the working principle, the negatively charged silver nanoparticles (AgNPs) can be destabilized by positively charged amino group at the end of PNA probe, resulting in nanoparticle aggregation with a detectable color change (**Figure 1.10**). In the presence of complementary DNA target, the anionic DNA-PNA duplex was formed and thus the aggregation of AgNPs was destroyed and the color returned to the original state. Thus, the result showed the low level of AgNPs aggregation in the presence of the target DNAs, while the high intensity of AgNPs aggregation was observed in the absence of the target DNA (**Figure 1.10b**). In this work, a paper-based device was designed to simultaneously detect three target DNAs including Middle East respiratory syndrome coronavirus (MERS-CoV), *Mycobacterium tuberculosis* (MTB) and human papillomavirus (HPV). The limit of detection was 1.53 (MERS-CoV), 1.27 (MTB), and 1.03 nM (HPV). Moreover, the pyrrolidinyl PNA probe exhibited high selectivity for the complementary oligonucleotides over single-base-mismatch, two-base-mismatch, and noncomplementary DNA targets.



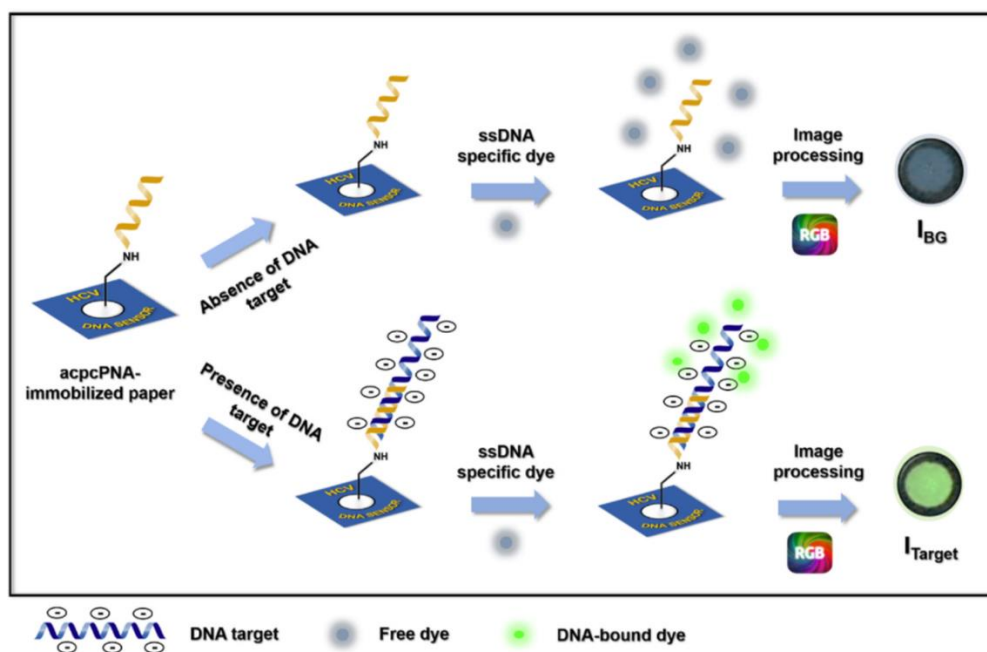
**Figure 1.10** a) The paper-based colorimetric assay for DNA detection based on pyrrolidinyl PNA-induced nanoparticle aggregation. b) Photograph of visual color changes obtained from detection of MERS-CoV, MTB, and HPV in the presence of complementary DNA.<sup>41</sup>

In 2021, a smartphone-assisted paper-based colorimetric assay employing the similar concept of the pyrrolidinyl PNA-induced nanoparticle aggregation was developed as shown in **Figure 1.11a**.<sup>42</sup> In this work, the dextrin-stabilized gold nanoparticles (d-AuNPs) were aggregated in the presence of PNA according to the aforementioned principle. This aggregation resulted in a distinctive color change from red to blue on the paper. The formation of hybrid between the pyrrolidinyl PNA probe and the DNA target d-AuNPs aggregation due to the decreased level of the residual PNA probe. The color change in the present and absent of target DNA was quantified by analyzing the color intensity through a smart phone application. The detection limit of 1 nM was achieved under the optimal conditions. As usual, the acpcPNA probe exhibited high selectivity for the complementary DNA over single-base-mismatch, two-base-mismatch, and non-complementary DNA targets as shown in **Figure 1.11b**.



**Figure 1.11** a) The concept of the pyrrolidinyl PNA-induced nanoparticle aggregation in the present and absent of DNA target.<sup>42</sup> b) The graph of  $\Delta$ intensity of complementary (c-DNA), single-base mismatched (Mis/1b-DNA), two-base mismatched (Mis/2b-DNA), and non-complementary DNA (NC-DNA).

In 2021, another fluorescent paper-based DNA sensor employing a pyrrolidinyl PNA probe for the detection of hepatitis C virus was reported by Teengam and coworkers.<sup>43</sup> The pyrrolidinyl PNA probe was covalently attached onto the oxidized cellulose paper through reductive alkylation between the amine group from the PNA probe and the aldehyde groups on the paper surface. The ssDNA-binding fluorescent dye was used to indirectly monitor the formation of PNA-DNA duplex via the binding of the dye to the overhang region of the single-stranded DNA target (**Figure 1.12**). The sensor showed a limit of detection of 5 pmol DNA/spot under the optimal condition and showed selectivity for complementary DNA over mismatched DNA sequences.



**Figure 1.12** The principle of the fluorescence-based detection of target DNA using the acpcPNA-immobilized paper-based sensor and ssDNA-specific fluorescence dye.<sup>43</sup>

#### 1.4 Impactful applications of the use of DNA sensors based on pyrrolidinyl PNA

Due to the outstanding performance of paper-based DNA sensor, the development of this technology has a high impact on many research topics. One of these is the clinical diagnosis because the mutation of genes may cause genetic disorders that can be life-threatening such as thalassemia, sickle cell anemia and diabetes. Genetic disorders are traditionally categorized into three main groups including single-gene, chromosomal, and multifactorial disorders.<sup>44</sup> Single-gene disorders are caused by the deletion or mutations in the DNA sequence of the individual's gene leading to genetic diseases. Multifactorial disorders are caused by multiple-gene mutation and environmental factors. Chromosomal disorders arise from a change in the number or structure of chromosomes. Thus, the accurate diagnosis of diseases is essential for appropriate treatment of patients, genetic counseling, and prevention strategies. In this work, the development of the paper-

based DNA sensor is applied in the detection of thalassemia disease, a common genetic disorder in Thailand.

Thalassemia is an inherited blood disorder which cause the body produces less hemoglobin or abnormal hemoglobin. As there are several types of mutation in thalassemia disease, accurate diagnosis is difficult and usually require the DNA-based diagnosis for identification of the genotype. Among several existing DNA-based methods for thalassemia diagnostics (**Table 1.1**), DNA sequencing is considered the most informative and accurate.<sup>45, 46</sup> However, this method is not applicable for routine analyses mainly due to the cost and highly demanding facilities and trained staff. The high-resolution melting technique suffers similar limitations. Allele-specific polymerase chain reaction (PCR),<sup>47-49</sup> on the other hand, offers a more practical solution to identify thalassemia genes. While this method requires less sophisticated equipment, it requires a tedious gel-based analysis. Furthermore, multiple reactions need to be performed when the homozygous and heterozygous states are to be differentiated. On the other hand, the reverse dot blot (RDB) hybridization is a relatively simple, economical, yet effective in providing specific genetic data of interest.<sup>46, 47</sup> The underlying principle is the immobilization of DNA probes designed to capture the specific DNA target onto a membrane. Subsequent enzyme-catalyzed visualization of the captured DNA target allows for clear diagnosis and applicable to all types of mutations. Unfortunately, with the typically employed DNA oligonucleotide probes, a strict control of temperature within a range of few degree Celsius is mandatory for the detection of single-point mutations due to the small difference between the stabilities of the complementary and single-mismatched duplexes.<sup>50, 51</sup> According to the aforementioned DNA binding properties of pyrrolidinyl PNA, we envisioned that the high specific pyrrolidinyl PNA will greatly distinguish full-matched DNA target from a single-base mismatched duplex.

**Table 1.1** Selected diagnostic methods at the DNA level for the identification of thalassemia genotypes

Method	Advantage	Drawback	Key Equipment
Allele-specific PCR <sup>47-49</sup>	Wide applicability for point mutations	The need of multiple reactions to distinguish between homozygotes and heterozygotes <sup>52</sup>	Thermal cycler and gel electrophoresis
High-resolution melting analysis <sup>53</sup>	High selectivity for point mutations	The need of positive controls for accurate identification	Real-time PCR instrument
Sanger sequencing <sup>46, 54</sup>	The ability to characterize nucleotide variants	Impracticality to characterizing large deletions	DNA sequencer
Next-generation sequencing <sup>45, 46</sup>	Comprehensiveness in terms of obtained genetic data	High cost and demanding resource requirement	Next-generation sequencer
Reverse dot blot hybridization <sup>37, 46</sup>	Relatively low cost, applicability for point mutations and deletions	Strict requirement of temperature control when identifying point mutations	Thermal cycler and water bath

Apart from the clinical diagnosis, the development of paper-based DNA sensor is highly attractive for the detection of foodborne pathogen, which is important in food industry. Foodborne pathogen is microorganisms, such as bacteria, virus, and parasite, that can cause a foodborne disease. Foodborne pathogens are causing a large number of diseases with severe threats to public health. According to the data collection from 1996 to 2005, 121,536 cases of laboratory-confirmed bacterial infections including 552 cases of deaths (5%) was reported by the Foodborne Diseases Active Surveillance Network.<sup>55</sup> Thus, the screening method for the detection of foodborne pathogens is necessary to prevent the outbreak of foodborne diseases and ensure the food safety.<sup>56</sup> At present, the routine identification of foodborne pathogen is the culture method and PCR-based detection technology.<sup>56-58</sup> Although conventional methods are simple and inexpensive, they have some critical disadvantages, for example, time-consuming and laborious. In recent years, a trend of the point-of-care testing approach with the visual detection method arises because it allows direct observation of the result with the naked



eye.<sup>57, 58</sup> Hence, our development of paper-based DNA sensor that fit with the trend was applied in the detection of *Bacillus cereus* — a toxin-producing bacteria is commonly found in food.

*Bacillus cereus* is a well-known pathogenic bacterium that can be found in multiple types of foods such as rice, wheat, and dairy products and is responsible for foodborne illnesses.<sup>59</sup> Due to its persistent nature including being facultative anaerobic, capable of forming endospores, and capable of synthesizing heat-stable toxins, foodborne illnesses related to *B. cereus* can be a serious problem if sufficient care in food handling is not taken.<sup>59, 60</sup> Hence, there is a high demand in food and agriculture industries for rapid, sensitive, and specific detection methods for *B. cereus*.<sup>61</sup>

Currently, colony counting on agar plates is still a standard method for the identification of *B. cereus* in many settings.<sup>62, 63</sup> While this method has relatively low cost, the long turnaround time (days) and the lack of species specificity are the key limitations. Therefore, methods based on molecular biology such as the polymerase chain reaction (PCR) with a gel-based detection or quantitative real-time PCR have been developed for the detection of *B. cereus* with greater accuracy and rapidness.<sup>64-69</sup> Nevertheless, highly specific detection methods of this species are still desirable due to its close genetic resemblance with other *Bacillus* species.<sup>61, 66, 69-72</sup> Instead of relying only on the detection of the PCR amplicons (which depends on the specificity of the primers in amplifying the correct region of the genetic markers alone), we surmised that the key to achieving high specificity lies in the use of powerful probes. Thus, pyrrolidinyl PNA with great performance in DNA affinity and specificity will be introduced as a probe for *B. cereus* detection.

### 1.5 Rationale and objective of this work

As mentioned earlier, there are still great demands for a DNA sensor that meets the criteria for point-of-care testing where simplicity, affordability, sensitivity, specificity, rapidity, and robustness are required. The objective of this work is to develop of a paper-based DNA analytical device for the detection of PCR amplicons from real samples. It was proposed that the limitation of conventional DNA probe, whereby the strictly temperature control is required to achieve perfect mismatch discrimination, should be overcome by using pyrrolidinyl PNA probes with high sequence specificity and strong affinity towards DNA instead of DNA probes. Although PNA probes have been used in many paper-based DNA sensors, the detection of PCR amplicons was still challenging. Herein, various factors such temperature and ionic strength were optimized to achieve this goal. In this work, the paper-based DNA sensor was fabricated by immobilization of the pyrrolidinyl PNA probes at specific locations via the amide bond formation through EDC/NHS chemistry. Strategic combinations of several PNA probes are incorporated into the same device to provide a self-validation mechanism. For the DNA detection process, the enzymatically amplified colorimetric assay which theoretically offers a high sensitivity was utilized to visualize the DNA target in this study. The immobilized pyrrolidinyl PNA probes were selectively hybridized with the target PCR amplicon bearing a biotin tag incorporated in the form of biotinylated primer. Next, streptavidin-alkaline phosphatase conjugated was captured by the biotinylated PCR amplicon that was previously captured by the immobilized PNA probe. The visible signal was finally generated through the enzymatic reaction with chromogenic substrates. The location of colored spots on the sensor that was determined by the complementarity between the sequences of the PNA probe and the DNA target reveals the identity of the DNA target by naked-eye detection or by using an image processing software. This whole process of sensor fabrication and detection was evaluated to two important applications including 1) the detection of a HbE thalassemia mutation in

human blood samples, and 2) the detection of the presence of *Bacillus cereus* genes in rice matrix.



## CHAPTER II

### EXPERIMENTAL SECTION

#### 2.1 Materials

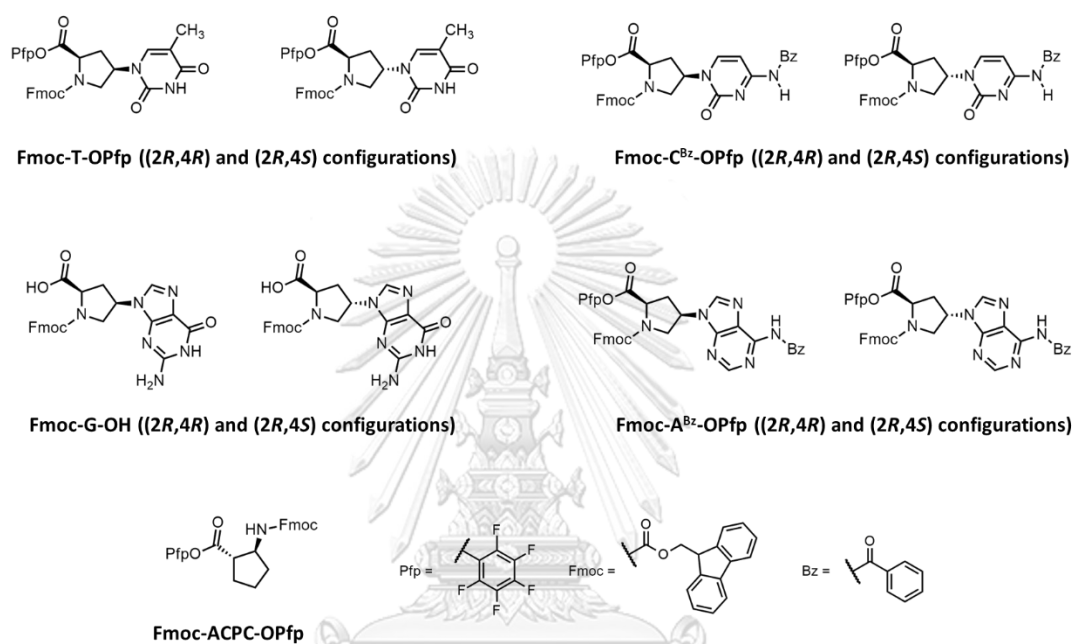
All chemicals for the synthesis of PNA monomers and PNA probes were purchased from Fluka, Merck, ChemImpex, GL Biochem or Sigma-Aldrich and were used as received without further purification. Anhydrous *N,N*-dimethylformamide (DMF, H<sub>2</sub>O ≤ 0.01%) for solid phase peptide synthesis was obtained from RCI Labscan and was dried over activated 4Å molecular sieves before use. The solid support for peptide synthesis (TentaGel S-RAM Fmoc resin, 0.24 mmol/g) was obtained from Fluka. Fmoc-L-Lys(Boc)-OPfp was purchased from Calbiochem Novabiochem. Nitrogen gas was obtained from Labgas (Thailand) Ltd. with high purity up to 99.995%. Chromatography paper (grade 1 Chr) was purchased from GE Healthcare. Carboxymethyl cellulose (CMC, average molecular weight = 9000, 99.5%) was purchased from Acros Organics. CaCl<sub>2</sub> (99%) was obtained from Suksapanphanit, Thailand. *N*-(3-dimethylaminopropyl)-*N'*-ethylcarbodiimide hydrochloride (EDC-HCl, 98%) and *N*-hydroxysuccinimide (NHS, 98%) were purchased from Merck. Alkaline phosphatase-streptavidin conjugate and the visualization agent, consisting of *p*-nitroblue tetrazolium chloride (NBT, 0.42 g/L) and 5-bromo-4-chloro-3-indolyl phosphate (BCIP, 0.21 g/L) in Genius buffer, were obtained from KPL, Gaithersburg, MD, USA.

#### 2.2 Synthesis of pyrrolidinyl PNA

##### 2.2.1 Pyrrolidinyl PNA monomer synthesis

The eight Fmoc-protected, Pfp-activated pyrrolidinyl PNA monomers namely Fmoc-A<sup>Bz</sup>-OPfp, Fmoc-C<sup>Bz</sup>-OPfp, Fmoc-G-OH and Fmoc-T-OPfp with the (2*R*,4*R*)- and (2*R*,4*S*) configurations for acpcPNA and *epi*-acpcPNA, respectively, (**Figure**

2.1 and 2.2) were synthesized by Mr. Nuttapon Jirakittiwut (Fmoc-A<sup>Bz</sup>-OPfp and Fmoc-C<sup>Bz</sup>-OPfp), Ms. Penthip Muangkaew (Fmoc-T-OPfp) and Mr. Chayan Charoenpakdee (Fmoc-G-OH) following the previously reported protocol.<sup>73, 74</sup> The activated spacer Fmoc-(1*S*,2*S*)-2-amino-1-cyclopentanecarboxylic acid pentafluorophenyl ester (Fmoc-ACPC-OPfp) was synthesized by Ms. Penthip Muangkaew.



**Figure 2.1** Structures of pyrrolidiny PNA monomers and ACPC spacer used in solid phase peptide synthesis of acpcPNA and *epi*-acpcPNA

## 2.2.2 Solid phase peptide synthesis

Pyrrolidiny PNAs were synthesized on Tentagel S-RAM resin following the standard solid phase peptide synthesis protocol at 1.5  $\mu$ mol scale by stepwise coupling of the four Fmoc-protected pyrrolidiny PNA monomers and the activated ACPC spacer as reported in literature.<sup>73</sup> The *N*-terminal Fmoc group on the resin was first removed by treatment with 100  $\mu$ L of 20% piperidine and 2% 1,8-diazabicyclo[5.4.0]undec-7-ene (DBU), in DMF for 5 minutes to provide the free *N*-terminal amino group. After an extensive DMF washing, the Fmoc-protected Pfp-activated monomers or spacer or other amino acids such as Fmoc-L-Lys(Boc)-OPfp

were directly coupled to the free amino groups on the resin by using 4 equiv. of the Pfp-activated amino acids, 4 equiv. 1-hydroxy-7-azabenzotriazole (HOAt), 4 equiv. *N,N*-diisopropylethylamine (DIEA) in DMF, 30 minutes single coupling (40 minutes for Fmoc-T-OPfp). In the case of Fmoc-G-OH, 1-[bis(dimethylamino)methylene]-1H-1,2,3-triazolo[4,5-b]pyridinium 3-oxide hexafluorophosphate (HATU)-activation was required before the coupling (4 equiv. free acid monomers, 4 equiv. HATU, 8 equiv. DIEA in DMF, 1 minute pre-activation, 40 minutes single coupling). Following another round of DMF washing, the capping step was performed to ensure the complete blocking of any unreacted free amino groups (5  $\mu$ L of acetic anhydride and 30  $\mu$ L of 7% DIEA in DMF). The deprotection-coupling-capping cycle was repeatedly performed with exhaustive DMF washing during each step until the desired sequence was obtained.

After the last amino acid was incorporated, the *N*-terminal Fmoc group was removed, and the free amino group was then acetylated. The nucleobase protecting groups (Bz for A and C) were next removed by heating with 1:1 aqueous ammonia-dioxane at 60 °C overnight. The resin was subsequently washed thoroughly with methanol and dried. The pyrrolidinyll PNA was cleaved from the resin by treatment with 500  $\mu$ L of trifluoroacetic acid (TFA) for 1 hour (3 times). The cleavage solution was dried under a stream of nitrogen gas and the residue was washed with diethyl ether to remove the remaining TFA. Purification was performed by reverse phase HPLC on Waters 600 HPLC System using a C-18 column (4.6x150 mm, 3.0  $\mu$ m of particle size). The sample elution was performed using a gradient of water (A) and methanol (B) containing 0.1% TFA (monitored by UV absorbance at 260 nm, 10% B for 5 minutes then linear gradient to 90% B over 60 minutes, flow rate 0.5 mL/minute). The purified PNA probe was characterized by MALDI-TOF mass spectrometry (Microflex, Bruker Daltonics) and the purity was determined by HPLC (10% B for 5 minutes then linear gradient to 90% B over 35 minutes, flow rate 0.5 mL/minute).

## 2.3 Preparation of DNA samples

### 2.3.1 for HbE detection

Genomic DNA was extracted from 300  $\mu$ L of peripheral blood using the Genra Puregene Blood Kit according to the manufacturer's protocol (Qiagen, Hilden, Germany; [www.qiagen.com](http://www.qiagen.com)). Thereafter, 100 ng of each genomic DNA sample was amplified using 2 $\times$  Hot Start PCR Master Mix (Biotechrabbit, Berlin, Germany; [www.biotechrabbit.com](http://www.biotechrabbit.com)), which contains Taq DNA polymerase, deoxynucleotide triphosphate mixtures, and a PCR buffer (total volume of 25  $\mu$ L). The primers (200 nmol of each primer per each amplification reaction) used in this study were China1 and China2 (**Figure 2.2a**), both of which were biotinylated at the 5'-end.<sup>37</sup> The PCR cycling reaction was performed in a programmable thermal cycler with the following steps: (1) the initial denaturation step at 95 °C for 2 minutes; (2) 35 cycles of 94 °C for 30 seconds, 55 °C for 45 seconds, and 72 °C for 45 seconds; and (3) the final extension step at 72 °C for 5 minutes. With this primer pair (China1/China2), a PCR product was obtained (**Figure 2.2b**). The size of which was confirmed by gel electrophoresis to be around 600 bp as expected from the base sequence (**Figure A4**).

- a) China1: 5' -GTACGGCTGTCATCACTTAGACCTCA-3'  
 China2: 5' -TGCAGCTTGTACAGTGCAGCTCACT-3'
- b) 1 5' -GTACGGCTGTCATCACTTAGACCTCACCCCTGTGGAGCCACACCCTAGGGTTGGCCAATCT  
 61 ACTCCAGGAGCAGGGAGGGCAGGAGCCAGGGCTGGGCATAAAAGTCAGGGCAGAGCCAT  
 121 CTATTGCTTACATTTGCTTCTGACACAACCTGTGTTCACTAGCAACCTCAAACAGACACCA  
 181 TGGTGCATCTGACTCCTGAGGAGAAGTCTGCCGTTACTGCCCTGTGGGGCAAGGTGAACG  
 241 TGGATGAAGTGGTGGTAAGGCCTGGGCAGGTTGGTATCAAGGTTACAAGACAGGTTTA  
 301 AGGAGACCAATAGAACTGGGCATGTGGAGACAGAGAAGACTCTTGGGTTTCTGATAGGC  
 361 ACTGACTCTCTGCTTATTGGTCTATTTTCCCACCCTTAGGCTGCTGGTGGTCTACCCT  
 421 TGGACCCAGAGGTTCTTTGAGTCCTTTGGGGATCTGTCCACTCCTGATGCTGTTATGGGC  
 481 AACCTAAGGTGAAGGCTCATGGCAAGAAAGTGCTCGGTGCCTTTAGTGATGGCCTGGCT  
 541 CACCTGGACAACCTCAAGGGCACCTTTGCCACACTGAGTGAGCTGCACTGTGACAAGCTG  
 601 CA-3'

**Figure 2.2** a) Sequence of primers, namely China1 and China2. b) Sequence of PCR amplicon from  $\beta$ -globin gene (grey highlight: primer sequences , red alphabets: detection region and a red alphabet with underline: a position of mutated base).

### 2.3.2 for *B. cereus* detection from isolated bacteria

A single colony of *B. cereus* was inoculated into 3 mL of Luria-Bertani (LB) medium, and incubated at 37 °C with shaking at 180 rpm. After 24-hour enrichment in LB, an aliquot of 3 mL of the bacterial culture was subjected to the genomic DNA extraction using GENEWIZ (Germany) as per manufacturer's instructions. The DNA concentration and quality were determined using a Nanodrop 2000 (Thermal Scientific, USA) and gel electrophoresis, respectively. The DNA concentration was adjusted to 1000 ng/ $\mu$ L by Milli-Q water and stored at -20 °C until used.

PCR was performed at a final volume of 25  $\mu$ L using Taq polymerase (Biolabs New England) as per manufacturer's instructions on the C1000™ Thermal Cycler (Biorad, USA). For the limit of detection test, the amount of the DNA template was varied from 0.0001-1 ng per reaction. The PCR reaction began with 1 cycle of 10 minutes at 95 °C, followed by 35 cycles of denaturing at 95 °C for 30 seconds, annealing at 50 °C for 30 seconds, and elongation at 68 °C for 30 seconds. An extra elongation step of 5 minutes at 68 °C was performed after the last PCR cycle. After



the PCR amplification, the product was analyzed by gel electrophoresis on a 1.5% pre-casted agarose gel with SYBR safe dye (Thermo Fisher Scientific, USA). The gels were imaged by a Gel Doc<sup>TM</sup> EZ Imaging System (Bio-Rad, USA).

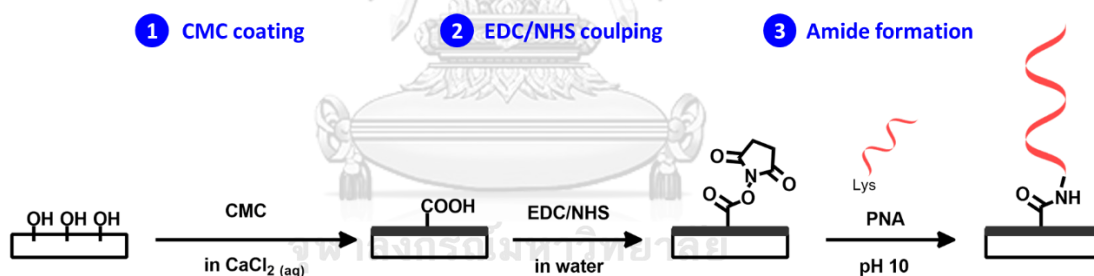
### 2.3.3 for *B. cereus* detection from spiked rice samples

Dry Jasmine rice (Hongthong Rice, Thailand) was purchased from a local supermarket. The dry rice samples were tested to confirm the absence of *B. cereus* contamination by the standard PCR method (**Section 2.3.2**). Twenty-five dry rice samples (25 g each) were ground into fine powder, autoclaved, and cooled down to room temperature. Thereafter, each portion of the fine rice powder was inoculated with 100  $\mu$ L of  $10^6$  CFU/mL of *B. cereus* ATCC 14579, followed by 225 mL of LB medium. After incubation at 37 °C with shaking at 180 rpm for 6 hours, the spiked samples were further centrifuged at 2,000 xg for 5 minutes to remove large debris. The suspensions were further centrifuged at 12,000 xg for 5 minutes. The pellets were then collected and washed twice with sterile milli-Q water, followed by being suspended again in 100  $\mu$ L of sterile milli-Q water. Genomic DNA was extracted by using GENEWIZ (Germany) as per the manufacturer's instructions. The DNA concentration and quality were determined using Nanodrop 2000 and gel electrophoresis, respectively. The genomic DNA obtained from this step was amplified through the same PCR conditions before being analyzed for the presence of *groEL*, *motB* and *16s rRNA* genes, respectively.

## 2.4 Preparation of the pyrrolidinyl PNA-immobilized paper sensor

Carboxymethylcellulose (CMC) was immobilized onto the cellulose paper following the method of Orelma and coworkers with slight modification.<sup>75</sup> Briefly, a sheet of Whatman cellulose chromatography paper with pencil-drawn grids of 0.5 cm  $\times$  0.5 cm was immersed in a 2 mg mL<sup>-1</sup> CMC solution containing 10 mM CaCl<sub>2</sub> (total volume = 20 mL) (**Scheme 2.1**). The resulting solution was shaken on an orbital

shaker (80 rpm) for 90 min. This was followed by successive washing with deionized water, 10 mM  $\text{CaCl}_2$  solution, and deionized water (5 min each), respectively. The CMC-coated paper was then immersed in a solution (total volume of 20 mL in MilliQ water) of EDC-HCl (0.1 M) and NHS (0.4 M).<sup>75</sup> The resulting solution was shaken on the orbital shaker for 20 min, followed by 10-min washing in deionized water. This modified paper was air-dried before proceeding to the next step. A solution of the PNA probe (10 pmol in 0.2  $\mu\text{L}$  of 0.05M sodium carbonate buffer, pH 10) was spotted on pre-defined areas on the paper sheet. Thereafter, the sheet was incubated by being laid on a plastic scaffold in a closed box filled with water at the bottom to maintain a high level of moisture for 16 h. The resultant paper sheet was washed by immersing in phosphate buffer (pH 7, 10 mM, 20 mL) for 10 min on an orbital shaker (80 rpm). This modified paper was air-dried and can be stored for at least 1 month under ambient conditions without any detectable loss of performance.



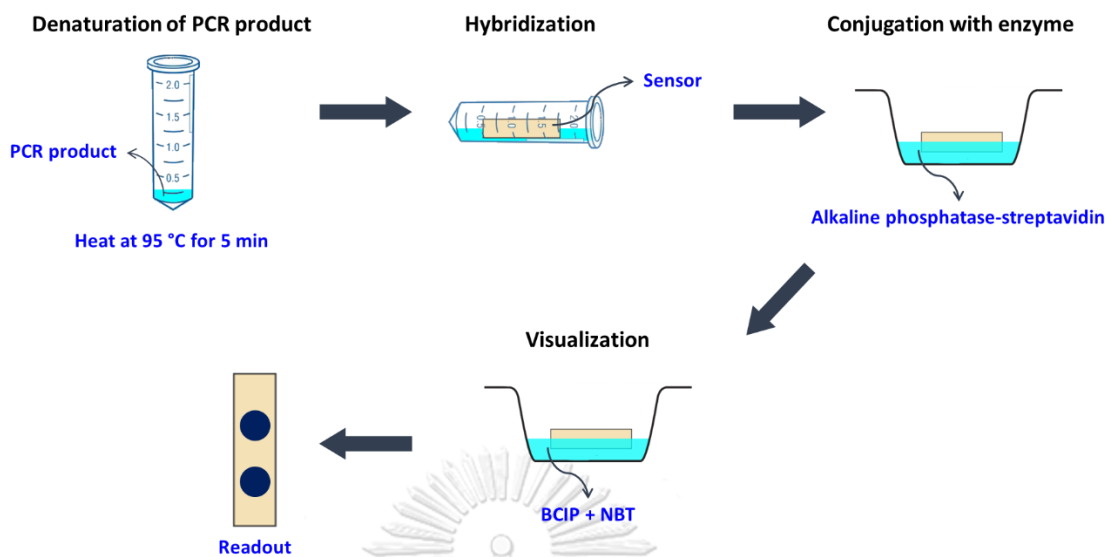
**Scheme 2.1** Preparation of pyrrolidinyl PNA-immobilized paper

## 2.5 DNA detection method

The PNA-immobilized paper was immersed in a 5-mL solution of 0.33 $\times$  SSC buffer containing 0.017% sodium dodecyl sulfate (SDS) for 5 min with shaking at 100 rpm.<sup>37</sup> In the meantime, the PCR product was denatured by adding 10  $\mu\text{L}$  of the PCR product into 100  $\mu\text{L}$  of pre-heated (95  $^{\circ}\text{C}$ , 5 min) solution of 0.33 $\times$  SSC buffer containing 0.017% SDS in another PCR tube (**Scheme 2.2**). The heating was continued for another 5 min, followed by a rapid quenching in an ice bath for 2 min.

Thereafter, the conditioned PNA-immobilized paper was transferred into the denatured DNA solution. The tube was then shaken at 100 rpm for 15 min at room temperature. The paper sheet was then transferred to another container having 2× SSC buffer containing 0.1% SDS (5 mL) and shaken for 10 min at 100 rpm.

One  $\mu\text{L}$  of alkaline phosphatase-streptavidin conjugate was mixed with 2 mL of 2× SSC buffer containing 0.1% SDS (**Scheme 2.2**). The modified paper from the previous step was immersed in this solution for 15 min with shaking at 100 rpm. The paper sheet was then transferred to another container containing 2× SSC buffer with 0.1% SDS (5 mL) and shaken at 100 rpm for 5 min. Next, the paper was immersed in Genius buffer (containing 100 mM Tris-Cl, pH 9.5, 5 mM  $\text{MgCl}_2$ , 100 mM NaCl; 1 mL) with shaking at 100 rpm for another 5 min.<sup>37</sup> Thereafter, the visualization agent containing p-nitroblue tetrazolium chloride (NBT,  $0.42 \text{ g L}^{-1}$ ) and 5-bromo-4-chloro-3-indolyl phosphate (BCIP,  $0.21 \text{ g L}^{-1}$ ) was mixed with the Genius buffer at the ratio of 1:1 with the total volume of 400  $\mu\text{L}$ . For visualization, the paper-bound DNA after the enzyme treatment was placed in this solution and shaken at 100 rpm for 30 min. This was followed by 5-min washing with water. The paper was air-dried and scanned to digitally record the data. It should be noted that the color stayed intact for months at ambient condition especially if kept in the dark.



**Scheme 2.2** DNA detection method by using pyrrolidinyI PNA-immobilized paper-based sensor and visualization of DNA target through enzymatic amplification assay

## 2.6 Image analysis by Scion Image software

Each image was processed by the Scion Image software (v.4.0.2) to extract the color intensity data for more quantitative analyses. Briefly, a straight line (profile plot line width at 25) from the selection tool was drawn across the all probe areas in the grayscale image of the paper-based sensor as shown in **Figure 2.3a**. The plot profile function was executed to give a profile plot as a peak which basically represents the spot intensities at different areas on the sensor as shown in **Figure 2.3b**. The peak areas were measured to give a set of numerical data for further processing as shown in **Figure 2.3c**.

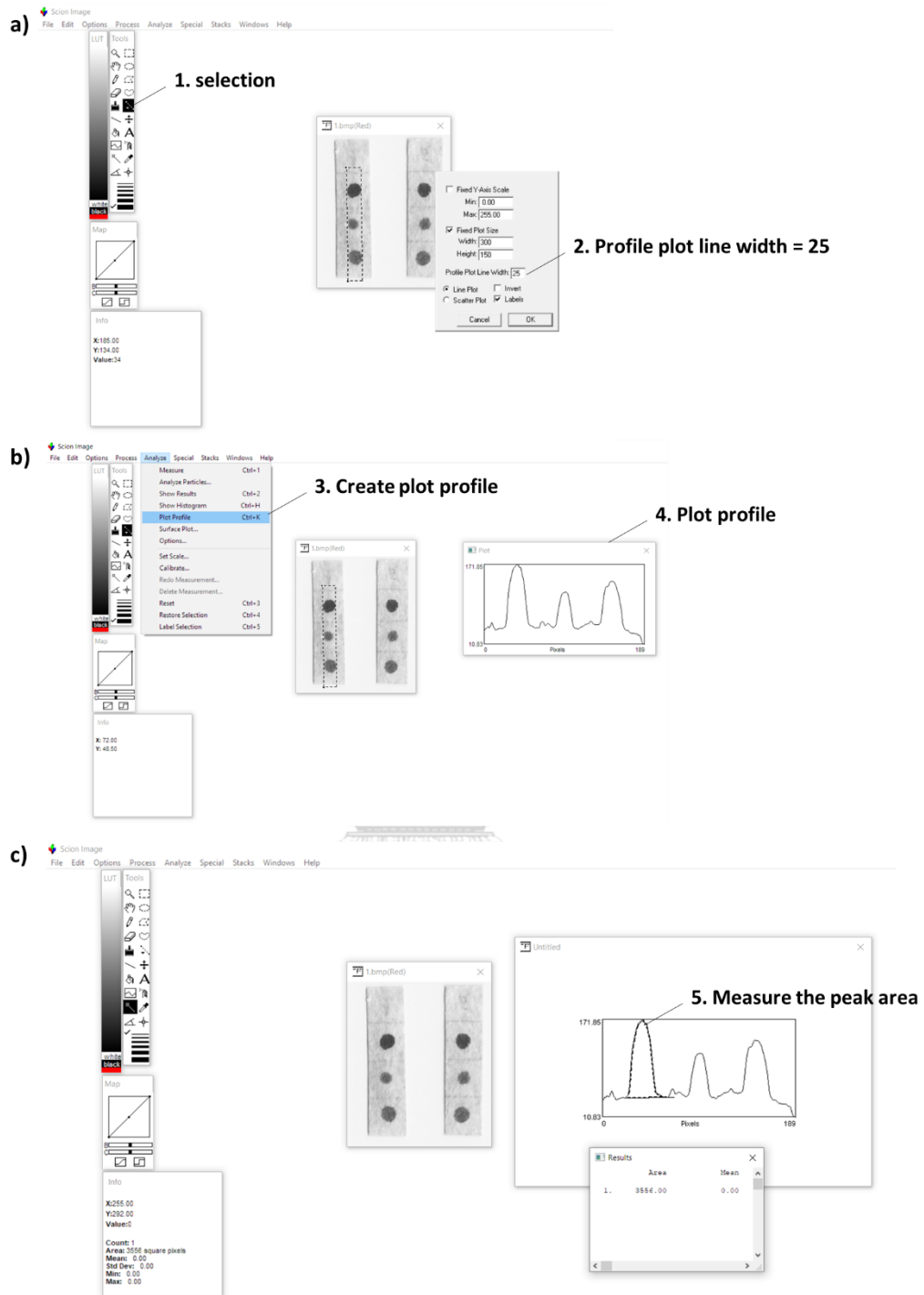


Figure 2.3 Image analysis by using Scion Image software consists of 3 steps: a) area selection, b) plot profile creation, and c) peak area measurement.

## CHAPTER III

### RESULTS AND DISCUSSION

#### 3.1 Synthesis and characterization of pyrrolidinyl PNA oligomers

The pyrrolidinyl PNA oligomers used in this work were designated as N, HbE, GroEL, 16s and MotB probes, in which N and HbE probes are *epi*-acpcPNA and GroEL, 16s and MotB probes are acpcPNA. The N and HbE probes were employed for thalassemia diagnosis, while the GroEL, 16s and MotB probes were used in the *B. cereus* detection. All PNA probes were synthesized by the solid phase synthesis method at 1.5  $\mu\text{mol}$  scale according to the previously developed protocol.<sup>73</sup> The pyrrolidinyl PNA probes were cleaved from the resin, purified by HPLC, and characterized by MALDI-TOF mass spectrometry. All pyrrolidinyl PNA provided the expected  $m/z$  values corresponding to the  $M+H^+$  signals and their purities were more than 90%, as confirmed by HPLC. The concentration was determined by UV spectrophotometry at 260 nm using molar extinction coefficient values calculated by an in-house web-based software (<http://www.chemistry.sc.chula.ac.th/pna/pna.asp>). The characterization data of all pyrrolidinyl PNA probes are summarized in **Table 3.1**.

**Table 3.1** Characterization data of PNA probes

Name	Type	PNA sequence	$t_R$ (minute)	Yield (%)	m/z (observed)	m/z (calculated)
N	<i>epi-acpcPNA</i>	Ac-Lys-GCCTC ACCACCA-NH <sub>2</sub>	28.3	10	4122.8	4123.4
HbE	<i>epi-acpcPNA</i>	Ac-Lys-GCCTT ACCACCA-NH <sub>2</sub>	28.1	13	4137.3	4138.4
GroEL	<i>acpcPNA</i>	Ac-GTAGGAA GCACAG-LysNH <sub>2</sub>	29.5	4	4649.3	4648.9
16s	<i>acpcPNA</i>	Ac-AACGAGC GCAAC-LysNH <sub>2</sub>	31.0	25	4235.2	4236.6
MotB	<i>acpcPNA</i>	Ac-CGAACGT TAAGCC-LysNH <sub>2</sub>	28.8	20	4558.1	4559.9

### 3.2 Sensor fabrication and DNA detection process

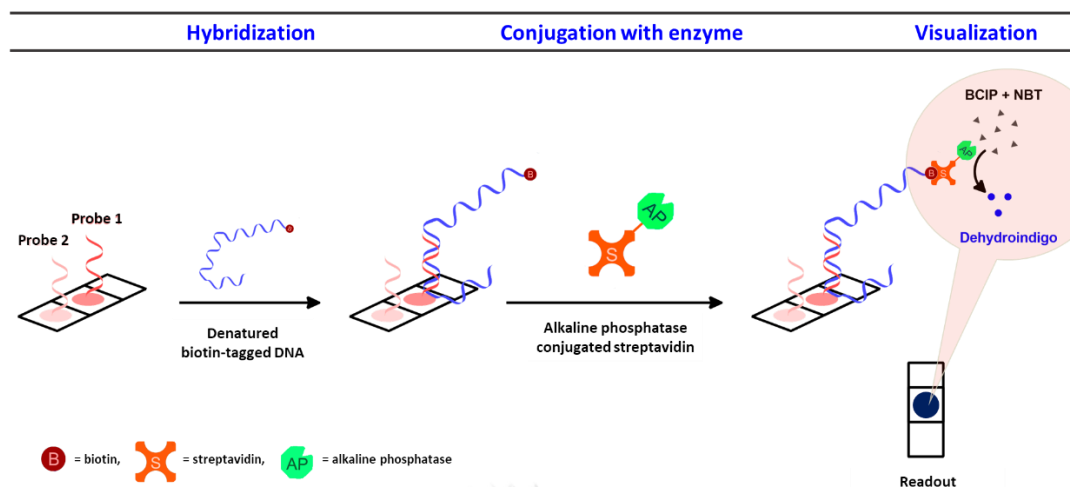
The paper-based sensing system was fabricated by employing a set of chemical modifications on cellulose paper. First, the cellulose surface of Whatman No. 1 filter paper was treated with CMC in the presence of Ca<sup>2+</sup> ion to generate the CMC-adsorbed cellulose membrane. This CMC adhesion chemistry was first reported by Orelma and coworkers, who proved that the presence of Ca<sup>2+</sup> as a background electrolyte is crucial to promote the adsorption of CMC onto the cellulose surface.<sup>75</sup> In that work, they utilized the EDC/NHS coupling chemistry for the antibody conjugation on the CMC-modified cellulose surface for quartz crystal microbalance experiments. A similar method was also successfully applied for the immobilization of DNA by Kargl and coworkers,<sup>76</sup> and for the fabrication of a paper based analytical device (PAD) for protein detection by Yang et al.<sup>77</sup> Hence, we surmised that this mild chemistry should also be directly amenable to the conjugation of PNA probes to the cellulose surface required for our purpose. In fact, its success may also lead to broader applications requiring the immobilization of PNA on paper, as the divinyl sulfone chemistry used in our previous work was proven to provide inconsistent

background signal in the current setting.<sup>40</sup> Thus, we decided to test this new chemistry for the PNA immobilization. It was found that the presence of both CMC and  $\text{Ca}^{2+}$  was crucial for selective immobilization (**Figure A5**). After the CMC coating, the carboxyl group of the CMC presented on the cellulose surface was activated via carbodiimide-NHS, resulting in an *N*-hydroxysuccinimidyl ester surface. The lysine-modified PNA probe was then allowed to react with this activated surface at pH 10 to shift the equilibrium of the lysine amino/ammonium group on the PNA probe to the unprotonated form. This condition led to a successful covalent attachment the PNA probe onto the cellulose paper via an amide bond. The pyrrolidinyl PNA-immobilized paper was then kept in a dry cabinet at room temperature before the DNA detection experiments.

Thereafter, the fabricated PNA-immobilized paper-based sensor was employed for the sensing of the DNA target (**Scheme 3.1**). We exploited a twofold signal enhancement mechanism whereby PCR was first used to amplify the DNA target, and an enzyme-catalyzed pigmentation was utilized for the visualization of the DNA binding event with concomitant signal amplification.<sup>37</sup> The process began with extracting the DNA samples. PCR was then performed on the extracted DNA samples employing biotin-tagged DNA primers, which would yield biotinylated PCR amplicons necessary for the enzyme-based colorimetric detection. The biotinylated PCR amplicons were next denatured and allowed to hybridize with the immobilized PNA probes on the paper-based sensor. Subsequently, the surface-bound biotinylated DNA sample was treated with streptavidin-alkaline phosphatase conjugate to immobilize the enzyme on the sensor surface via the very strong and highly specific biotin-streptavidin interaction. Finally, a pair of signaling substrates including NBT and BCIP was added to produce the highly intense blue-colored pigments under the catalysis of the immobilized alkaline phosphatase enzyme. This color was found to be stable for prolonged storage (at least 10 months). In addition, it can be clearly seen in all images of the paper-based sensor reported herein that



the background signal was generally low despite having multiple components involved in each spot. It should be noted that the background signal on the CMC-coated paper was much lower than the previously reported DVS chemistry<sup>40</sup> as well as unmodified paper (see **Figure A5**). Thus, the CMC modification not only provided the carboxyl handle necessary for the subsequent PNA immobilization but also contribute to the reduced background signal. The lowering of the nonspecific signal can be explained by the repulsion between the negatively charged carboxylate groups of CMC and other components including DNA (negatively charged with no Watson-Crick hydrogen bonding formed in the background area), streptavidin-alkaline phosphatase (both proteins have acidic pI values in the range of 4–5), as well as the enzyme substrate (BCIP, also negatively charged). Although the carboxyl groups were converted to the NHS esters followed by subsequent PNA immobilization, it was conceivable that only parts of the NHS ester were reacted with the PNA probe, and the remaining would be hydrolyzed back to the carboxyl groups under the aqueous basic conditions employed for the immobilization of the PNA probe. Importantly, after some optimizations, all of these steps can be conducted at ambient temperature (25–30 °C), hence no precise temperature control is required as in conventional dot blot analysis<sup>15, 37, 78</sup> and thus reducing the complexity of the assay (see below).

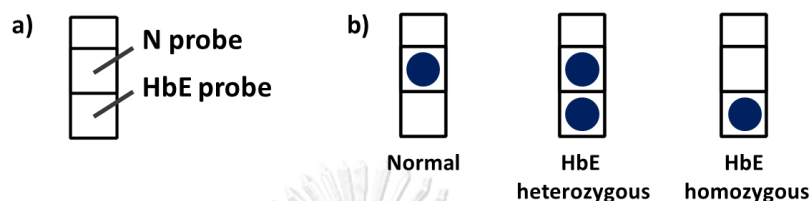


**Scheme 3.1** A schematic representation of the working principle of the paper-based DNA sensor. The PCR-amplified biotinylated DNA sample was denatured and captured by the paper-immobilized PNA probe, followed by the immobilization of enzyme and signal generation. The color pigments remain adsorbed on the paper, and the scanned images of these paper-based sensors were converted to numerical data by imaging software for further analysis

### 3.3 Optimization of the DNA detection method

In order to maximize the performance of the paper-based sensor, the optimization of various factors such as additional probe spacer (**Figure A2**), type of the pyrrolidinyl PNA probe (**Figure A3**), temperature and salt concentration is of high importance. The full optimization was conducted on the paper-based sensor designed for the detection of HbE mutation, a common mutation of thalassemia. The DNA sequence of the HbE genotype has only one base position that is different from the normal genotype. In human population, there are three possible scenarios including normal, HbE heterozygous (het HbE) and HbE homozygous genotypes. The paper-based sensor for HbE was prepared by immobilizing two PNA probes (normal and HbE) on the same piece of paper, which upon treatment with the DNA sample followed by enzymatic color development should provide three possible patterns as shown in **Figure 3.1b**. We expected that the high specificity of our pyrrolidinyl PNA-

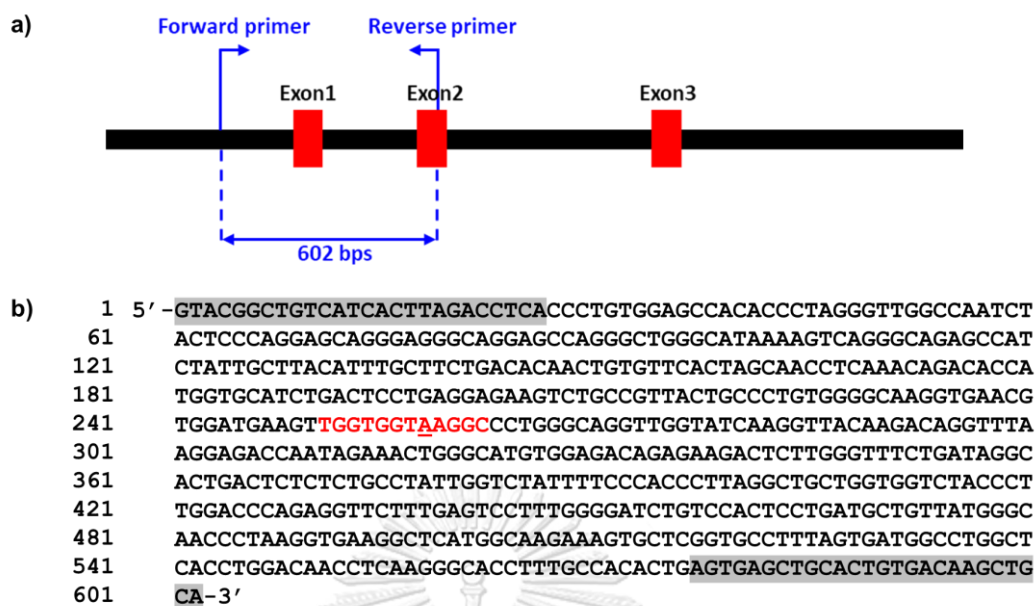
based sensor should allow us to distinguish between complementary and single-base mismatched sequences under the optimal condition without the requirement of elevated and precisely controlled incubation temperature as in conventional dot blot hybridization employing normal DNA probes.<sup>37</sup>



**Figure 3.1** a) Layout of PNA-immobilized paper for the detection of HbE mutation and b) three expected patterns of the results from DNA detection of normal, HbE heterozygous and HbE homozygous genotypes. N probe = normal probe

### 3.3.1 Design of the sequences of PNA probes and DNA primers for HbE detection

In this study, the primers were designed to obtain a 602 bps PCR amplicon that cover various types of  $\beta$ -thalassemia including the HbE mutation (Figure 3.2a and 3.2b).<sup>37</sup> While the DNA sequence was longer than actually necessary for the detection of HbE mutation, the long PCR amplicon was chosen as it can be used for the detection of multiple mutations in the future. For the design of the PNA probe sequence, the position of the mutated base was placed at the middle of sequence to maximize the discrimination ability (Figure 3.2b).

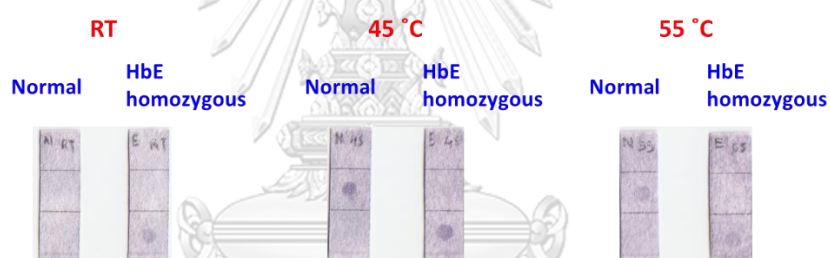


**Figure 3.2** a) Position of PCR product on  $\beta$ -globin gene. b) Sequence of PCR amplicon from  $\beta$ -globin gene (grey highlight: primer sequences, red alphabets: detection region and a red alphabet with underline: a position of mutated base).

### 3.3.2 Effect of temperature

We started by analyzing the underlying reason behind the need of increased binding temperature in the previously reported RDB method.<sup>37</sup> At room temperature, the RDB assay suffered from severe nonspecific binding whereby the normal DNA sample displayed intense signals for both normal (N) and HbE probes (and vice versa). This is due to the fact that the single-mismatched DNA-DNA hybrid ( $T_m = 38.02$  °C, calculated from <https://arep.med.harvard.edu/cgi-bin/adnan/tm.pl>), differing by only one base from the complementary hybrid ( $T_m = 50.18$  °C), is still fairly stable at room temperature, thus resulting in similar binding and signaling behavior to the complementary hybrid. Raising the temperature helped improve the selectivity by selectively destroying the less stable mismatched duplex. In the current study whereby PNA probes were used in place of DNA probes, the results were remarkably different (**Figure 3.3**,  $T_m = 64.5$ – $64.8$  °C and  $81.2$ – $81.6$  °C in the cases of single-based mismatch and complementary PNA-DNA duplexes,

respectively). Although 45 °C was still better than ambient temperature (25–30 °C), the behavior differed from the DNA case in that the ambient condition gave weak signals but without nonspecific binding. The absence of nonspecific binding in this case was consistent with the expectation based on the much higher discriminatory power of the pyrrolidinyl PNA probe in distinguishing single mismatched DNA targets.<sup>35</sup> Nevertheless, the low signal intensity was presumably caused by the formation of stable secondary structures of the DNA target that may interfere with the PNA probe binding, which was destroyed once the temperature was raised. Based on this hypothesis, we surmised that this problem could be solved if salt concentration of buffer in hybridization environment was lowered to destabilize the secondary structure of the DNA without affecting the stability of the PNA-DNA hybrids.



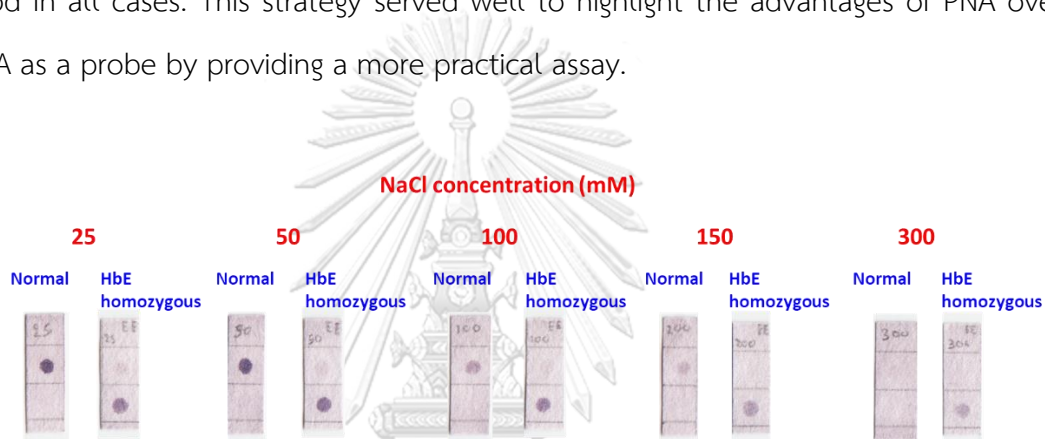
**Figure 3.3** The effect of temperature to the performance of the paper-based DNA sensor.

จุฬาลงกรณ์มหาวิทยาลัย  
CHULALONGKORN UNIVERSITY

### 3.3.3 Effect of salt concentration

Since cationic species such as  $\text{Na}^+$  and  $\text{Mg}^{2+}$  reduce the electrostatic repulsion of the phosphate groups and can bridge the phosphate groups together, secondary structures of DNA and RNA are stabilized by these cations. While the presence of salt is necessary in the case of DNA probes to facilitate the hybrid formation, the duplex formation between PNA and DNA is much less sensitive to electrostatic effects since PNA does not carry any charges.<sup>79-81</sup> Hence, it was proposed that lowering the salt concentrations may lower the stability of secondary structures in the DNA samples without interfering with the formation of PNA-DNA

duplex. Indeed, this approach was found to be the key for obtaining high signal intensities in the PNA-based assay with good discrimination between the normal and HbE genotypes at ambient temperature (**Figure 3.4**). Following the optimization, the lowest salt concentration at 25 mM of Na<sup>+</sup> ion (as 1/6 of 1× SSC buffer) was eventually selected as the optimal salt concentration that permit ambient temperature detection with reasonable signal intensity. At higher salt concentrations, the signals became progressively weaker, but the mismatch discrimination was still good in all cases. This strategy served well to highlight the advantages of PNA over DNA as a probe by providing a more practical assay.



**Figure 3.4** The effect of salt concentration to the performance of paper-based DNA sensor

### 3.4 The performance of pyrrolidinyl PNA-immobilized sensor in thalassemia diagnosis

#### 3.4.1 Specificity

The correct identification of genotype is the key to indicate the performance of thalassemia diagnostic methods. Although there are several types of thalassemia mutation, this work specifically focused on HbE which is the most common mutation in Thai population.<sup>82</sup> The high specificity of the paper-based sensor with immobilized pyrrolidinyl PNA probes has already been demonstrated in the previous experiments (**Section 3.3.3**). However, the experiments were performed with the normal and HbE homozygous genotypes only, thus the discrimination

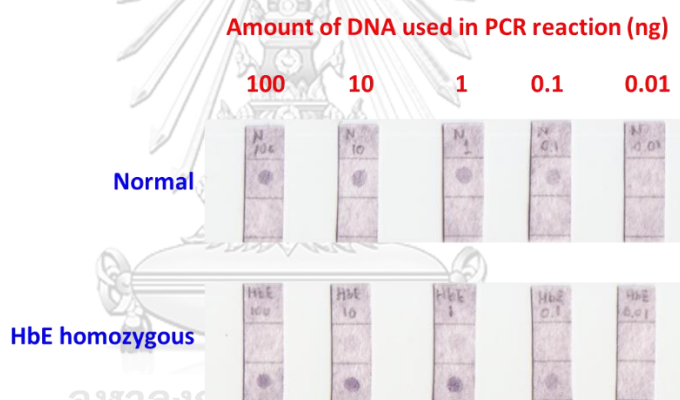
among normal, HbE homozygous and HbE heterozygous genotypes has not yet been proven. The sensor was next tested with samples with three different genotypes including normal, HbE homozygous and HbE heterozygous under the optimal conditions obtained from the previous experiments. As expected, the normal and HbE homozygous genotypes DNAs gave only one signal for each sample at the expected positions on the sensor, i.e., at the N and HbE channels, respectively (**Figure 3.5**). On the other hand, two signals with equal but lower intensities were observed in the case of HbE heterozygous genotype. This is because the sample of the HbE heterozygous genotype has only one copy of each of the normal and HbE genes. Accordingly, the concentration of each DNA was lower than the homozygous cases by a half, assuming equal PCR amplification efficiencies for both genotypes. In summary, the identification of three genotypes in HbE mutation was achieved by the developed pyrrolidinyI PNA-based sensor, in which the presence of signal at the N channel (top) indicated the presence of normal hemoglobin DNA, and the signal at the HbE channel indicated the presence of HbE DNA. The homozygous genotypes were characterized by the presence of only one signal, and two signals of equal intensities indicated HbE heterozygous cases.



**Figure 3.5** The results from the DNA detection of each genotypes including normal, HbE heterozygous and HbE homozygous genotypes providing different spot patterns

### 3.4.2 Limit of detection

Next, the limit of detection was determined to identify the lowest amounts of DNA that can be detected by the sensor. Although this metric is not of high importance for this particular sensing purpose, this knowledge can show the limitation of the sensor and can increase the confidence for real usages. In **Figure 3.6**, it can be seen that this paper-based sensing device can detect both normal and HbE genotypes down to the level of around 0.1 ng (~ 29 copies) of total DNA extracted. This was well below a typical range of the amount of DNA (5 to 100 ng or ~ 1,450 to 29,000 copies of DNA) that can be obtained from a single extraction from 300  $\mu$ L of typical blood samples from patients - thanks to the double signal enhancements used in this sensor.



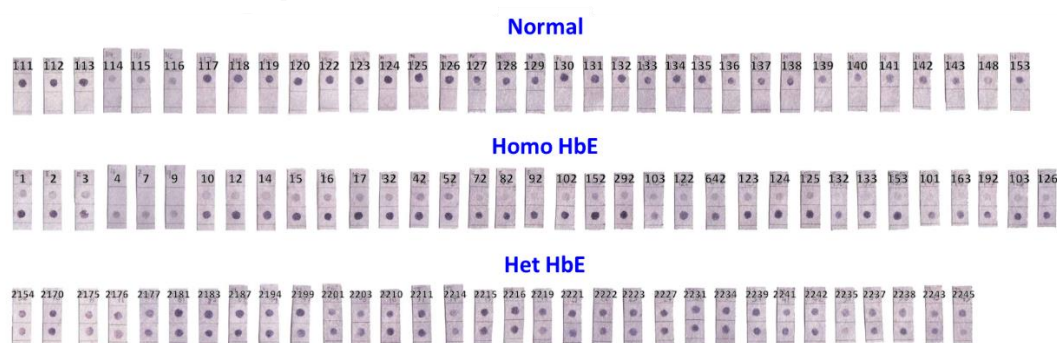
**Figure 3.6** Limit of detection of the paper-based DNA sensor for HbE detection (top row – normal genotype; bottom row – HbE homozygous genotype). The amount of DNA presented the amounts of the template used for subsequent amplifications.

### 3.4.3 The validation of the method with real samples

After the optimization was completed, we proceeded to assess the performance of the sensor in a larger pool of real samples. In this section, the biosafety was approved by Faculty of Science Institute Biosafety Committee (biosafety approval number: SC CU-IBC-005/2018, ethical approval number: COA No. 138/2018). The DNA was extracted from leukocytes of each subject, whose age and

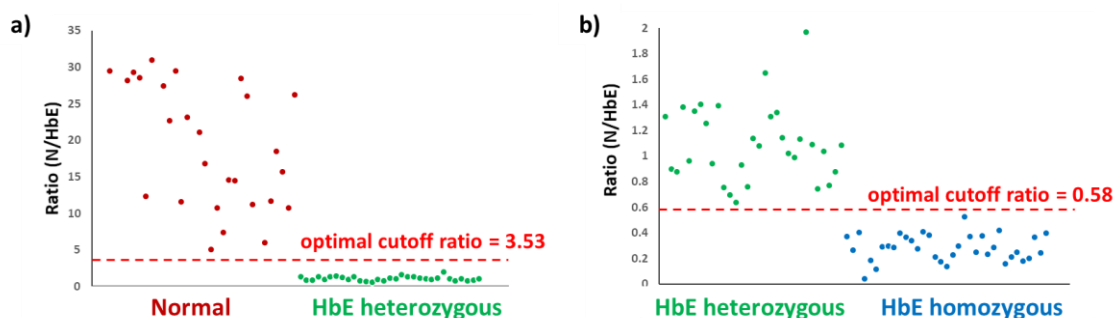


gender varies (**Table A1**). Thereafter, the genotype of each DNA sample was identified to be either normal, HbE homozygous, or HbE heterozygous genotypes by a combination of conventional methods including CBC, hemoglobin typing, and RDB hybridization (this part of the work was performed by Thongperm Munkongdee at the Thalassemia Research Center, Institute of Molecular Biosciences, Mahidol University). Since the combined results of CBC and hemoglobin typing are considered sufficient for confident identification of HbE genotype,<sup>83</sup> the use of the three methods together thus led to a set of reliable data that can be treated as authentic results. Indeed, all three methods gave unanimous genotype identification for all samples (**Table A1**).<sup>84</sup><sup>85</sup> Hence, we proceeded to use our sensor to evaluate all samples, which can be divided into 34 normal genotypes, 35 HbE homozygotes, and 31 HbE heterozygotes. According to **Figure 3.7**, it can be seen that most samples exhibited clear visual signals, thus allowing one to assign each case to a specific genotype with confidence (normal, top spot only; HbE homozygote, bottom spot only; HbE heterozygote, both spots are present). To allow for more systematic and objective evaluation of the assay, however, the software Scion Image was used to convert all images to numerical data (details in the experimental section). These were then used to assist the decision making as discussed below.



**Figure 3.7** A scanned image of 100 paper-based sensor that were tested against 100 real samples.

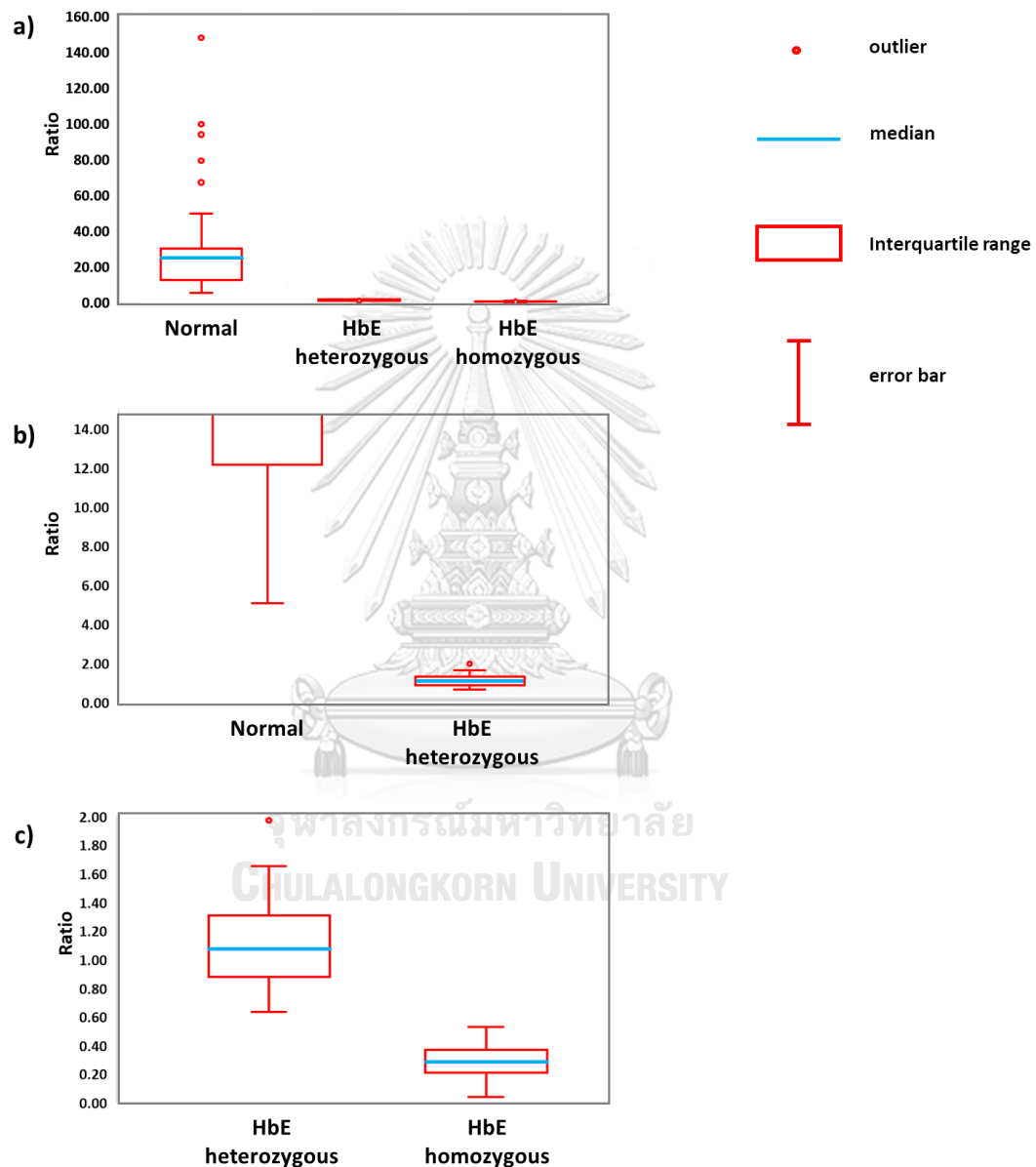
It is important to note that despite having the same amounts of immobilized PNA probes and DNA samples (generally present in large excess over the immobilized probe), the digitized signals from the N and HbE channels are not exactly of equal intensity. To compensate for the variation of signal intensities between different genotypes, a ratio value was used where the signal intensity of the N probe was divided by that of the HbE probe (N/HbE). In general sense, the higher ratio signifies that there is more binding extent in the normal probe on paper than in the HbE probe — this, in turn, implies that the DNA sequence should be the normal (N) gene (and vice versa). Weak signals observed in the HbE channel could result from non-specific binding between the probe and the single mismatched DNA target. In principle, the HbE heterozygous cases would show equal intensity in the N and HbE channels, i.e. the intensity ratio of  $N/HbE = 1$ . In practice, the value is hardly exactly unity, and there will be a range of ratios in between the two homozygous genotypes. In order to find a suitable set of cutoff ratios for distinguishing between normal, HbE homozygous, and HbE heterozygous genotypes, we first calculated the ratios of all samples (all numerical data can be found in the associated spreadsheet in **Tables 3.4** and **3.5**). As depicted in **Figure 3.8**, our sensor can produce well distinguished N/HbE signal ratios for all three possible cases, thus allowing one to confidently identify the genotype of each sample.



**Figure 3.8** Plots of intensity ratios with suggested optimized ratios as obtained from the generation of ROC curves between a) normal vs HbE heterozygous genotypes and b) HbE heterozygous vs HbE homozygous genotypes. It should be noted that normal samples with intensity ratios above 35 were not shown for the sake of clarity at the cutoff area.

To probe the effects of outliers on the determination of optimal ratios, a set of box plots is also highlighted in **Figure 3.9**. In this presentation, the interquartile range (IQR), defined as the difference between the 25- and 75-percentile marks, is used to identify outliers. The outliers are those data that have values outside  $1.5 \times$  interquartile range (IQR). Clearly, this kind of presentation shows that large deviations were found only at the higher end of the values from the normal case. This, in a practical sense, merely means that these values were either from very high color intensity in the N probe or with very low background signal from the HbE probe. That is, these outliers would pose no difficulty in interpreting as a normal case and should even give more confidence in interpreting as such. Interestingly, there is only one more outlier in the HbE heterozygous genotype, but this data point is significantly below the error bar of the normal case (**Figure 3.9b**), which implies the non-outlier minimum value. In addition, two types of statistical tests, namely, two-sample *t*-tests and two-sample F-tests, were also performed to give further information about the difference of the data of each genotype group from one another. The results in **Tables 3.2** and **3.3** clearly indicate that each group indeed differs statistically from

all others, thus giving further confidence in our methodology of data interpretation. In brief, these analyses suggest that a set of optimal ratios can be found where unambiguous identifications are minimal and, if present, can be readily recognized as such so that repeat experiments can be performed when necessary.



**Figure 3.9** Box plots showing median, IQR, and outliers of ratios from each genotype data set with a) the total view of all data, b) the borderline between normal and HbE heterozygous genotypes, and c) the borderline between HbE heterozygous and HbE homozygous genotypes.

**Table 3.2** Two sample *t*-tests between each pair of genotypes.

	Population 1	Population 2	df	<i>t</i> Stat	<i>t</i> Critical two-tail	<i>p</i> -value
<i>t</i> -Test	Normal	HbE heterozygous	63	5.59	2.65	< 0.01
	HbE heterozygous	HbE homozygous	64	15.14	2.65	< 0.01
	Normal	HbE homozygous	67	6.10	2.65	< 0.01

**Table 3.3** Two sample F-tests between each pair of genotypes.

	Population 1	Population 2	df1	df2	F	F Critical one-tail	<i>p</i> -value
F-Test	Normal	HbE heterozygous	33	30	10976	1.82	< 0.01
	HbE heterozygous	HbE homozygous	30	34	8.18	1.79	< 0.01
	Normal	HbE homozygous	33	34	89791.00	1.77	< 0.01

Also, to provide a systematic way in determining an optimal set of threshold ratios for future genotype classification, the binary-valued diagnostic test involving true positive (TP), false positive (FP), false negative (FN), true negative (TN), the sensitivity, and specificity were calculated with various cutoff ratios as exemplified in **Table 3.4** (normal vs HbE heterozygous genotypes) and **Table 3.5** (HbE homozygous vs HbE heterozygous genotypes).<sup>86</sup> Although the sensitivity and the specificity have an inverse relationship when the cutoff threshold was changed, there is an optimal set of cutoff ratios at 3.53 and 0.58 for **Table 3.4** and **3.5**, respectively, that gave 100% sensitivity and specificity. In addition, we also generated ROC curves from a larger set of cutoff ratios (**Figure 3.10**).<sup>86</sup> ROC curve is a graph showing the performance of a classification model by plotting between sensitivity and 1-specificity from all cutoff ratio. The area under the curve (AUC) was calculated to

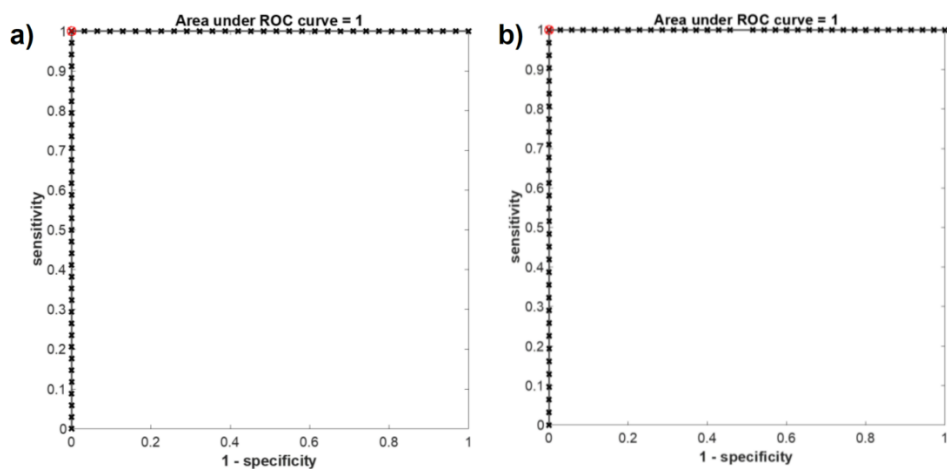
measure the performance. The results confirmed that the two ROC curves represent the perfect classification by achieving the AUC of 1.0. All aforementioned results ensure that the sensing system illustrated herein has a high margin of accuracy and thus has a great potential for real applications.

**Table 3.4** Effect of the cutoff ratios to the performance of the sensor in distinguishing between normal (34 samples) and HbE heterozygous genotypes (31 samples)

Cutoff ratio	Normal genotype (TP)	HbE heterozygote			Sensitivity	Specificity
		FN	FP	TN		
1.40	34/34	3	0	28/31	1	0.90
1.53	34/34	2	0	29/31	1	0.94
1.81	34/34	1	0	30/31	1	0.97
3.53	34/34	0	0	31/31	1	1
5.54	33/34	0	1	31/31	0.97	1
6.68	32/34	0	2	31/31	0.94	1
10.79	30/34	0	3	31/31	0.88	1

**Table 3.5** Effect of the cutoff ratios to the performance of the sensor in distinguishing between HbE homozygous (35 samples) and heterozygous genotypes (31 samples)

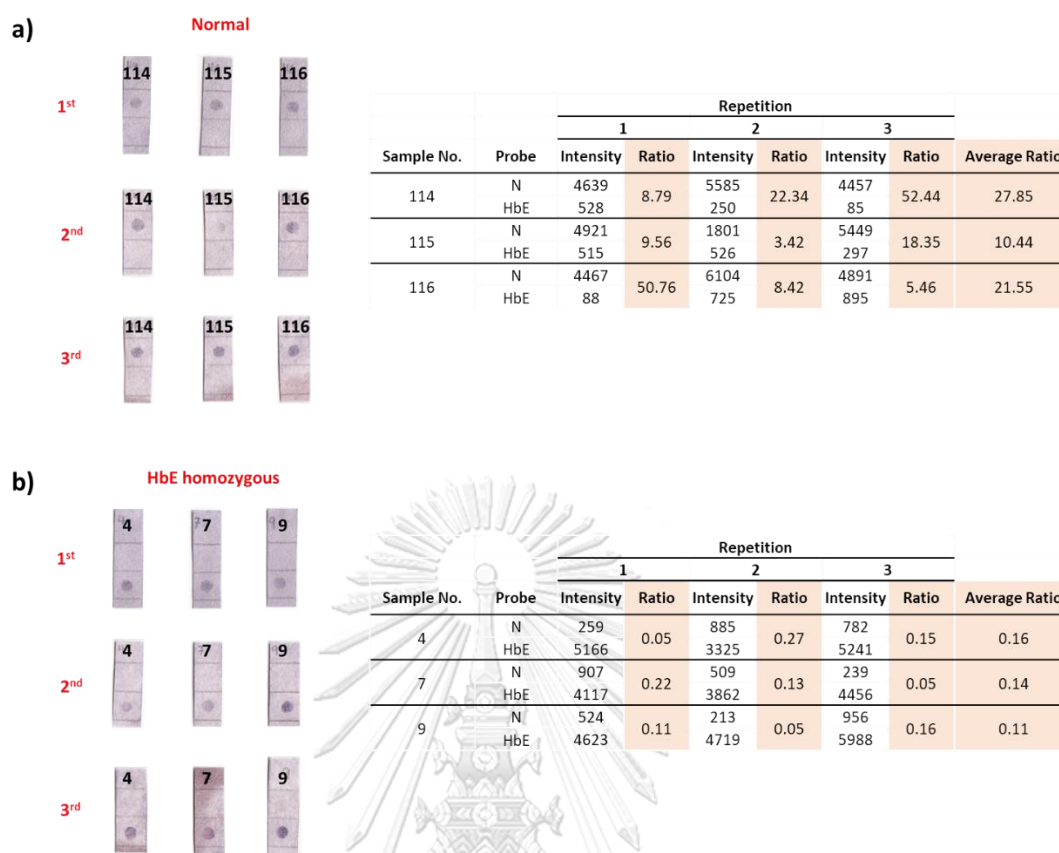
Cutoff ratio	HbE homozygote (TP)	HbE heterozygote			Sensitivity	Specificity
		FN	FP	TN		
0.38	28/35	0	7	31/31	0.80	1
0.41	32/35	0	3	31/31	0.91	1
0.47	34/35	0	1	31/31	0.97	1
0.58	35/35	0	0	31/31	1	1
0.67	35/35	1	0	30/31	1	0.97
0.75	35/35	3	0	28/31	1	0.90
0.82	35/35	6	0	25/31	1	0.81



**Figure 3.10** ROC curves of the discrimination between a) normal vs HbE heterozygous genotypes, and b) HbE heterozygous vs HbE homozygous genotypes

#### 3.4.4 Repeatability

Additionally, although the good outcome from the 100-sample test as discussed above should already be an indirect evidence of good reproducibility, a formal evaluation on reproducibility was also conducted. This was done by testing selected samples carrying each genotype multiple times to assess the consistency of signal intensities. The results, as shown in **Figure 3.11**, indicated that the signals were generally consistent (as evaluated visually and by numerical data). In rare cases where there may be unexpectedly low signal intensities (likely due to the sensor preparation by incomplete immobilization of the PNA probe), repetitions, which are totally practical with our sensing system, can effectively compensate with this. Given the very clear-cut nature of the resulting optimal ratio, this flawed piece of sensor would eventually cause no effect in the genotype identification.



**Figure 3.11** Reproducibility test on two genotypes (a – normal; b – HbE homozygous). Each genotype was evaluated by testing three samples for three repetitions.

### 3.4.5 Shelf life

The paper-based device was also evaluated for its shelf life. This was done by storing the PNA-immobilized paper for longer periods of time up to 3 months under different conditions. As shown in **Figure 3.12**, at ambient temperature the sensors performed well up to the age of 1 month without any significant deterioration of sensing performance. If kept in a desiccator, the sensor can be used up to 3 months with partial loss of overall signal intensities. It should be noted, however, that this partial loss of the maximum performance should still permit correct genotype identifications in all cases.



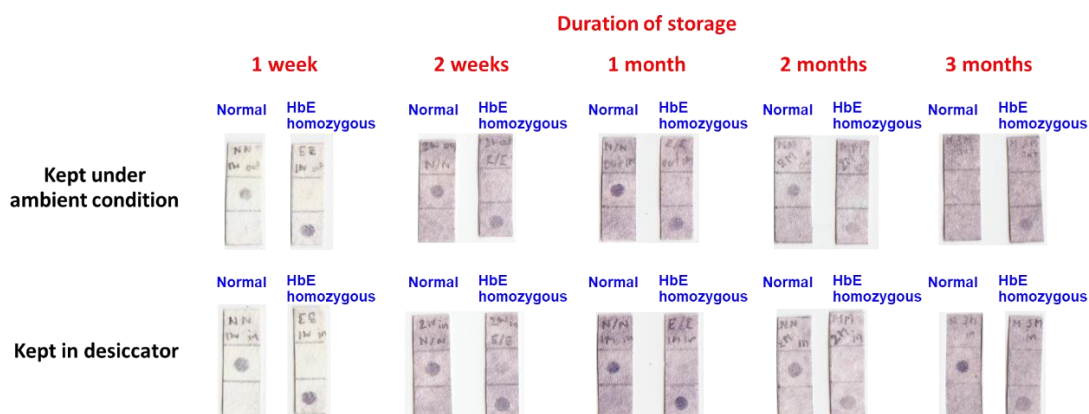


Figure 3.12 The effect of storage periods on the performance of the sensor

### 3.5 The performance of the PNA-immobilized sensor for pathogen detection

The excellent performance of the PNA-immobilized sensor for thalassemia diagnosis suggests a good opportunity to apply the same sensor for other applications by simply changing the PNA probe sequence. In this section, the sensor was fabricated and optimized for the detection of *Bacillus cereus* genes. The sensor was designed with internal controls that provide a self-check mechanism to assist the evaluation of the results with high confidence. The performance of the sensor was then evaluated by testing the ability to identify several strains of *B. cereus* among various other species and determining the detection limit. Lastly, its application in the detection of *B. cereus* in raw rice matrix was demonstrated.

#### 3.5.1 Genomic analysis of suitable gene candidates for species identification

The *B. cereus* group includes *Bacillus anthracis*, *B. cereus*, *Bacillus thuringiensis*, *Bacillus mycoides*, *Bacillus pseudomycoides*, and *Bacillus weihenstephanesis*.<sup>70</sup> Based on the genome sequences of *B. cereus* and related species deposited in public databases (<https://www.ncbi.nlm.nih.gov/gene> and <https://www.genome.jp/kegg>), we analyzed the presence of three categories of genes including the stress-responsive genes (focusing on heat shock genes), the cytochrome

P450 genes, and the genes encoding motility protein from 34 entire genomes. These are *B. anthracis* (11 strains), *B. cereus* (3 strains), *B. thuringiensis* (15 strains), *B. mycooides* (3 strains), *B. pseudomycooides* (1 strain), and *B. subtilis* (1 strain). Among the three categories of the target gene groups, multiple alignments revealed that the gene encoding the molecular chaperone GroEL (accession number, NCBI-GENE ID: NP\_830146) and the chemotaxis encoding gene MotB (accession number, NCBI-GENE ID: 1206857) are two possible candidates as gene markers that are unique for *B. cereus* among other members of the genus *Bacillus*. Primer pairs for each gene were then designed and optimized, resulting in the final primer sets shown in **Table 3.6**. The expected sequences of the amplicons deriving from the final primer sets were then used to design the PNA probes (**Table 3.1**) (see **Figure 3.13** for detailed alignment of the probe sequences within their respective amplicon).

**Table 3.6** Sequences of primers used in this study.

Gene	Sequence
Forward <i>groEL</i>	5'-CTGTAGTTGAAGGT -3'
Reverse <i>groEL</i>	5'-biotin-CACGAGTTGAGTT-3'
Forward <i>motB</i>	5'-GTGAATGTATATCGA-3'
Reverse <i>motB</i>	5'-biotin-CTGCATATCCTAC-3'
Forward <i>16s rRNA</i>	5'-GTCGTCAGCTCGTGT-3'
Reverse <i>16s rRNA</i>	5'-biotin-CGATTACTAGCGATTCC-3'

A) 1 5' - **GTG**TAGTTGAAGGT**GTAGGAAGCAG**AACAAATCGAAGCTCGCATCGGTCAAATCCGTG  
61 CGCAATTAGAAGAAACAACCTTCTGAATTCGATCGTGAAAAATTACAAGAGCGTCTTGCTA  
121 AACTAGCAGGTGGCGTACCAGTAATTAAGTAGGTGCAGCAACTGAAACTGAGTTAAAAG  
181 AGCGCAAACCTTCGATTGAAGATGCACTTAACTCAACTCGTG-3'

B) 1 5' - **GTGAATGTATATCGAGAGGATACAGGGTAAGCGTCGTTATAGTAGATAATTTAATATTT**  
61 GATACAGGCGATG**CGAACGTTAAGCC**CGAAGCGAAAGGGATAATAAGTCAATTAGTTGGA  
121 TTTTTTCAATCCGTACCTAACCCAATTGTTGTAGAGGGACATACAGATAGTAGACCTATT  
181 CATAACGAGAAATTCCTTCTAATTGGGAGTTATCTTCAGCACGAGCGGCAAATATGATT  
241 CACCATTTAATTGAAGTGATAATGTGGACGATAAAAGGCTAGCTGCGGTAGGATATGCA  
301 G-3'

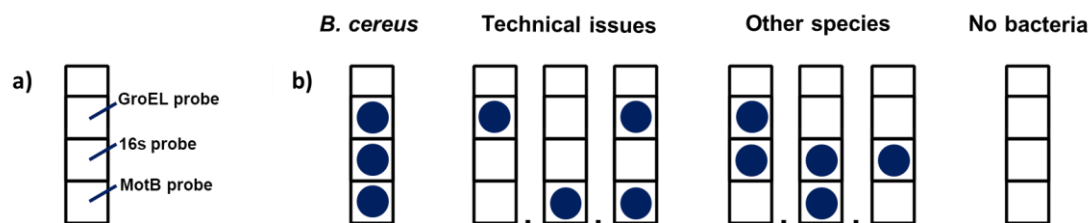
C) 1 5' - **GTCGTCAGCTCGTGTGTCGAGATGTTGGGTTAAGTCCCGCAACGAGCGCAAC**CCCTTGATC  
61 TTAGTTGCCATCATTAAAGTTGGGCACTCTAAGGTGACTGCCGGTGACAAACCGGAGGAAG  
121 GTGGGGATGACGTCAAATCATCATGCCCTTATGACCTGGGCTACACACGTGCTACAATG  
181 GACGGTACAAAGAGCTGCAAGACCGCGAGGTGGAGCTAATCTCATAAAACCGTTCTCAGT  
241 TCGGATTGTAGGCTGCAACTCGCTACATGAAGCTGGAATCGCTAGTAATCG-3'

**Figure 3.13** Putative sequences of the amplicons from the gene A) *groEL*, B) *motB* and C) *16s rRNA* (grey highlight: primer sequences and red alphabets: detection region).

### 3.5.2 Design of the sensor

In terms of the layout of the sensor, we decided to incorporate some mechanisms for validating the results into the sensor. Specifically, three PNA probes were immobilized including both genes that are specific for *B. cereus*, *i.e.*, *groEL* and *motB*, as indicated from the aforementioned genomic analysis, along with the *16s rRNA* gene as a control (**Figure 3.14a**). This allows us to cover all possible outcomes of any tests (**Figure 3.14b**). That is, positive signals for all three genes indicate the presence of *B. cereus*, while all negative signals indicate the absence of any bacterial species. The absence of *16s rRNA* signal also serves to identify any technical issues of the assay, *e.g.*, DNA isolation and/or amplification. Importantly, the inclusion of both indicative genes of *B. cereus* is to further prevent any artifacts that may occur when the sensor is used to analyze various types of samples with different bacterial species. Indeed, it was later found that such artifact did happen when analyzed with

other species (see below), but thanks to this failproof design, the analysis can be performed with minimal ambiguity.



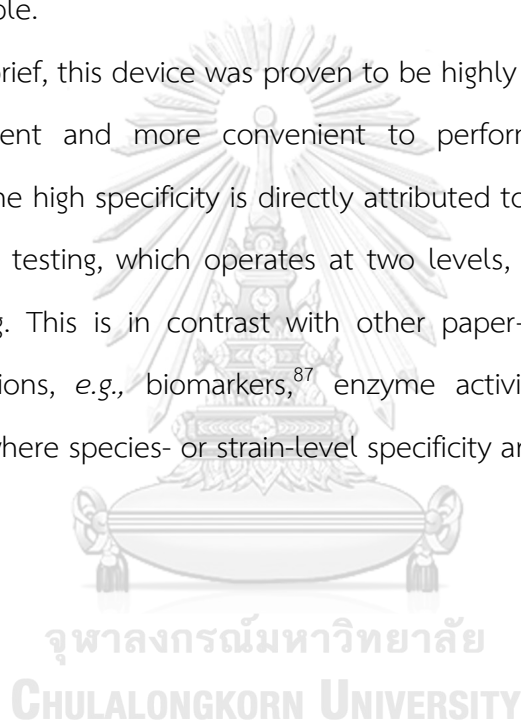
**Figure 3.14** a) Schematic layout of the paper-based sensor showing the locations and the sequences of the PNA probes used in this study, along with b) the list of all possible outcomes of the sensor.

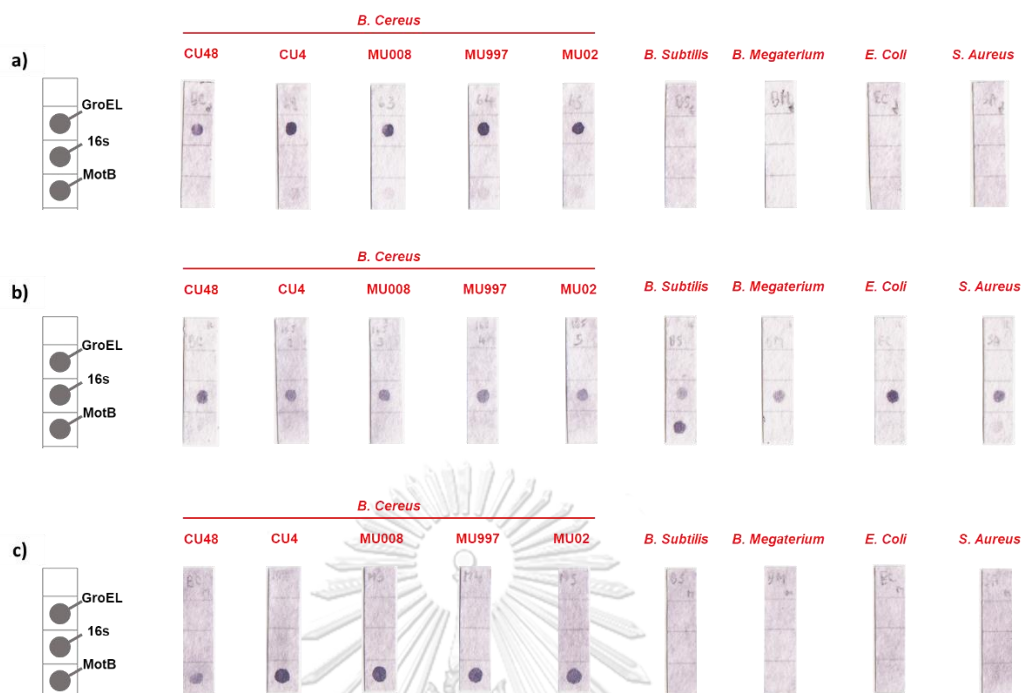
### 3.5.3 Specificity

After successful fabricating the paper-based sensor, we evaluated it in a series of experiments (biosafety approval number: SC CU-IBC-012/2018). First, the species specificity was assessed by comparing the color signals from a variety of *B. cereus* strains including ATCC 14579, CU48, CU4, MU008, MU997, and MU02, in comparison with four other bacterial species including *B. subtilis* ATCC 6633, *Bacillus megaterium* ATCC 14581, *Staphylococcus aureus* ATCC 6538P, and *Escherichia coli* ATCC 8739. In each case, three sets of the biotinylated primers corresponding to the three *B. cereus* genes (*groEL*, *motB*, *16s*) were used for PCR amplifying the genomic DNA extracted from each species. The resulting PCR-amplified DNA samples were then incubated with the paper-based sensor carrying the immobilized PNA probes corresponding to all three *B. cereus* genes. The results in **Figure 3.15** indicated that the sensor exhibited great species specificity as only the DNA samples from all *B. cereus* strains gave clear signals at all three positions in the sensor indicating the presence of all three *B. cereus* genes. The results were also in line with gel electrophoresis (**Figure A6**) where clear bands of anticipated sizes were observed in the case of *B. cereus*. On the other hand, all bacterial species including the *B. cereus* strains exhibited clear spots at the 16s probe position, thus confirming the validity of

the control probe per the design discussed above. Interestingly, the PCR amplicon obtained from the genomic DNA from *B. subtilis* employing the *16s rRNA* primers also gave an intense signal at the MotB probe position in addition to the expected signal at the 16s probe position (**Figure 3.15**). A close inspection of the sequences of the probe and the amplicon revealed that they indeed share some similarity (**Figure A7**). Nevertheless, the requirement of having both positive signals in the GroEL and MotB channels confidently rejects this outcome as a positive result, *i.e.*, the existence of *B. cereus* in the sample.

In brief, this device was proven to be highly specific to *B. cereus*, while being more efficient and more convenient to perform than conventional gel electrophoresis. The high specificity is directly attributed to the specific nature of the nucleic-acid-based testing, which operates at two levels, the PCR amplification and the probe binding. This is in contrast with other paper-based sensors with other modes of detections, *e.g.*, biomarkers,<sup>87</sup> enzyme activities,<sup>88</sup> or the amount of amplified DNA,<sup>89</sup> where species- or strain-level specificity are difficult to achieve.



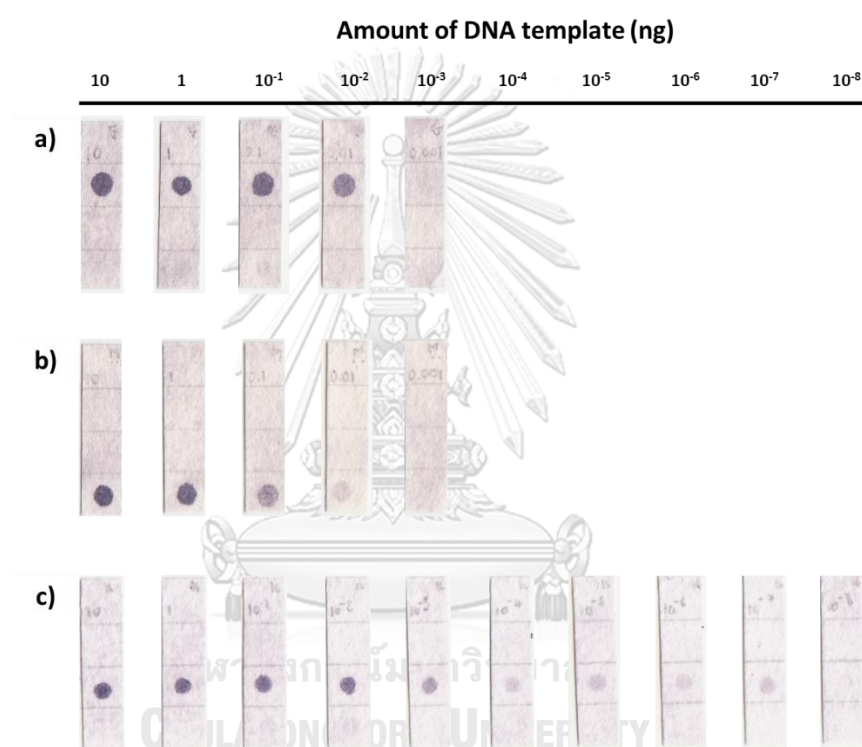


**Figure 3.15** Species specificity of the sensor carrying three immobilized PNA probes, namely GroEL, 16s, and MotB with DNA samples from amplification with a) *groEL* primers, b) *motB* primers and c) *16s rRNA* primers.

### 3.5.4 Limit of detection

Next, the limit of detection of this sensor was evaluated. According to the strong binding affinity of pyrrolidinyl PNA towards its complementary DNA target, the sensor was found to exert decent sensitivity to all genes tested in this study (**Figure 3.16**). Notably, these results are in line with their associated gel electrophoresis results (**Figure A8**), where the detection of *groEL* was slightly more sensitive than *motB* genes probably due to the more efficient PCR amplification. In both cases, the lowest detectable signal was approximately at 0.01 ng of the starting DNA template. Interestingly, the *16s rRNA* gene showed exceptionally low limit of detection. Even though the signal on the paper-based sensor of this gene at high DNA template amounts appeared to be less intense than the respective *groEL* and *motB* genes, the signal can be observed by naked eyes down to  $10^{-7}$  ng of DNA,

which is also significantly more sensitive ( $10^4$ -folds) than its respective result from gel electrophoresis (Figure A8.b). The exceptionally low limit of detection in this case can be attributed to the presence of multiple copies of *16s rRNA* in the *B. cereus* genome (Figure A9). On the other hand, the difference between the results from the paper-based sensor and gel electrophoresis may be explained by the double amplification feature of the sensor.



**Figure 3.16** Limit of detection of the sensor carrying three immobilized PNA probes, namely GroEL, 16s, and MotB with DNA samples from amplifications of varying amounts of genomic DNA template with a) *groEL* primers, b) *motB* primers and c) *16s rRNA* primers.

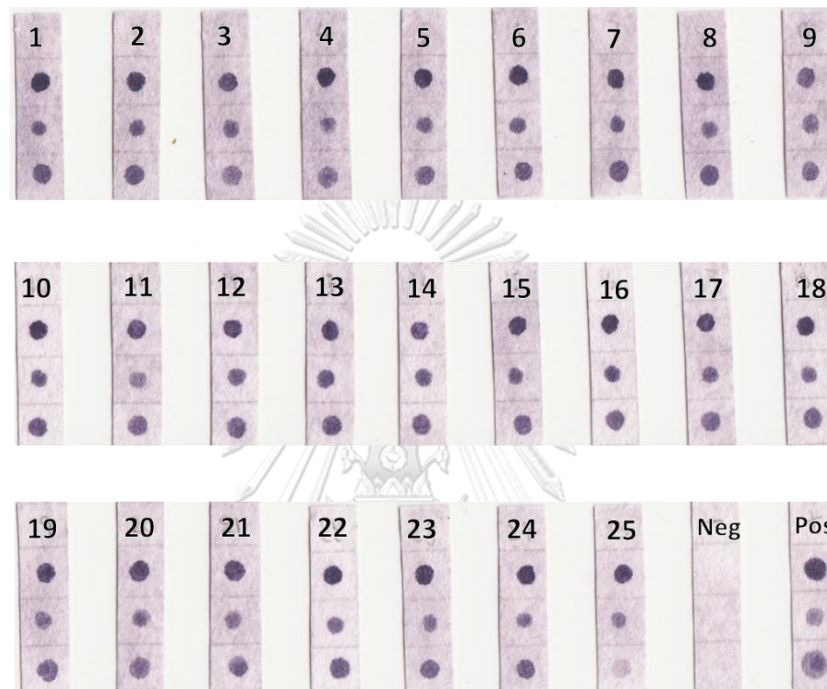
### 3.5.5 The performance evaluation in real samples

Encouraged by the outcomes of the performance evaluations above, we proceeded to test the sensor in a more realistic environment setting. Herein, 25 rice samples were spiked with *B. cereus* at 4,000 CFU/g of rice. This initial amount of spiked bacteria could be lowered but at a cost of longer incubation time. Thus, we decided to conduct all experiment at this amount, which is already below the unsafe level according to the UK and Australia/New Zealand standard.<sup>90, 91</sup> Thereafter, the DNA samples were extracted and separately amplified using the respective biotinylated primers for the three genes. The mixture of three sets of PCR amplicons for each sample was then analyzed with the paper-based sensor as described earlier. Simple visual examination of the results shown in **Figure 3.17** clearly suggest that the sensor was able to detect all three genes in more complex matrices such as rice samples. However, one borderline case in the sample #25 was observed whereby the signal of the *motB* gene was weaker than expected. In this case, repeating the test on this sample should suffice to confirm the positive results.

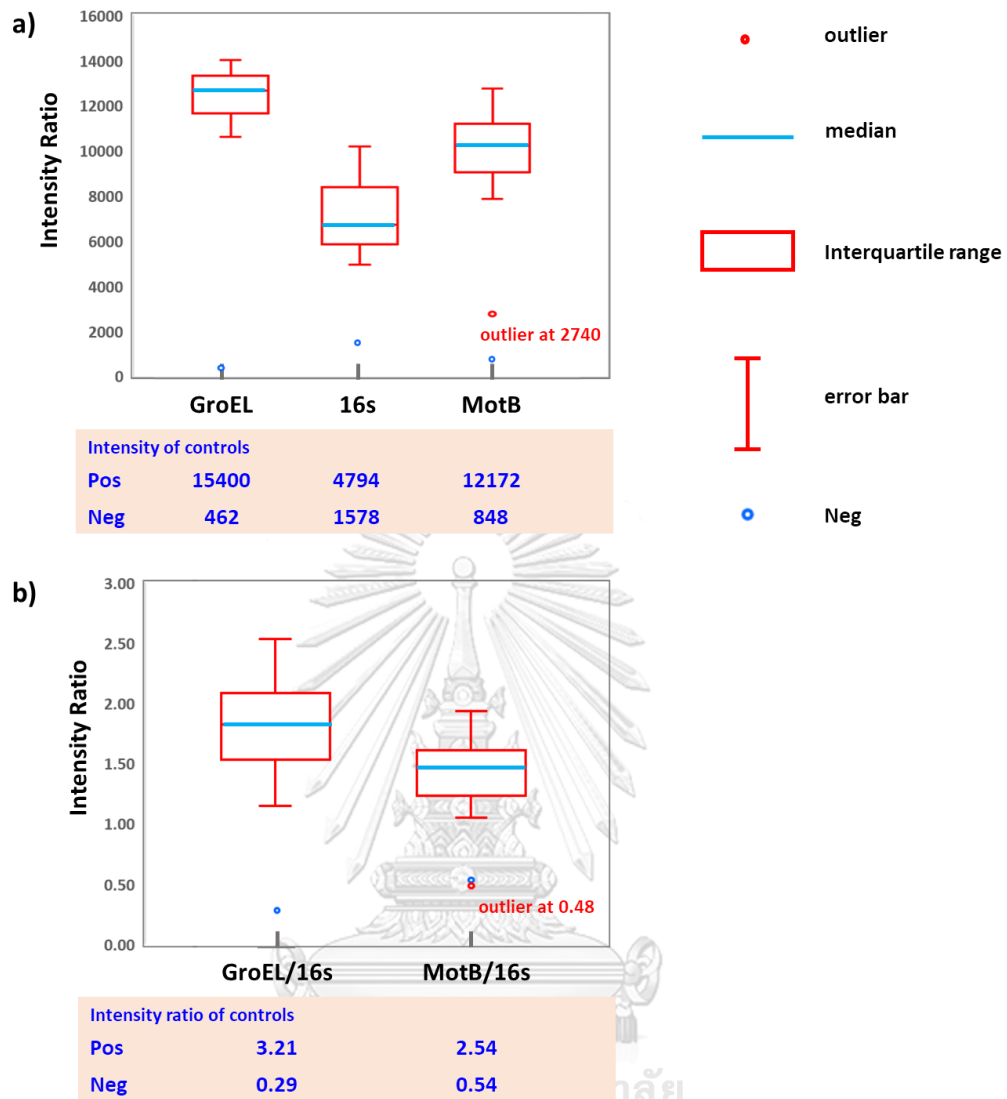
To provide a more objective method of analysis, a scanned image containing all sensors was analyzed with Scion Image. Box plots were then created to illustrate general statistical features of the data (full numerical data can be found in **Table A2**). **Figure 3.18a** shows the absolute intensities of all probes. In each case, the signals in the real samples were all higher than the negative controls of each probe, including even the outlier in the case of the MotB probe in the sensor #25 (2740 vs 848). Nevertheless, the ratios between the intensities of the signals in each probe, with that from 16s probe as a control, were also calculated. This is to further provide another layer of caveat prevention on the data. The results in **Figure 3.18b** suggested that all samples except #25 exhibited clear signals indicating the presence of *B. cereus*. That is, the data from real samples (means of 1.82 and 1.46 for GroEL/16s and MotB/16s, respectively) are statistically different from those from the negative control (0.29 and 0.54 for GroEL/16s and MotB/16s, respectively). Notably,



the weak signal of the MotB probe in the sample #25 is reflected in the ratio of MotB/16s (0.48), which is statistically considered to be an outlier. Hence, this methodology allows users to gain more confidence in analyzing the result, and thus makes the use of the sensor more robust.



**Figure 3.17** A scanned image of paper-based sensors for the detection of *B. cereus* in 25 spiked rice samples. Neg = negative control, which is a rice sample subjected to the same experimental protocol but without bacteria inoculation. Pos = the positive control, which is a direct amplification from isolated bacteria solution (no rice matrix).

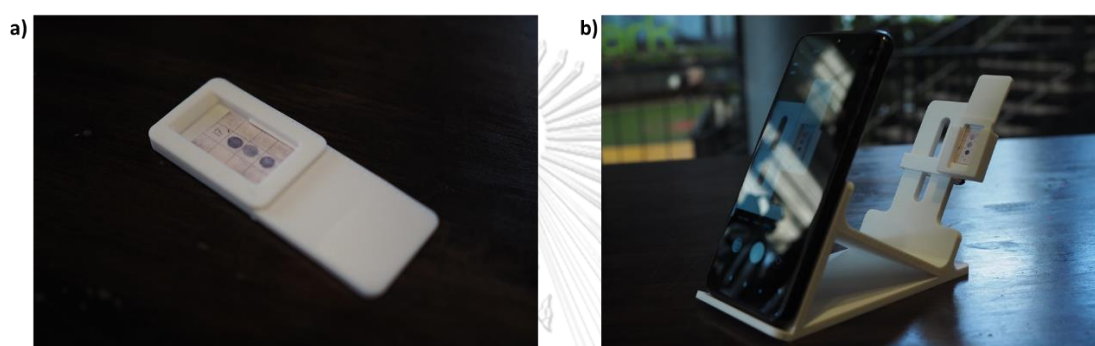


**Figure 3.18** Box plot illustrating a) the absolute intensities of signals from GroEL, 16s and MotB probes, and b) the intensity ratios of signals from GroEL and MotB probes, with 16s probe as a control, *i.e.*, the denominator of ratio calculations. Pos and Neg samples are defined in the previous figure.

### 3.5.6 The concept of smartphone application

Last but not least, the whole workflow could also be elaborated further for field operations by utilizing a smartphone and a suitable image processing application. While the development of a dedicated smartphone application is not a focus of this work, a demonstration of a more rugged device based on our PNA-

immobilized sensor is reported herein. In particular, 3D printing was used to create a smartphone holder and cassettes for holding a sheet of paper-based sensors (**Figure 3.19**). Thanks to the versatility of 3D printing, the construction of the smartphone holder to suit different phones (having different camera properties) can be done relatively easily. The constructed cassette can be used to perform the hybridization and color generation steps from pre-immobilized PNA paper sheets. This enhances the practicality and accessibility of this sensor for broader applications.



**Figure 3.19** The pictures that show a) PNA-immobilized paper sheet held in a cassette after DNA detection and b) the setup of the smartphone holder with a smartphone and a sensor cassette being in place.

## CHAPTER IV

### CONCLUSION

In this study, a colorimetric paper-based DNA sensor employing immobilized pyrrolidinyl PNA as a recognition probe was successfully developed for the specific detection of PCR amplicons at ambient temperature. The visualization of the captured biotinylated DNA target was carried out through enzyme-catalyzed pigmentation. The pyrrolidinyl PNA probe offered better specificity over conventional DNA probes so that the discrimination of complementary and mismatched DNA targets could be performed at ambient temperature. The sensor performance was evaluated in two diverse areas of application including clinical diagnosis of thalassemia and foodborne pathogen detection. In the thalassemia diagnosis, the key target gene was HbE. The sensor was designed to contain two *epi*-acpcPNA probes corresponding to the normal and HbE genes in the same sensor. The high specificity of the sensor allows discrimination between the three possible genotypes including normal, HbE homozygote, and HbE heterozygote by simply comparing the intensity ratio of the colored spot at each location, either by naked eyes or via image analysis software. Furthermore, the sensor provided high reproducibility as well as good stability with up to 3-month storage in desiccator. The limit of detection was observed at 0.1 ng of DNA template — which is more than enough to detect DNA extracted from patients. Importantly, 100% sensitivity and specificity were achieved from the genotyping of 100 human blood samples.

For the detection of *B. cereus* as a foodborne pathogen model, three genes including *groEL*, *motB*, and *16s rRNA* were chosen as the targets based on bioinformatics design. Three acpcPNA probes corresponding to the three genes were included in the same sensor to provide a self-check system, whereby the *groEL*, *motB* were specific for *B. cereus* and the *16s rRNA* serves as a control gene that indicates the presence of any bacterial species. The sensor demonstrated a high

species specificity that can distinguish *B. cereus* from other related bacteria species and showed low limits of detection at 0.01 ng of the starting DNA template of *groEL* and *motB*. Additionally, the performance of the sensor showed was evaluated in 25 samples of rice matrix that were spiked with *B. cereus*, providing highly accurate results thus demonstrating its practical usefulness.

This study provided the first prototype of a paper-based DNA sensor featuring pyrrolidinyl PNA probes that offer great performance in terms of specificity and sensitivity without strict temperature control. In addition, the sensor was simple to fabricate, low-cost, easy to use – all of which are highly desirable features for point-of-care testing. Yet, there are possibilities for future improvement including the elimination of the complicated PCR step that still requires a thermal cycler by employing isothermal amplification such as loop-mediated isothermal amplification (LAMP), recombinase polymerase amplification (RPA), rolling circle amplification (RCA), or related techniques. The sensor can be further designed for high throughput screening that allows the detection of various mutations or several different bacteria species at once. Finally, the whole process should be further streamlined by combining the DNA sample preparation, the data collection by a smartphone, and automated analysis of the results by an image analysis software.

## REFERENCES

1. Tang, R. H.; Liu, L. N.; Zhang, S. F.; He, X. C.; Li, X. J.; Xu, F.; Ni, Y. H.; Li, F. A review on advances in methods for modification of paper supports for use in point-of-care testing. *Microchim. Acta* **2019**, *186*, 521.
2. Hu, J.; Wang, S.; Wang, L.; Li, F.; Pinguan-Murphy, B.; Lu, T. J.; Xu, F. Advances in paper-based point-of-care diagnostics. *Biosens. Bioelectron.* **2014**, *54*, 585-597.
3. Liana, D. D.; Raguse, B.; Gooding, J. J.; Chow, E. Recent advances in paper-based sensors. *Sensors* **2012**, *12*.
4. Kaur, N.; Toley, B. J. Paper-based nucleic acid amplification tests for point-of-care diagnostics. *Analyst* **2018**, *143*, 2213-2234.
5. Paniel, N.; Baudart, J.; Hayat, A.; Barthelmebs, L. Aptasensor and genosensor methods for detection of microbes in real world samples. *Methods* **2013**, *64*, 229-240.
6. Lee, K.-M.; Runyon, M.; Herrman, T. J.; Phillips, R.; Hsieh, J. Review of Salmonella detection and identification methods: Aspects of rapid emergency response and food safety. *Food Control* **2015**, *47*, 264-276.
7. Lo, Y.-T.; Shaw, P.-C. DNA-based techniques for authentication of processed food and food supplements. *Food Chem.* **2018**, *240*, 767-774.
8. Abi, A.; Safavi, A. Targeted detection of single-nucleotide variations: progress and promise. *ACS Sens.* **2019**, *4*, 792-807.
9. Böhme, K.; Calo-Mata, P.; Barros-Velázquez, J.; Ortea, I. Review of recent DNA-based methods for main food-authentication topics. *J. Agric. Food Chem.* **2019**, *67*, 3854-3864.
10. McCord, B. R.; Gauthier, Q.; Cho, S.; Roig, M. N.; Gibson-Daw, G. C.; Young, B.; Taglia, F.; Zapico, S. C.; Mariot, R. F.; Lee, S. B.; Duncan, G. Forensic DNA analysis. *Anal. Chem.* **2019**, *91*, 673-688.
11. Butler, J. M.; Willis, S. Interpol review of forensic biology and forensic DNA typing 2016-2019. *Forensic Sci. Int.: Synergy* **2020**, 352-367.

12. Lu, X.; Cui, M.; Yi, Q.; kamrani, A. Detection of mutant genes with different types of biosensor methods. *TRAC-Trend. Anal. Chem.* **2020**, 115860.
13. Ziyaina, M.; Rasco, B.; Sablani, S. S. Rapid methods of microbial detection in dairy products. *Food Control* **2020**, *110*, 107008.
14. Bhat, A. I.; Rao, G. P. Dot-blot hybridization technique. In *Characterization of Plant Viruses : Methods and Protocols*, Bhat, A. I.; Rao, G. P., Eds. Springer US: New York, **2020**; 303-321.
15. Saiki, R. K.; Bugawan, T. L.; Horn, G. T.; Mullis, K. B.; Erlich, H. A. Analysis of enzymatically amplified  $\beta$ -globin and HLA-DQ $\alpha$  DNA with allele-specific oligonucleotide probes. *Nature* **1986**, *324*, 163-166.
16. Eshaque, B.; Dixon, B. Technology platforms for molecular diagnosis of cystic fibrosis. *Biotechnol. Adv.* **2006**, *24*, 86-93.
17. Blok, V. C.; Ziegler, A.; Scott, K.; Dangora, D. B.; Robinson, D. J.; Murant, A. F. Detection of groundnut rosette umbravirus infections with radioactive and non-radioactive probes to its satellite RNA. *Ann. Appl. Biol.* **1995**, *127*, 321-328.
18. Smith, G. R.; Clarke, M. L.; Van de Velde, R.; Dale, J. L. Chemiluminescent detection of Fiji disease virus with biotinylated DNA probes. *Arch. Virol* **1994**, *136*, 325-334.
19. Roy, B. P.; AbouHaidar, M. G.; Alexander, A. Biotinylated RNA probes for the detection of potato spindle tuber viroid (PSTV) in plants. *J. Virol. Methods* **1989**, *23*, 149-155.
20. Saiki, R. K.; Walsh, P. S.; Levenson, C. H.; Erlich, H. A. Genetic analysis of amplified DNA with immobilized sequence-specific oligonucleotide probes. *Proc. Natl. Acad. Sci.* **1989**, *86*, 6230-6234.
21. Magro, L.; Escadafal, C.; Garneret, P.; Jacquelin, B.; Kwasiborski, A.; Manuguerra, J.-C.; Monti, F.; Sakuntabhai, A.; Vanhomwegen, J.; Lafaye, P.; Tabeling, P. Paper microfluidics for nucleic acid amplification testing (NAAT) of infectious diseases. *Lab Chip* **2017**, *17*, 2347-2371.
22. Qiu, W.; Xu, H.; Takalkar, S.; Gurung, A. S.; Liu, B.; Zheng, Y.; Guo, Z.; Baloda, M.; Baryeh, K.; Liu, G. Carbon nanotube-based lateral flow biosensor for

- sensitive and rapid detection of DNA sequence. *Biosens. Bioelectron.* **2015**, *64*, 367-372.
23. Henderson, W. A.; Xiang, L.; Fourie, N. H.; Abey, S. K.; Ferguson, E. G.; Diallo, A. F.; Kenea, N. D.; Kim, C. H. Simple lateral flow assays for microbial detection in stool. *Anal. Methods* **2018**, *10*, 5358-5363.
24. Yang, Z.; Yi, C.; Lv, S.; Sheng, Y.; Wen, W.; Zhang, X.; Wang, S. Development of a lateral flow strip biosensor based on copper oxide nanoparticles for rapid and sensitive detection of HPV16 DNA. *Sens. Actuators B Chem.* **2019**, *285*, 326-332.
25. Takalkar, S.; Baryeh, K.; Liu, G. Fluorescent carbon nanoparticle-based lateral flow biosensor for ultrasensitive detection of DNA. *Biosens. Bioelectron.* **2017**, *98*, 147-154.
26. Meredith, N. A.; Quinn, C.; Cate, D. M.; Reilly, T. H.; Volckens, J.; Henry, C. S. Paper-based analytical devices for environmental analysis. *Analyst* **2016**, *141*, 1874-1887.
27. Scida, K.; Li, B.; Ellington, A. D.; Crooks, R. M. DNA detection using origami paper analytical devices. *Anal. Chem.* **2013**, *85*, 9713-9720.
28. Nielsen Peter, E.; Egholm, M.; Berg Rolf, H.; Buchardt, O. Sequence-selective recognition of DNA by strand displacement with a thymine-substituted polyamide. *Science* **1991**, *254*, 1497-1500.
29. Lundin, K. E.; Good, L.; Strömberg, R.; Gråslund, A.; Smith, C. I. E. Biological activity and biotechnological aspects of peptide nucleic acid. *Adv Genet* **2006**, *56*, 1-51.
30. Shakeel, S.; Karim, S.; Ali, A. Peptide nucleic acid (PNA) — a review. *J. Chem. Technol. Biotechnol.* **2006**, *81*, 892-899.
31. Egholm, M.; Buchardt, O.; Nielsen, P. E.; Berg, R. H. Peptide nucleic acids (PNA). Oligonucleotide analogs with an achiral peptide backbone. *J. Am. Chem. Soc.* **1992**, *114*, 1895-1897.
32. Sforza, S.; Corradini, R.; Tedeschi, T.; Marchelli, R. Food analysis and food authentication by peptide nucleic acid (PNA)-based technologies. *Chem. Soc. Rev.* **2011**, *40*, 221-232.



33. Shi, H.; Yang, F.; Li, W.; Zhao, W.; Nie, K.; Dong, B.; Liu, Z. A review: Fabrications, detections and applications of peptide nucleic acids (PNAs) microarray. *Biosens. Bioelectron.* **2015**, *66*, 481-489.
34. Choi, J.-J.; Jang, M.; Kim, J.; Park, H. Highly sensitive PNA array platform technology for single nucleotide mismatch discrimination. *J Microbiol Biotechnol* **2010**, *20*, 287-293.
35. Vilaivan, T. Pyrrolidinyl PNA with alpha/beta-dipeptide backbone: from development to applications. *Acc Chem Res* **2015**, *48*, 1645-56.
36. Liu, Y.; Zhan, L.; Qin, Z.; Sackrison, J.; Bischof, J. C. Ultrasensitive and highly specific lateral flow assays for point-of-care diagnosis. *ACS Nano* **2021**, *15*, 3593-3611.
37. Winichagoon, P.; Saechan, V.; Sripanich, R.; Nopparatana, C.; Kanokpongsakdi, S.; Maggio, A.; Fucharoen, S. Prenatal diagnosis of beta-thalassaemia by reverse dot-blot hybridization. *Prenatal Diag* **1999**, *19*, 428-435.
38. Sayers, J.; Payne, R. J.; Winssinger, N. Peptide nucleic acid-templated selenocystine-selenoester ligation enables rapid miRNA detection. *Chem. Sci.* **2018**, *9*, 896-903.
39. Laopa, P. S.; Vilaivan, T.; Hoven, V. P. Positively charged polymer brush-functionalized filter paper for DNA sequence determination following Dot blot hybridization employing a pyrrolidinyl peptide nucleic acid probe. *Analyst* **2013**, *138*, 269-277.
40. Jirakittiwut, N.; Panyain, N.; Nuanyai, T.; Vilaivan, T.; Praneenarat, T. Pyrrolidinyl peptide nucleic acids immobilised on cellulose paper as a DNA sensor. *RSC Adv.* **2015**, *5*, 24110-24114.
41. Teengam, P.; Siangproh, W.; Tuantranont, A.; Vilaivan, T.; Chailapakul, O.; Henry, C. S. Multiplex paper-based colorimetric DNA sensor using pyrrolidinyl peptide nucleic acid-induced AgNPs aggregation for detecting MERS-CoV, MTB, and HPV oligonucleotides. *Anal. Chem.* **2017**, *89*, 5428-5435.
42. Naorungroj, S.; Teengam, P.; Vilaivan, T.; Chailapakul, O. Paper-based DNA sensor enabling colorimetric assay integrated with smartphone for human papillomavirus detection. *New J. Chem.* **2021**, *45*, 6960-6967.

43. Teengam, P.; Nisab, N.; Chuaypen, N.; Tangkijvanich, P.; Vilaivan, T.; Chailapakul, O. Fluorescent paper-based DNA sensor using pyrrolidinyl peptide nucleic acids for hepatitis C virus detection. *Biosens. Bioelectron.* **2021**, *189*, 113381.
44. Mahdieh, N.; Rabbani, B. An overview of mutation detection methods in genetic disorders. *Iran J Pediatr* **2013**, *23*, 375-388.
45. Clark, B. E.; Shooter, C.; Smith, F.; Brawand, D.; Thein, S. L. Next-generation sequencing as a tool for breakpoint analysis in rearrangements of the globin gene clusters. *Int. J. Lab. Hematol.* **2017**, *39*, 111-120.
46. Sabath, D. E. Molecular diagnosis of thalassemias and hemoglobinopathies: an ACLPS critical review. *Am. J. Clin. Pathol.* **2017**, *148*, 6-15.
47. Gu, X.; Zeng, Y. A review of the molecular diagnosis of thalassemia. *Hematology* **2002**, *7*, 203-209.
48. Quek, D. L.; Ng, Y.-Y.; Wang, W.; Tan, A. S. C.; Tang-Lim, G.-I.; Ng, I. S. L.; Law, H.-Y.; Chong, S. S. Rapid carrier screening for  $\beta$ -thalassemia by single-step allele-specific PCR and detection. *Clin. Biochem.* **2007**, *40*, 427-430.
49. Liu, X.; Law, H. Y.; Tan, Y. M.; Hong, Y. High-throughput  $\beta$ -thalassemia carrier screening by allele-specific Q-primer real-time polymerase chain reaction. *Anal. Biochem.* **2010**, *404*, 97-99.
50. Naiser, T.; Ehler, O.; Kayser, J.; Mai, T.; Michel, W.; Ott, A. Impact of point-mutations on the hybridization affinity of surface-bound DNA/DNA and RNA/DNA oligonucleotide-duplexes: comparison of single base mismatches and base bulges. *BMC Biotechnol* **2008**, *8*, 48-48.
51. Su, X.; Li, L.; Wang, S.; Hao, D.; Wang, L.; Yu, C. Single-molecule counting of point mutations by transient DNA binding. *Sci. Rep.* **2017**, *7*, 43824.
52. Yang, Y. P.; Corley, N.; Garcia-Heras, J. Reverse dot-blot hybridization as an improved tool for the molecular diagnosis of point mutations in congenital adrenal hyperplasia caused by 21-hydroxylase deficiency. *Mol Diagn* **2001**, *6*, 193-9.
53. Charoenkwan, P.; Sirichotiyakul, S.; Phusua, A.; Suanta, S.; Fanhchaksai, K;

- Sae-Tung, R.; Sanguansermisri, T. High-resolution melting analysis for prenatal diagnosis of beta-thalassemia in northern Thailand. *Int J Hematol* **2017**, *106*, 757-764.
54. Fan, D. M.; Yang, X.; Huang, L. M.; Ouyang, G. J.; Yang, X. X.; Li, M. Simultaneous detection of target CNVs and SNVs of thalassemia by multiplex PCR and next-generation sequencing. *Mol Med Rep* **2019**, *19*, 2837-2848.
55. Barton Behravesh, C.; Jones, T. F.; Vugia, D. J.; Long, C.; Marcus, R.; Smith, K.; Thomas, S.; Zansky, S.; Fullerton, K. E.; Henao, O. L.; Scallan, E.; FoodNet Working, G. Deaths associated with bacterial pathogens transmitted commonly through food: foodborne diseases active surveillance network (FoodNet), 1996–2005. *J. Infect. Dis.* **2011**, *204*, 263-267.
56. Wei, X.; Zhao, X. Advances in typing and identification of foodborne pathogens. *Curr. Opin. Food Sci.* **2021**, *37*, 52-57.
57. Law, J. W.-F.; Ab Mutalib, N.-S.; Chan, K.-G.; Lee, L.-H. Rapid methods for the detection of foodborne bacterial pathogens: principles, applications, advantages and limitations. *Front. Microbiol.* **2015**, *5*, 770.
58. Wang, K.; Wang, Z.; Zeng, H.; Luo, X.; Yang, T. Advances in portable visual detection of pathogenic bacteria. *ACS Appl. Bio Mater.* **2020**, *3*, 7291-7305.
59. Granum, P. E.; Lund, T. *Bacillus cereus* and its food poisoning toxins. *FEMS Microbiol. Lett.* **1997**, *157*, 223-228.
60. Frenzel, E.; Kranzler, M.; Stark, T. D.; Hofmann, T.; Ehling-Schulz, M. The endospore-forming pathogen *Bacillus cereus* exploits a small colony variant-based diversification strategy in response to aminoglycoside exposure. *mBio* **2015**, *6*, e01172-15.
61. Ramarao, N.; Tran, S.-L.; Marin, M.; Vidic, J. Advanced methods for detection of *Bacillus cereus* and its pathogenic factors. *Sensors* **2020**, *20*, 2667.
62. Schulten, S. M.; P.H.; Nagelkerke, N. J. D.; Scotter, S.; M.L; Rollier, P.; Lahellec, C. Evaluation of the ISO 7932 standard for the enumeration of *Bacillus cereus* in foods. *Int. J. Food Microbiol.* **2000**, *57*, 53-61.
63. Chon, J.-W.; Kim, Y.-J.; Kim, D.-H.; Song, K.-Y.; Kim, H.; Seo, K.-H.

- Supplementation of modified mannitol-yolk-polymyxin B agar with cefuroxime for quantitative detection of *Bacillus cereus* in food. *Journal of Food Science* **2019**, *84*, 133-137.
64. Zhang, Z.; Feng, L.; Xu, H.; Liu, C.; Shah, N. P.; Wei, H. Detection of viable enterotoxin-producing *Bacillus cereus* and analysis of toxigenicity from ready-to-eat foods and infant formula milk powder by multiplex PCR. *J. Dairy Sci.* **2016**, *99*, 1047-1055.
  65. Sadek, Z. I.; Abdel-Rahman, M. A.; Azab, M. S.; Darwesh, O. M.; Hassan, M. S. Microbiological evaluation of infant foods quality and molecular detection of *Bacillus cereus* toxins relating genes. *Toxicol. Rep.* **2018**, *5*, 871-877.
  66. Sánchez-Chica, J.; Correa, M. M.; Aceves-Diez, A. E.; Castañeda-Sandoval, L. M. A novel method for direct detection of *Bacillus cereus* toxin genes in powdered dairy products. *Int. Dairy J.* **2020**, *103*, 104625.
  67. Yabutani, M.; Agata, N.; Ohta, M. A new rapid and sensitive detection method for cereulide-producing *Bacillus cereus* using a cycleave real-time PCR. *Lett. Appl. Microbiol.* **2009**, *48*, 698-704.
  68. Fischer, C.; Hünninger, T.; Jarck, J.-H.; Frohnmeyer, E.; Kallinich, C.; Haase, I.; Hahn, U.; Fischer, M. Food sensing: aptamer-based trapping of *Bacillus cereus* spores with specific detection via real time PCR in milk. *J. Agric. Food Chem.* **2015**, *63*, 8050-8057.
  69. Cattani, F.; Barth, V. C., Jr.; Nasário, J. S. R.; Ferreira, C. A. S.; Oliveira, S. D. Detection and quantification of viable *Bacillus cereus* group species in milk by propidium monoazide quantitative real-time PCR. *J. Dairy Sci.* **2016**, *99*, 2617-2624.
  70. Helgason, E.; Økstad, O. A.; Caugant, D. A.; Johansen, H. A.; Fouet, A.; Mock, M.; Hegna, I.; Kolstø, A.-B. *Bacillus anthracis*, *Bacillus cereus*, and *Bacillus thuringiensis*—One Species on the Basis of Genetic Evidence. *Appl. Environ. Microbiol.* **2000**, *66*, 2627.
  71. Kim, K.; Seo, J.; Wheeler, K.; Park, C.; Kim, D.; Park, S.; Kim, W.; Chung, S.-I.; Leighton, T. Rapid genotypic detection of *Bacillus anthracis* and the *Bacillus cereus* group by multiplex real-time PCR melting curve analysis. *FEMS Microbiol.*

- Immunol.* **2005**, *43*, 301-310.
72. Oliwa-Stasiak, K.; Molnar, C. I.; Arshak, K.; Bartoszcze, M.; Adley, C. C. Development of a PCR assay for identification of the *Bacillus cereus* group species. *J. Appl. Microbiol.* **2010**, *108*, 266-273.
73. Vilaivan, T.; Srisuwannaket, C. Hybridization of pyrrolidinyl peptide nucleic acids and DNA: selectivity, base-pairing specificity, and direction of binding. *Org. Lett.* **2006**, *8*, 1897-1900.
74. Taechalertpaisarn, J.; Sriwarom, P.; Boonlua, C.; Yotapan, N.; Vilaivan, C.; Vilaivan, T. DNA-, RNA- and self-pairing properties of a pyrrolidinyl peptide nucleic acid with a (2'R,4'S)-prolyl-(1S,2S)-2-aminocyclopentanecarboxylic acid backbone. *Tetrahedron Lett.* **2010**, *51*, 5822-5826.
75. Orelma, H.; Teerinen, T.; Johansson, L.-S.; Holappa, S.; Laine, J. CMC-modified cellulose biointerface for antibody conjugation. *Biomacromolecules* **2012**, *13*, 1051-1058.
76. Kargl, R.; Vorraber, V.; Ribitsch, V.; Kostler, S.; Stana-Kleinschek, K.; Mohan, T. Selective immobilization and detection of DNA on biopolymer supports for the design of microarrays. *Biosens Bioelectron* **2015**, *68*, 437-441.
77. Yang, C.-H.; Chen, C.-A.; Chen, C.-F. Surface-modified cellulose paper and its application in infectious disease diagnosis. *Sens. Actuators B Chem.* **2018**, *265*, 506-513.
78. Sutcharitchan, P.; Saiki, R.; Fucharoen, S.; Winichagoon, P.; Erlich, H.; Embury, S. H. Reverse dot-blot detection of Thai  $\beta$ -thalassaemia mutations. *Br. J. Haematol.* **1995**, *90*, 809-816.
79. Geiger, A.; Lester, A.; Kleiber, J.; Ørum, H. PNA array technology in molecular diagnostics. *Nucleos. Nucleot.* **1998**, *17*, 1717-1724.
80. Egholm, M.; Buchardt, O.; Christensen, L.; Behrens, C.; Freier, S. M.; Driver, D. A.; Berg, R. H.; Kim, S. K.; Norden, B.; Nielsen, P. E. PNA hybridizes to complementary oligonucleotides obeying the Watson-Crick hydrogen-bonding rules. *Nature* **1993**, *365*, 566-568.
81. Ananthanawat, C.; Vilaivan, T.; Hoven, V. P.; Su, X. Comparison of DNA,

- aminoethylglycyl PNA and pyrrolidiny PNA as probes for detection of DNA hybridization using surface plasmon resonance technique. *Biosens. Bioelectron.* **2010**, *25*, 1064-1069.
82. Ruengthanoo, P.; Lithanatudom, P.; Inthi, P.; Termphiriyakit, J.; Laphyai, P.; Kangwanpong, D.; Smith, D. R.; Kampuansai, J. Endogamous marriage and the prevalence of hemoglobin E in ethnic groups of northern Thailand. *Asian Pacific Journal of Tropical Medicine* **2017**, *10*, 414-417.
83. Fucharoen, G.; Sanchaisuriya, K.; Sae-ung, N.; Dangwibul, S.; Fucharoen, S. A simplified screening strategy for thalassaemia and haemoglobin E in rural communities in South-East Asia. *Bull. World Health Organ.* **2004**, *82*, 364-372.
84. Fucharoen, S.; Winichagoon, P. Hemoglobinopathies in Southeast Asia: molecular biology and clinical medicine. *Hemoglobin* **1997**, *21*, 299-319.
85. Fucharoen, S.; Winichagoon, P.; Wisedpanichkij, R.; Sae-Ngow, B.; Sriphanich, R.; Oncoung, W.; Muangsapaya, W.; Chowthaworn, J.; Kanokpongsakdi, S.; Bunyaratvej, A.; Piankijagum, A.; Dewaele, C. Prenatal and postnatal diagnoses of thalassemiias and hemoglobinopathies by HPLC. *Clin. Chem.* **1998**, *44*, 740-8.
86. Fawcett, T. An introduction to ROC analysis. *Pattern Recognit. Lett.* **2006**, *27*, 861-874.
87. Na, M.; Zhang, S.; Liu, J.; Ma, S.; Han, Y.; Wang, Y.; He, Y.; Chen, H.; Chen, X. Determination of pathogenic bacteria—*Bacillus anthrax* spores in environmental samples by ratiometric fluorescence and test paper based on dual-emission fluorescent silicon nanoparticles. *J. Hazard. Mater.* **2020**, *386*, 121956.
88. Jokerst, J. C.; Adkins, J. A.; Bisha, B.; Mentele, M. M.; Goodridge, L. D.; Henry, C. S. Development of a paper-based analytical device for colorimetric detection of select foodborne pathogens. *Anal. Chem.* **2012**, *84*, 2900-2907.
89. Saengsawang, N.; Ruang-areerate, T.; Kesakomol, P.; Thita, T.; Mungthin, M.; Dungchai, W. Development of a fluorescent distance-based paper device using loop-mediated isothermal amplification to detect *Escherichia coli* in urine. *Analyst* **2020**, *145*, 8077-8086.

90. *Ready-to-eat foods: microbiological safety assessment guidelines*.  
<https://www.gov.uk/government/publications/ready-to-eat-foods-microbiological-safety-assessment-guidelines> (accessed 7 September 2021).
91. *Compendium of microbiological criteria for food*.  
<https://www.foodstandards.gov.au/publications/pages/compendium-of-microbiological-criteria-for-food.aspx> (accessed 7 September 2021).
92. Arlinghaus, H. F.; Schröder, M.; Feldner, J. C.; Brandt, O.; Hoheisel, J. D.; Lipinsky, D. Development of PNA microarrays for gene diagnostics with TOF-SIMS. *Appl. Surf. Sci.* **2004**, 231-232, 392-396.

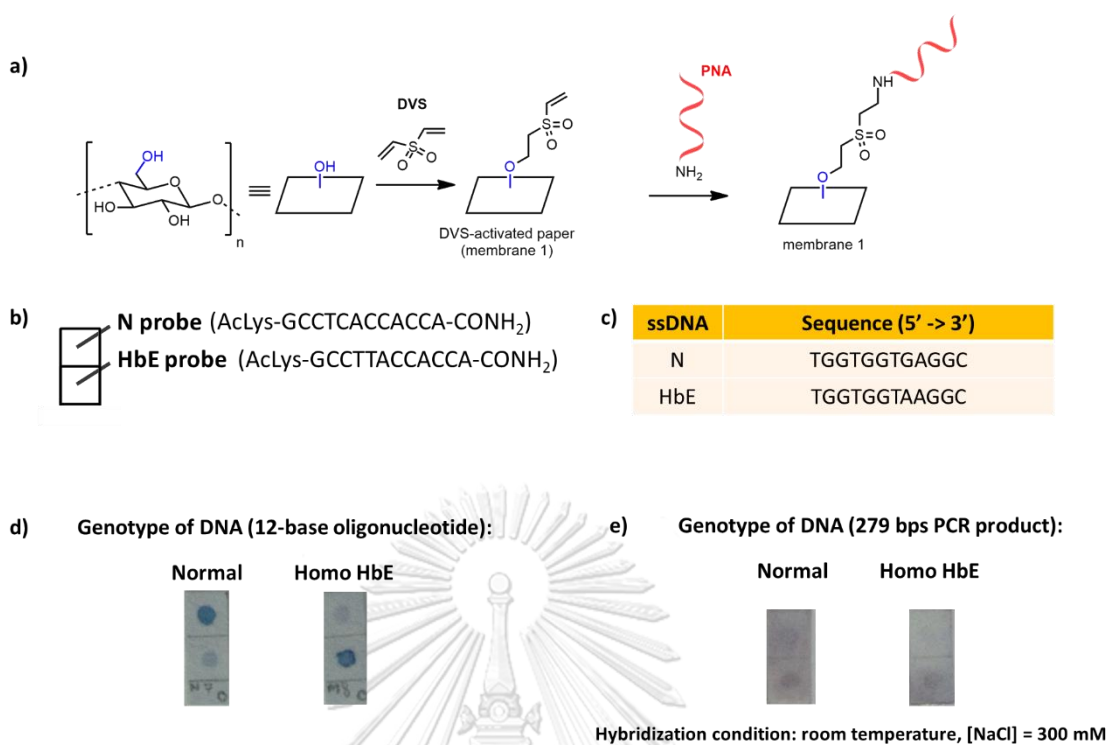


## Optimization of the DNA detection method by using the divinyl sulfone (DVS) method for PNA immobilization

### Preparation of PNA-immobilized paper by using DVS

Pyrrolidinyl PNA was covalently attached onto the paper surface by employing a previously published protocol (**Figure A1a.**)<sup>40</sup> DVS carries two reactive electrophilic moieties – one of which can link with the hydroxy group of the cellulose and the other with the amino group from the PNA probe. Then, the detection of 12-base ssDNA oligonucleotide corresponding to normal/HbE genes (**Figure A1c.**) was performed by employing the acpcPNA-immobilized paper. The intense signal was observed as well as discrimination ability between complementary and single-base mismatched sequences (hybridization at room temperature, in 300 mM NaCl). Unfortunately, while the acpcPNA probe immobilized this way was able to detect and discriminate biotinylated synthetic DNA oligonucleotides (**Figure A1d.**), the detection of PCR product was not successful (**Figure A1e.**).

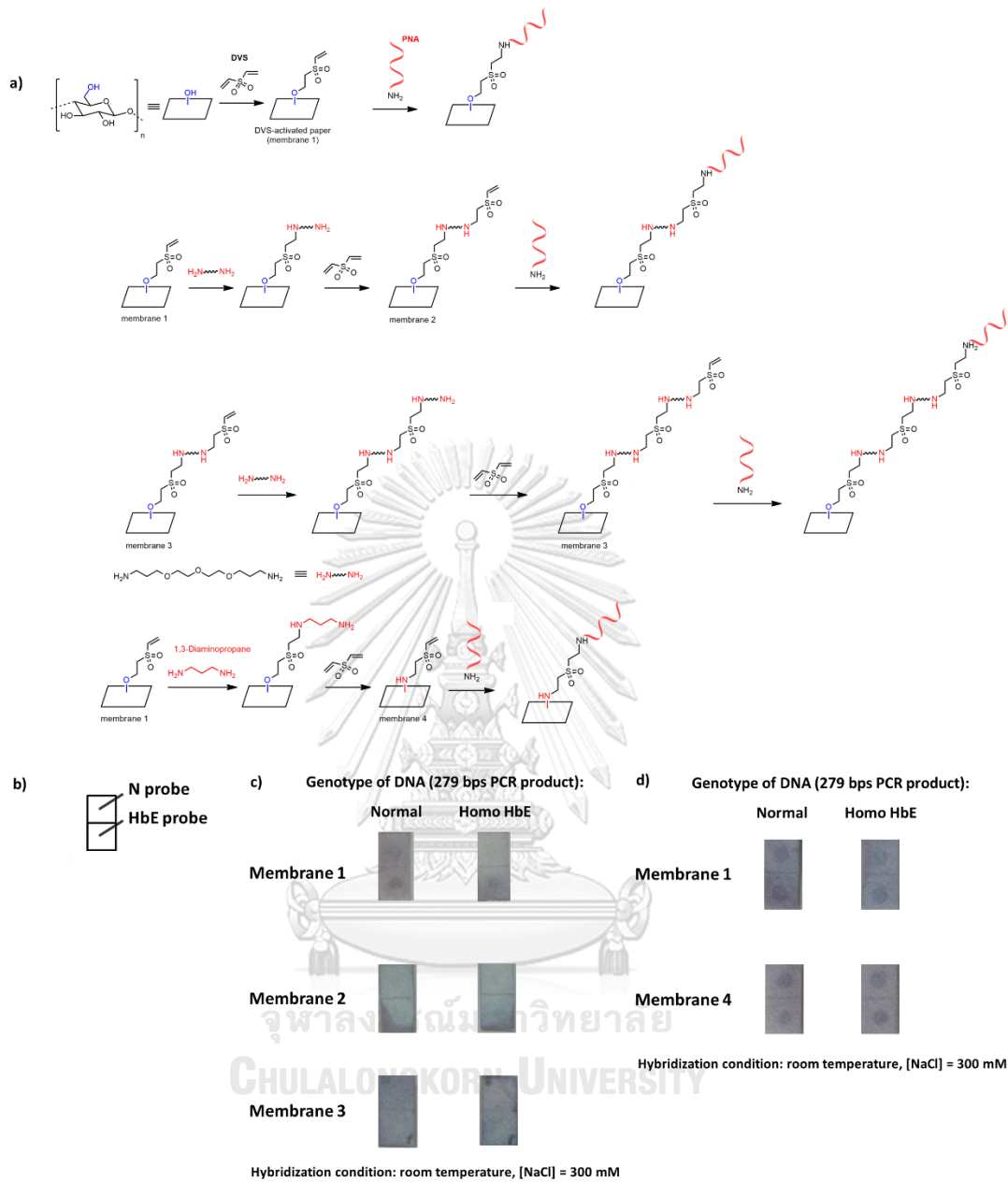




**Figure A1.** a) Scheme of preparation method for PNA immobilization by using divinyl sulfone. b) The layout showing the position of probes on the sensor. The photo of sensor testing with c) ssDNAs and d) PCR products.

### The effect of spacer between paper surface and PNA probe

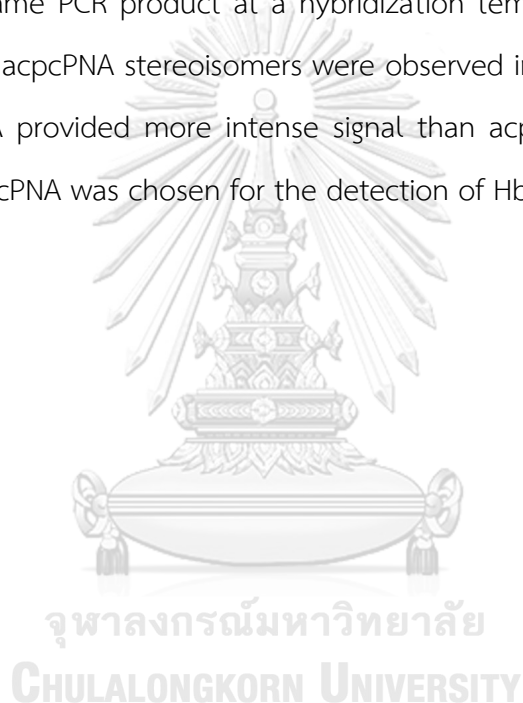
According to the literature,<sup>92</sup> the length of the spacer between the capture probe and the paper surface can be a major factor that contribute to the hybridization efficiency. Larger distance between probe and sensor surface could provide greater performance for the DNA binding. The papers with different surface modifications were prepared to compare the performance of the DNA binding. The linker length between the probe and the paper surface in membrane 3 was longer than in membrane 2 and membrane 1, respectively. However, the signal intensities from the three membranes after testing with the PCR products were similar. From the results, it was concluded that the spacer between the probe and surface did not affect the DNA binding. When the DNA detection was repeated with membrane 4 which was similar to membrane 2 but with a shorter diamine linker (1,3-propanediamine vs 4,7,10-trioxa-1,13-tridecanediamine), the same results were obtained and thus no linkers were used in the subsequent experiments.

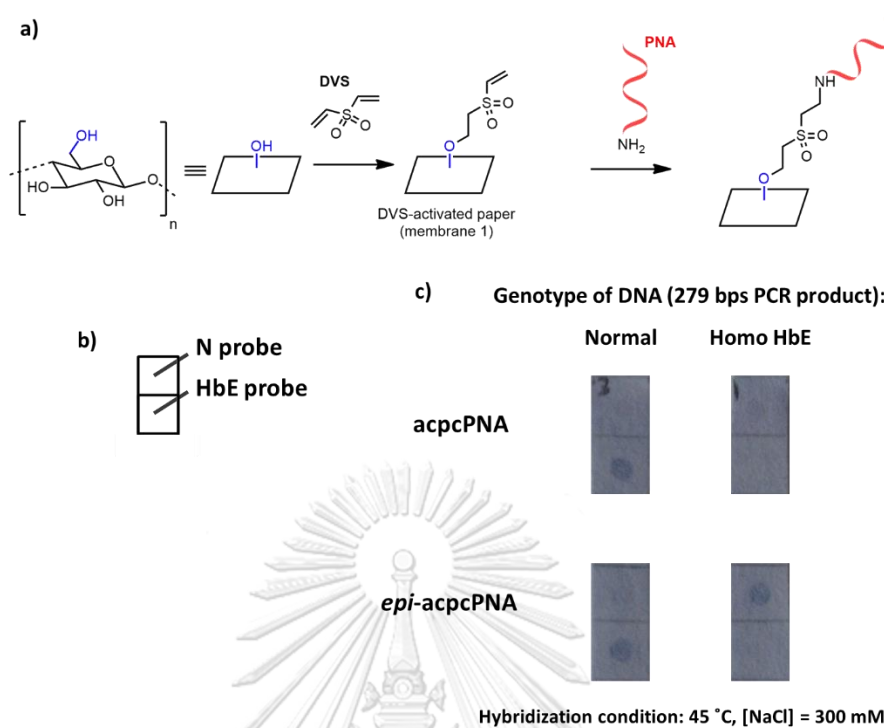


**Figure A2.** a) Scheme illustrating the preparation method of membrane 1–3 to compare the effect of spacer. b) The layout showing the position of probes on the sensor. c) The photo of sensor testing of PCR products with membrane 1–3. d) The photo of sensor testing of PCR products with membrane 1 and 4.

### The effect of type of pyrrolidinyl PNA

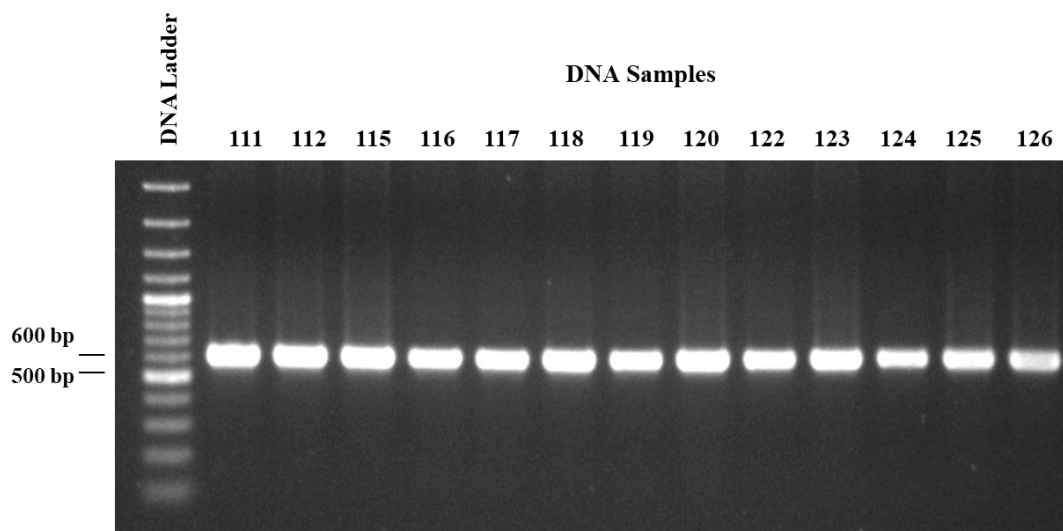
According to the literature,<sup>35</sup> *acpcPNA* and *epi-acpcPNA* are related by the different stereochemistry at the C4 position, but they showed similar DNA binding properties with some subtle differences. The binding strength of *epi-acpcPNA*-DNA duplex is slightly lower than the corresponding *acpcPNA*-DNA duplex, while the discrimination ability is still good. The performance of *acpcPNA* and *epi-acpcPNA* was compared in this experiment. The same sequence of *acpcPNA* and *epi-acpcPNA* was tested with the same PCR product at a hybridization temperature of 45 °C. Similar results of the two *acpcPNA* stereoisomers were observed in the case of the N probe, while *epi-acpcPNA* provided more intense signal than *acpcPNA* for the HbE probe. Therefore, *epi-acpcPNA* was chosen for the detection of HbE mutation.



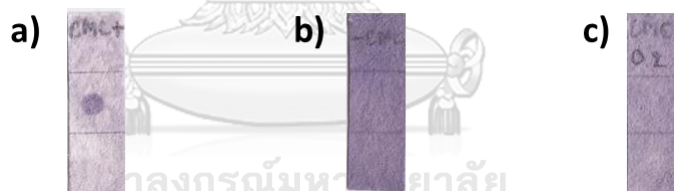


**Figure A3.** a) Scheme of preparation method for PNA immobilization of two stereoisomers by using divinyl sulfone. b) The layout showing the position of probes on the sensor. The photo of sensor testing with PCR product. It noted that the hybridization was performed at 45 °C.

## Gel electrophoresis of DNA samples used in the thalassemia diagnosis












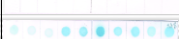










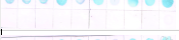






**Figure A4.** Agarose gel electrophoresis of biotinylated PCR products from selected real samples using China1/China2 primers (602 bp)

The effect of  $\text{Ca}^{2+}$  ion in CMC coating

**Figure A5.** The effect of CMC and  $\text{Ca}^{2+}$  ion to the immobilization efficiency of PNA on paper using the normal gene target. a) = control (CMC +  $\text{Ca}^{2+}$ ); b) = unmodified paper (no CMC and no  $\text{Ca}^{2+}$ ); c) = CMC but no  $\text{Ca}^{2+}$

**Table A1.** Comparison of the data from standard tests for HbE (CBC, hemoglobin typing, RDB hybridization), and from the PNA-based sensor (absolute intensities and intensity ratios) from 100 DNA samples extracted from human blood. The standard tests were performed by Thalassemia Research Center.

No.	Age	Gender	CBC		Hb type	RDB	Intrepretation	PNA sensor			
			Hb (g/dL)	MCV (fL)				Top spot intensity (normal probe)	Bottom spot intensity (HbE probe)	Ratio	Suggestion
111	18	Female	12.3	84.9	A2A		Normal hemoglobin type	5281	79	66.85	Normal
112	20	Female	13.8	82.6	A2A		Normal hemoglobin type	5291	67	78.97	Normal
113	23	Male	12.5	84.7	A2A		Normal hemoglobin type	5991	203	29.51	Normal
114	30	Female	13.1	83	A2A		Normal hemoglobin type	1989	20	99.45	Normal
115	31	Female	14.5	84.4	A2A		Normal hemoglobin type	4808	105	45.79	Normal
116	33	Female	14.3	88.4	A2A		Normal hemoglobin type	4792	170	28.19	Normal
117	22	Male	13.1	81.8	A2A		Normal hemoglobin type	6456	220	29.35	Normal
118	40	Female	12.7	84.1	A2A		Normal hemoglobin type	6225	218	28.56	Normal
119	32	Male	15.3	83.3	A2A		Normal hemoglobin type	5397	436	12.38	Normal
120	50	Female	15.9	85.5	A2A		Normal hemoglobin type	6357	205	31.01	Normal
122	47	Male	13.1	82.2	A2A		Normal hemoglobin type	6502	44	147.77	Normal
123	60	Male	11.1	91.5	A2A		Normal hemoglobin type	6003	219	27.41	Normal
124	18	Female	15.5	86.6	A2A		Normal hemoglobin type	6412	283	22.66	Normal
125	42	Male	11	84	A2A		Normal hemoglobin type	7028	238	29.53	Normal
126	37	Female	12.2	84.4	A2A		Normal hemoglobin type	6702	579	11.58	Normal
127	51	Female	11.9	84.6	A2A		Normal hemoglobin type	5021	217	23.14	Normal
128	24	Male	15.9	86.8	A2A		Normal hemoglobin type	5988	64	93.56	Normal
129	26	Female	15.7	82.1	A2A		Normal hemoglobin type	6076	288	21.10	Normal
130	44	Male	12.8	87.9	A2A		Normal hemoglobin type	6083	361	16.85	Normal
131	27	Male	11.7	83.7	A2A		Normal hemoglobin type	5940	1166	5.09	Normal
132	34	Male	12.4	84.1	A2A		Normal hemoglobin type	6247	579	10.79	Normal
133	36	Female	17	89.4	A2A		Normal hemoglobin type	5787	784	7.38	Normal
134	46	Female	13.3	88.1	A2A		Normal hemoglobin type	6376	436	14.62	Normal
135	30	Female	12.6	82.5	A2A		Normal hemoglobin type	6205	427	14.53	Normal
136	20	Female	14.8	82.1	A2A		Normal hemoglobin type	5210	183	28.47	Normal
137	48	Male	13.3	88.3	A2A		Normal hemoglobin type	4991	192	25.99	Normal
138	55	Female	14.1	87.2	A2A		Normal hemoglobin type	6309	563	11.21	Normal

No.	Age	Gender	CBC		Hb type	RDB <small>                     -βE (A-&gt;G)                      CD17 (A-&gt;T)                      CD19 (A-&gt;G)                      CD26: HbE (G-&gt;A)                      IVS-1 (G-&gt;T)                      IVS-5 (G-&gt;C)                      CD35 (C-&gt;A)                      CD44:2 (TCTT)                      CD71:71 (T-A)                      IVS1:654 (C-&gt;T)                 </small>	Intpretation	PNA sensor			
			Hb (g/dL)	MCV (fL)				Top spot intensity (normal probe)	Bottom spot intensity (HbE probe)	Ratio	Suggestion
139	40	Female	15.2	88.1	A2A		Normal hemoglobin type	5615	114	49.25	Normal
140	23	Male	14.8	81.1	A2A		Normal hemoglobin type	5158	862	5.98	Normal
141	47	Male	13.3	80.7	A2A		Normal hemoglobin type	6120	525	11.66	Normal
142	29	Female	13.4	86.1	A2A		Normal hemoglobin type	5942	321	18.51	Normal
143	38	Male	14.1	88	A2A		Normal hemoglobin type	5826	372	15.66	Normal
148	33	Female	13.5	87.3	A2A		Normal hemoglobin type	6345	588	10.79	Normal
153	32	Female	12.9	92.1	A2A		Normal hemoglobin type	5697	217	26.25	Normal
1	28	Male	11.8	56.6	EE		Hb E homozygote	2056	5548	0.37	HbE homozygous
2	29	Male	11.6	55.5	EE		Hb E homozygote	1516	5728	0.26	HbE homozygous
3	46	Male	12.7	61.6	EE		Hb E homozygote	2142	5343	0.40	HbE homozygous
4	63	Female	12.2	65.0	EE		Hb E homozygote	206	5034	0.04	HbE homozygous
7	21	Female	11.9	60.6	EE		Hb E homozygote	764	4128	0.19	HbE homozygous
9	19	Male	13.0	57.0	EE		Hb E homozygote	519	4550	0.11	HbE homozygous
10	18	Male	12.3	52.9	EE		Hb E homozygote	1726	5964	0.29	HbE homozygous
12	33	Male	11.1	57.4	EE		Hb E homozygote	1759	5974	0.29	HbE homozygous
14	38	Female	10.9	78.9	EE		Hb E homozygote	1894	6622	0.29	HbE homozygous
15	42	Male	13.9	64.1	EE		Hb E homozygote	2444	6175	0.40	HbE homozygous
16	50	Male	9.7	61.7	EE		Hb E homozygote	2026	5548	0.37	HbE homozygous
17	58	Female	13.7	63.7	EE		Hb E homozygote	2001	5885	0.34	HbE homozygous
32	35	Male	12.4	57.7	EE		Hb E homozygote	1728	6259	0.28	HbE homozygous
42	31	Male	13.5	61.0	EE		Hb E homozygote	2741	6701	0.41	HbE homozygous
52	22	Male	9.2	56.8	EE		Hb E homozygote	2407	6335	0.38	HbE homozygous
72	34	Female	12.2	65.0	EE		Hb E homozygote	995	4722	0.21	HbE homozygous
82	23	Female	10.5	55.2	EE		Hb E homozygote	922	5219	0.18	HbE homozygous
92	56	Male	10.0	54.9	EE		Hb E homozygote	854	6159	0.14	HbE homozygous
101	53	Male	9.9	56.3	EE		Hb E homozygote	1439	6269	0.23	HbE homozygous
102	34	Female	11.1	56.4	EE		Hb E homozygote	1672	5661	0.30	HbE homozygous



No.	Age	Gender	CBC		Hb type	RDB -28 (A->G) CD17 (A->T) CD19 (A->G) CD26: HbE (G->A) IVS-1 (G->T) IVS-5 (G->C) CD35 (C->A) CD41/2 (TCTT) CD171 (T-A) IVS1-654 (C->T)	Intrepretation	PNA sensor			
			Hb (g/dL)	MCV (fL)				Top spot intensity (normal probe)	Bottom spot intensity (HbE probe)	Ratio	Suggestion
103	26	Female	11.7	62.3	EE		Hb E homozygote	2906	5514	0.53	HbE homozygous
103	37	Male	10.5	62.3	EE		Hb E homozygote	1877	5072	0.37	HbE homozygous
122	40	Female	10.5	63.0	EE		Hb E homozygote	1651	6584	0.25	HbE homozygous
123	27	Female	13.6	67.0	EE		Hb E homozygote	2107	5591	0.38	HbE homozygous
124	22	Male	10.6	58.0	EE		Hb E homozygote	1479	6410	0.23	HbE homozygous
125	53	Male	13.1	62.6	EE		Hb E homozygote	1894	6622	0.29	HbE homozygous
126	35	Female	11.4	55.0	EE		Hb E homozygote	2125	5059	0.42	HbE homozygous
132	60	Male	11.7	59.6	EE		Hb E homozygote	895	5611	0.16	HbE homozygous
133	28	Male	12.6	64.2	EE		Hb E homozygote	1145	5394	0.21	HbE homozygous
152	34	Female	9.5	57.6	EE		Hb E homozygote	1549	6226	0.25	HbE homozygous
153	32	Male	10.6	54.9	EE		Hb E homozygote	1157	6393	0.18	HbE homozygous
163	30	Female	9.4	54.6	EE		Hb E homozygote	1186	5865	0.20	HbE homozygous
192	47	Female	14.8	66.4	EE		Hb E homozygote	1809	4922	0.37	HbE homozygous
292	25	Male	10.3	55.6	EE		Hb E homozygote	1422	5854	0.24	HbE homozygous
642	34	Female	10.5	62.3	EE		Hb E homozygote	2158	5409	0.40	HbE homozygous
2154	25	Female	12.4	74.2	EA		Hb E heterozygote	5997	4590	1.31	HbE heterozygous
2170	24	Female	11.9	75.5	EA		Hb E heterozygote	4740	5290	0.90	HbE heterozygous
2175	50	Female	10.7	73.1	EA		Hb E heterozygote	5351	6086	0.88	HbE heterozygous
2176	55	Female	14.8	70.2	EA		Hb E heterozygote	5847	4221	1.39	HbE heterozygous
2177	19	Female	12.7	70.7	EA		Hb E heterozygote	5443	5670	0.96	HbE heterozygous
2181	21	Male	12.7	74.8	EA		Hb E heterozygote	6209	4602	1.35	HbE heterozygous
2183	41	Female	11.5	73	EA		Hb E heterozygote	6519	4641	1.40	HbE heterozygous
2187	56	Male	11.7	73.6	EA		Hb E heterozygote	5727	4563	1.26	HbE heterozygous
2194	32	Male	12.8	74.6	EA		Hb E heterozygote	5379	5730	0.94	HbE heterozygous
2199	36	Male	11.6	71.6	EA		Hb E heterozygote	6258	4497	1.39	HbE heterozygous
2201	49	Female	10.8	67.8	EA		Hb E heterozygote	4156	5520	0.75	HbE heterozygous
2203	18	Male	12.7	68.8	EA		Hb E heterozygote	4538	6529	0.70	HbE heterozygous

No.	Age	Gender	CBC		Hb type	RDB -28 (A->G) CD17 (A->T) CD19 (A->G) CD26: HbE (G->A) IVS1-1 (G->T) IVS1-5 (G->C) CD35 (C->A) CD41/42 (TCTT) CD71/71 (e/A) IVS1/654 (C->T)	Intpretation	PNA sensor			
			Hb (g/dL)	MCV (fL)				Top spot intensity (normal probe)	Bottom spot intensity (HbE probe)	Ratio	Suggestion
2210	40	Female	10.8	85.3	EA		Hb E heterozygote	3493	5497	0.64	HbE heterozygous
2211	33	Male	10.3	71.8	EA		Hb E heterozygote	4778	5139	0.93	HbE heterozygous
2214	24	Male	16	71.2	EA		Hb E heterozygote	3914	5152	0.76	HbE heterozygous
2215	27	Female	11.8	76	EA		Hb E heterozygote	5671	4988	1.14	HbE heterozygous
2216	19	Female	12.5	78.6	EA		Hb E heterozygote	6545	6068	1.08	HbE heterozygous
2219	30	Male	11.9	70.8	EA		Hb E heterozygote	5096	3086	1.65	HbE heterozygous
2221	45	Female	13.8	73.9	EA		Hb E heterozygote	5328	4080	1.31	HbE heterozygous
222	48	Male	13.6	75	EA		Hb E heterozygote	5378	4012	1.34	HbE heterozygous
2223	55	Female	12	75.4	EA		Hb E heterozygote	5760	5044	1.14	HbE heterozygous
2227	18	Male	12.2	78	EA		Hb E heterozygote	5274	5157	1.02	HbE heterozygous
2231	31	Male	13.9	74.8	EA		Hb E heterozygote	4885	4937	0.99	HbE heterozygous
2234	28	Male	12.1	72	EA		Hb E heterozygote	5965	5269	1.13	HbE heterozygous
2235	27	Female	11.5	73.3	EA		Hb E heterozygote	6694	3398	1.97	HbE heterozygous
2237	60	Male	14.8	71.6	EA		Hb E heterozygote	5660	5196	1.09	HbE heterozygous
2238	53	Male	11.9	78.4	EA		Hb E heterozygote	4163	5610	0.74	HbE heterozygous
2239	35	Female	11.6	73.5	EA		Hb E heterozygote	5775	5559	1.04	HbE heterozygous
2241	40	Female	13.1	78.2	EA		HbE heterozygote	4130	5374	0.77	HbE heterozygous
2242	34	Male	13.8	79.8	EA		HbE heterozygote	4581	5228	0.88	HbE heterozygous
2243	41	Male	12.2	75.6	EA		HbE heterozygote	5397	4980	1.08	HbE heterozygous

Gel electrophoresis results and data of PCR sequences used in the detection of *B. cereus*

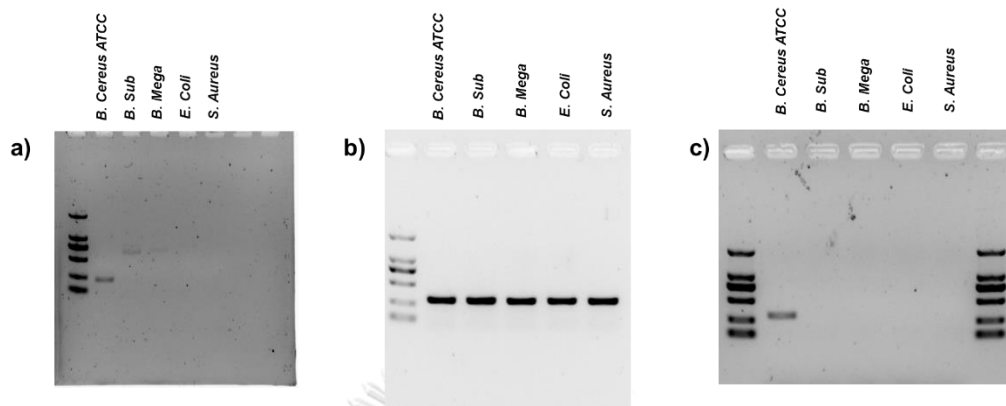


Figure A6. Gel electrophoresis results from PCR reaction of a) *groEL*, b) *16s* and c) *motB* genes used in the selectivity test

**16s RNA gene of *B. subtilis*:**

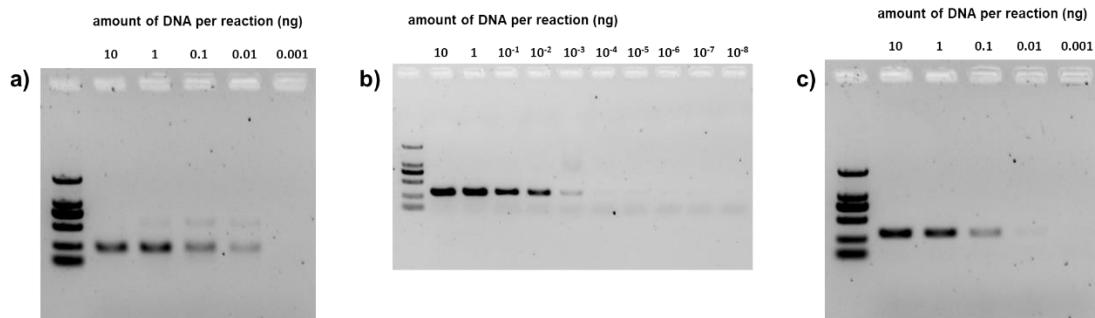
```

1 5' -GTCGTCAGCTCGTGTCTGAGATGTTGGGTTAAGTCCCGCAACGAGCGCAACCCCTTGATC
61  TTAGTTGCCAGCATTTCAGTTGGGCACCTAAGGTGACTGCCGGTGACAAACCGGAGGAAG
121  GTGGGGATGACGTCAAATCATCATGCCCTTATGACCTGGGCTACACACGTGCTACAATG
181  GACAGAACAAAGGGCAGCGAAACCGGAGGTTAAGCCAATCCACAAATCTGTTCTCAGT
241  TCGGATCGCAGTCTGCAACTCGACTGCGTGAAGCTGGAATCGCTAGTAATCG-3'

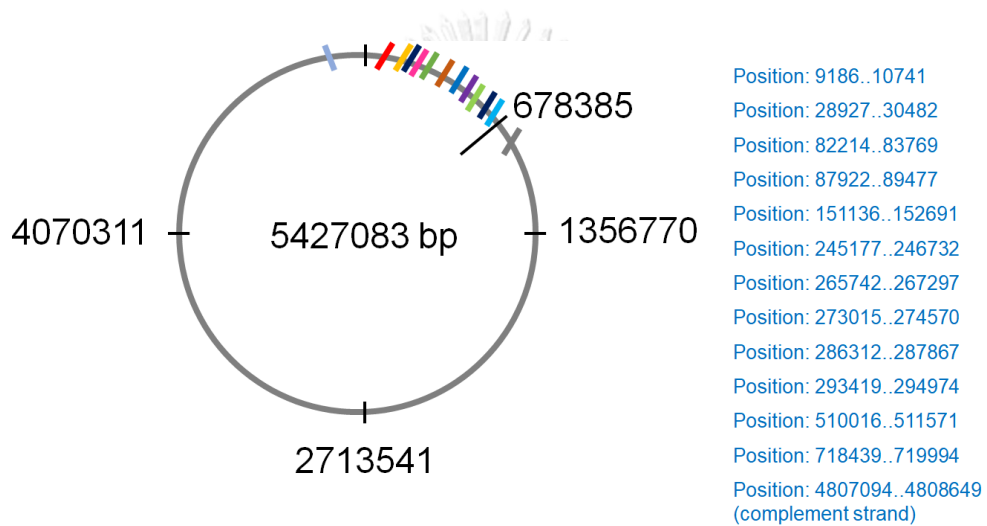
```

***motB* probe:** Ac-CGAACGTTAAGCC-Lys

Figure A7. Similarity of sequences between PCR amplicons from *16s* gene of *B. subtilis* and *motB* probe (grey: primer sequences, blue: the binding region of *16sRNA* probe, red: the region that is similar to *motB* probe)



**Figure A8.** Gel electrophoresis results from PCR reaction of a) *groEL*, b) *16sRNA* and c) *motB* genes that was utilized in sensitivity test

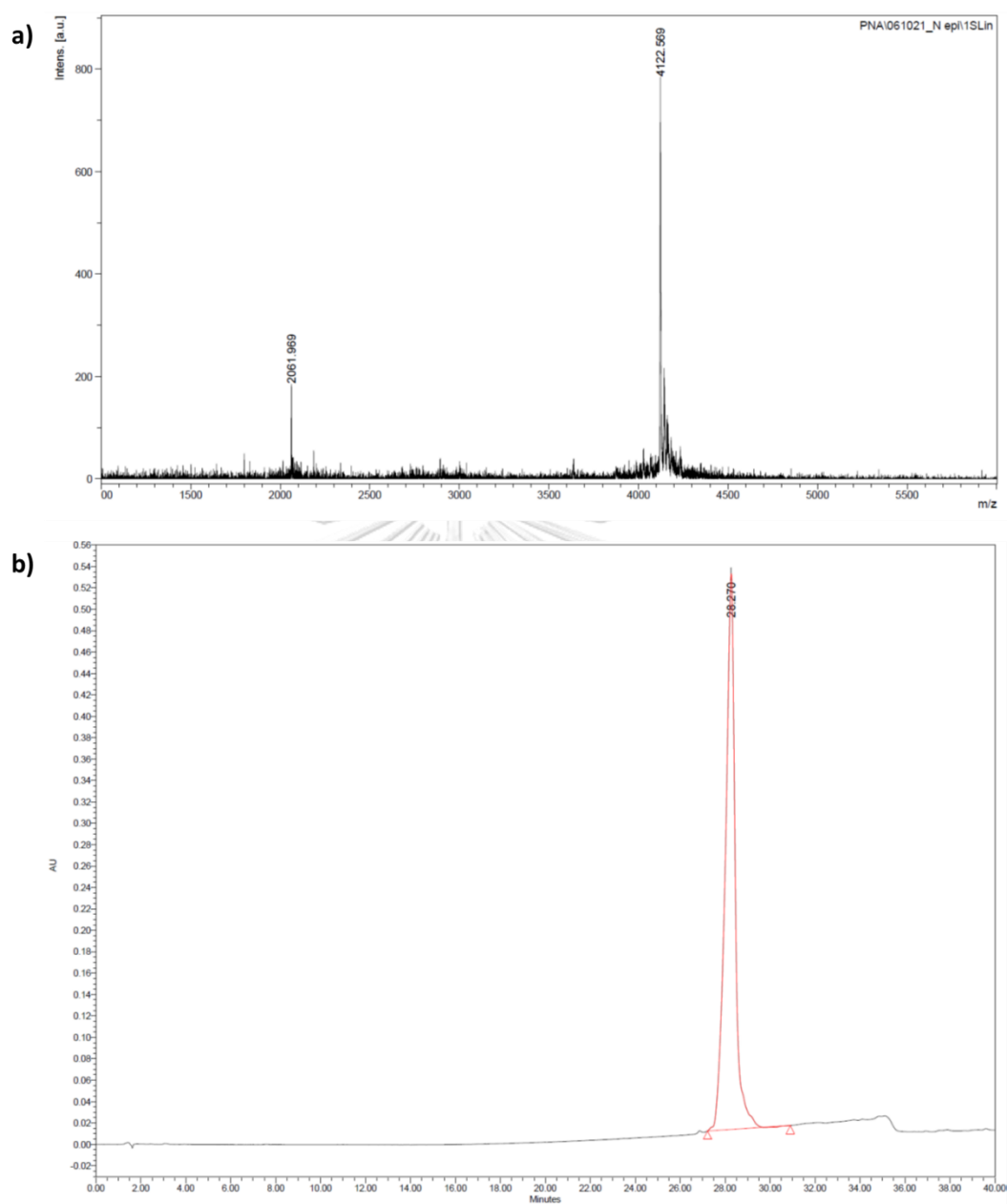


**Figure A9.** The *B. cereus* genome showing approximated locations of multiple copies of *16s rRNA* genes (<http://www.genome.jp/kegg/>).

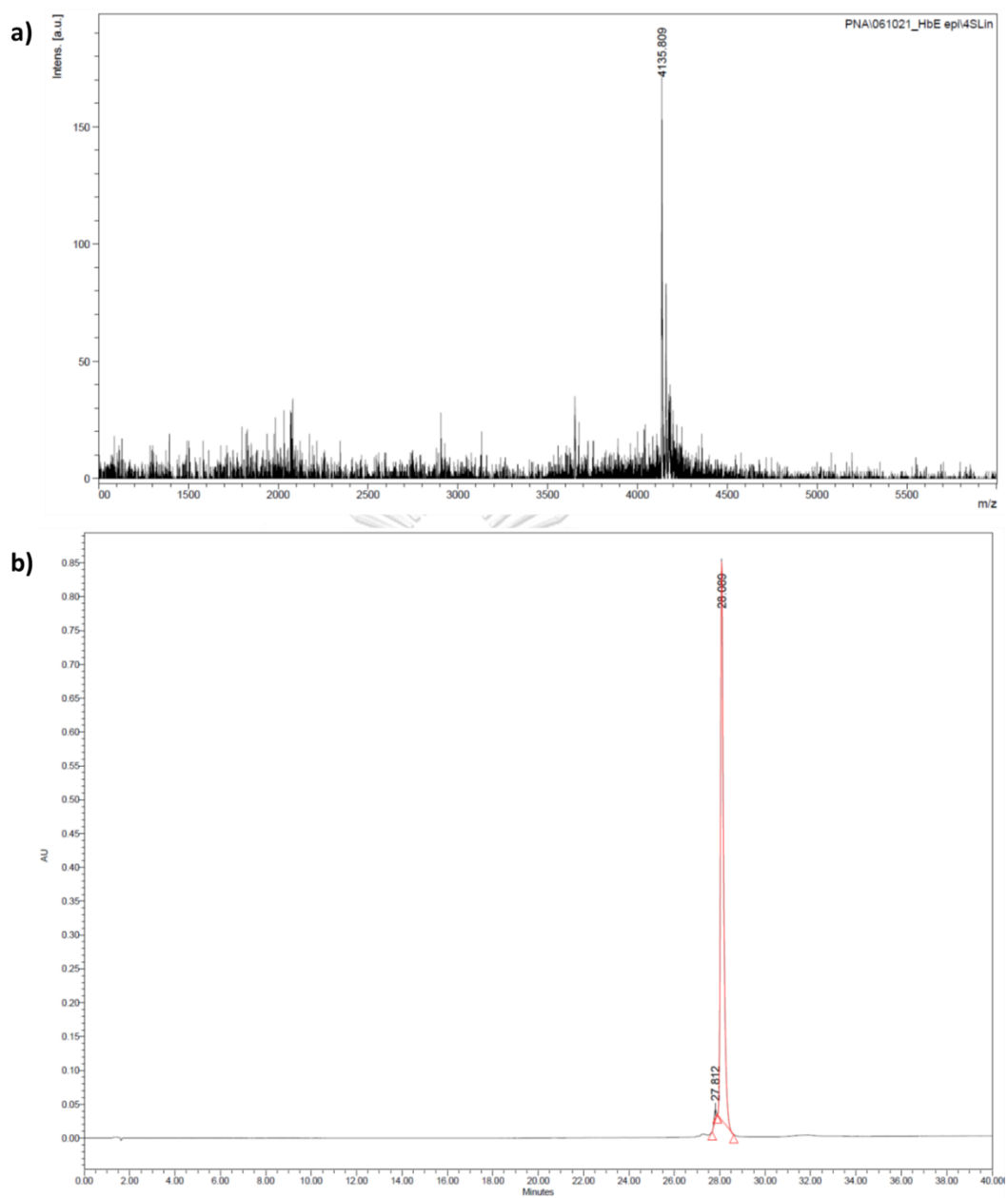
**Table A2.** Signal intensities from different channels (GroEL, 16s and MotB) as determined from Scion Image software in the analysis of 25 rice samples spiked with *B. cereus* by the paper-based sensor

Sample No.	Signal intensity			GroEL/16s	MotB/16s
	GroEL	16s	MotB		
1	13818	5692	10334	2.43	1.82
2	12803	7665	11441	1.67	1.49
3	11871	8297	8708	1.43	1.05
4	12489	4935	7835	2.53	1.59
5	11506	6541	8469	1.76	1.29
6	12683	6691	8719	1.90	1.30
7	11619	7155	11519	1.62	1.61
8	10621	5705	10125	1.86	1.77
9	13382	8796	9723	1.52	1.11
10	14011	8437	10779	1.66	1.28
11	12048	6615	10204	1.82	1.54
12	12961	10081	12751	1.29	1.26
13	13048	10095	11645	1.29	1.15
14	11691	10175	12111	1.15	1.19
15	11276	6636	9240	1.70	1.39
16	13981	9055	10849	1.54	1.20
17	11211	7676	10278	1.46	1.34
18	12771	6818	10939	1.87	1.60
19	10775	5538	10702	1.95	1.93
20	12657	6162	8983	2.05	1.46
21	12912	6118	9297	2.11	1.52
22	13509	7236	12098	1.87	1.67
23	13444	5424	9066	2.48	1.67
24	13270	5985	9640	2.22	1.61
25	12181	5678	2740	2.15	0.48
negative	462	1578	848	0.29	0.54
positive	15400	4794	12172	3.21	2.54

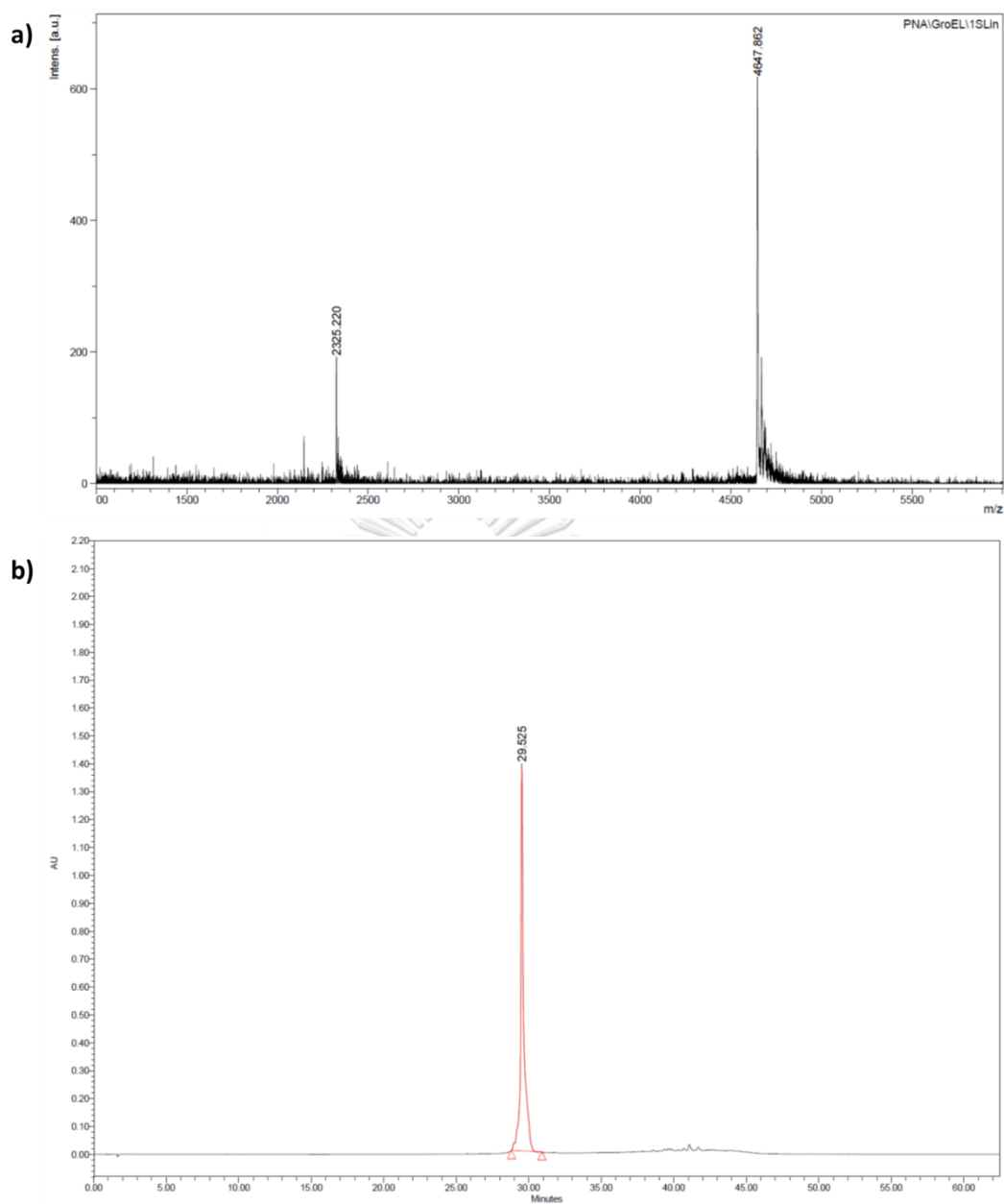
## Characterization of pyrrolidinyl PNA



**Figure A10.** a) MALDI-TOF mass spectrum and b) HPLC chromatogram of N probe (sequence: AcLys-GCCTCACCACCA-NH<sub>2</sub>, expected mass:  $m/z$  4123.4). For the HPLC conditions see **section 2.2.2**.

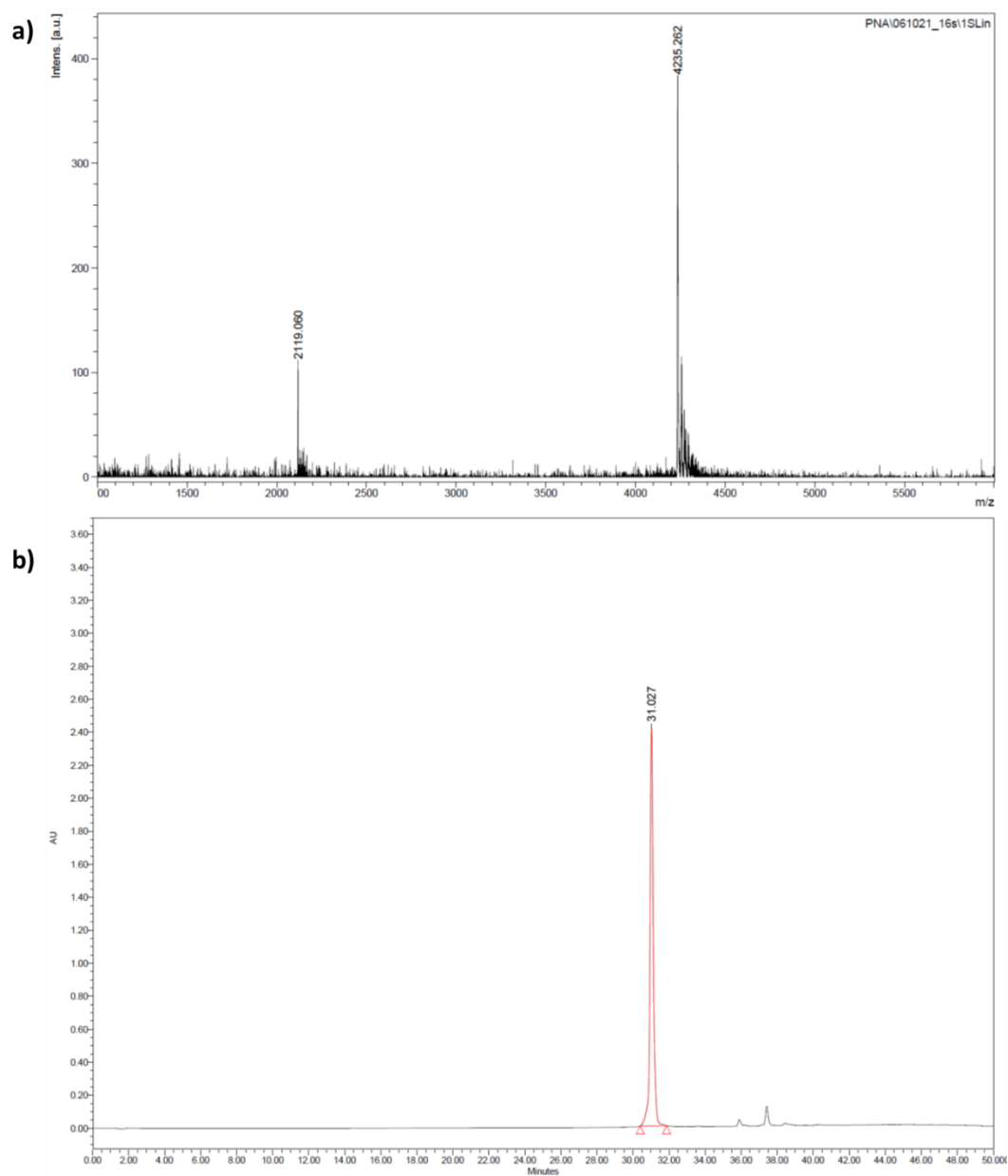


**Figure A11.** a) MALDI-TOF mass spectrum and b) HPLC chromatogram of HbE probe (sequence: AcLys-GCCTTACCACCA-NH<sub>2</sub>, expected mass:  $m/z$  4138.4). For the HPLC conditions see **section 2.2.2**.

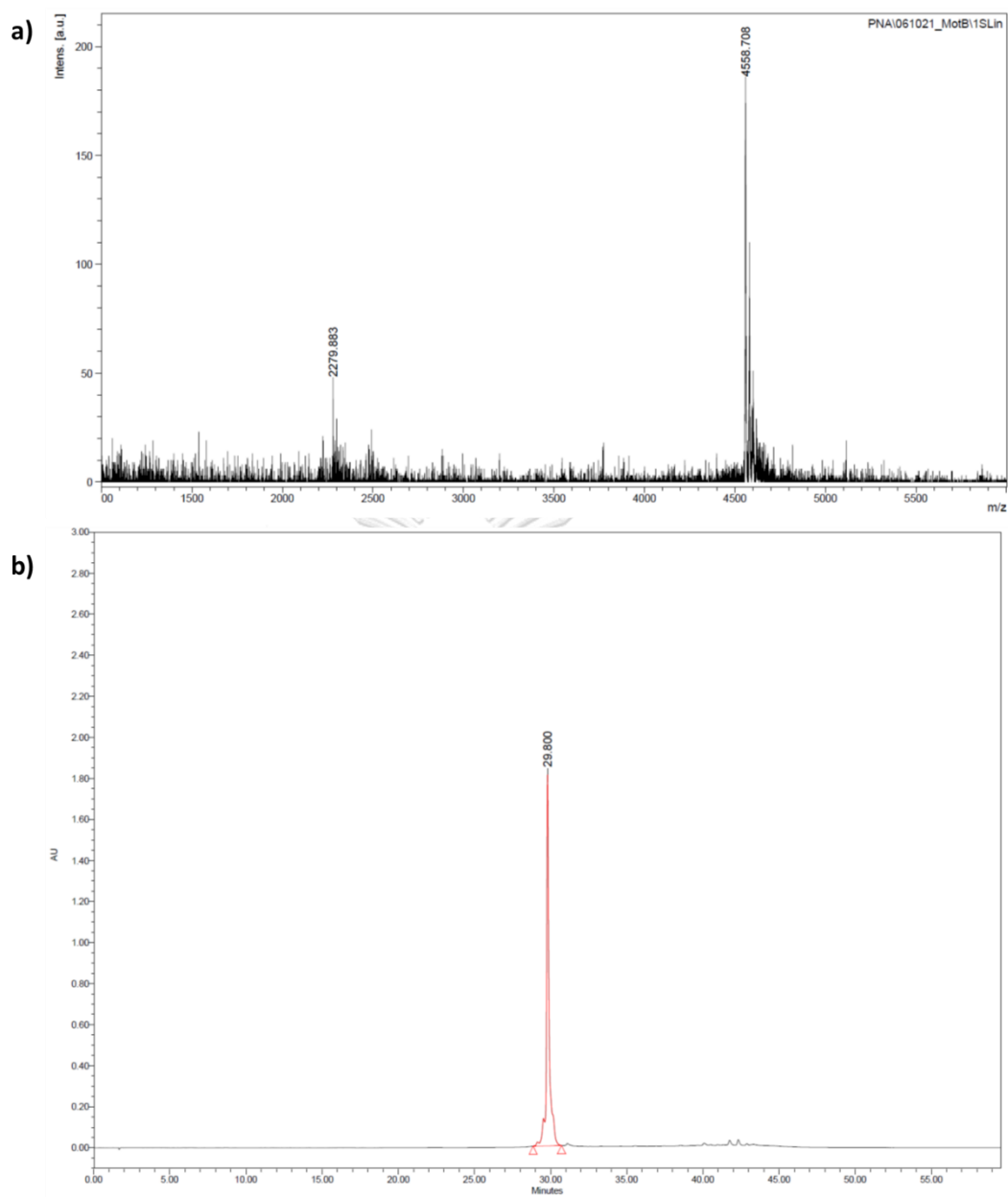


**Figure A12.** a) MALDI-TOF mass spectrum and b) HPLC chromatogram of GreEL probe (sequence: Ac-GTAGGAAGCACAG-LysNH<sub>2</sub>, expected mass:  $m/z$  4648.9). For the HPLC conditions see **section 2.2.2**.





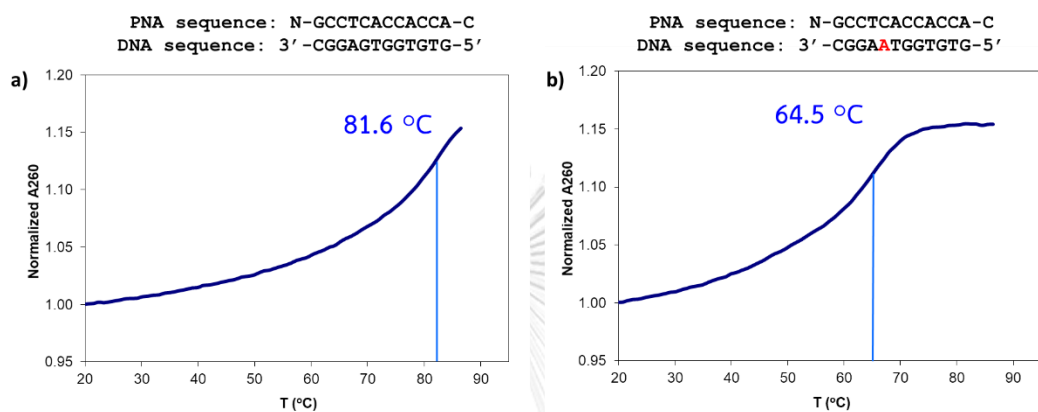
**Figure A13.** a) MALDI-TOF mass spectrum and b) HPLC chromatogram of 16s probe (sequence: Ac-AACGAGCGCAAC-LysNH<sub>2</sub>, expected mass:  $m/z$  4236.6). For the HPLC conditions see **section 2.2.2**.



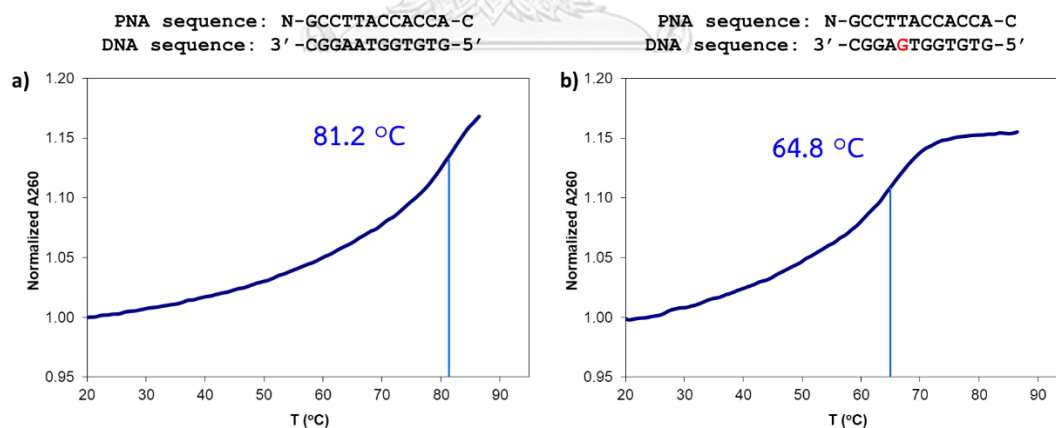
**Figure A14.** a) MALDI-TOF mass spectrum and b) HPLC chromatogram of MotB probe (sequence: Ac-CGAACGTTAAGCC-LysNH<sub>2</sub>, expected mass:  $m/z$  4559.9). For the HPLC conditions see **section 2.2.2**.

### Thermal denaturation experiments

A 1:1 mixture of PNA and DNA solution (1  $\mu\text{M}$  each) was prepared in 10 mM phosphate buffer, pH 7.4. The  $T_m$  experiment was carried out by UV/Vis spectrometry at 260 nm with 1.0  $^{\circ}\text{C}/\text{minute}$  of heating rate. Finally, the  $T_m$  curve was normalized and analyzed by using KaleidaGraph software.



**Figure A15.**  $T_m$  curve of N probe with a) complementary DNA and b) single-base mismatched DNA.



**Figure A16.**  $T_m$  curve of HbE probe with a) complementary DNA and b) single-base mismatched DNA.

## VITA

**NAME** Nuttapon Jirakittiwut

**DATE OF BIRTH** 20 Jan 1991

**PLACE OF BIRTH** Chiang Mai

**INSTITUTIONS ATTENDED** Department of Chemistry, Faculty of Science

**HOME ADDRESS** Tha parkland Tak Sin Road, Bukkhalo, Thon Buri, Bangkok  
10600

**PUBLICATION**

1. Jirakittiwut, N.; Panyain, N.; Nuanyai, T.; Vilaivan, T.; Praneenarat, T. Pyrrolidinyl peptide nucleic acids immobilised on cellulose paper as a DNA sensor. RSC Adv. 2015, 5, 24110-24114.
2. Jirakittiwut, N.; Munkongdee, T.; Wongravee, K.; Sripichai, O.; Fucharoen, S.; Praneenarat, T.; Vilaivan, T. Visual genotyping of thalassemia by using pyrrolidinyl peptide nucleic acid probes immobilized on carboxymethylcellulose-modified paper and enzyme-induced pigmentation. Microchim. Acta 2020, 187, 238.
3. Jirakittiwut, N.; Patipong, T.; Cheiwchanchamnangij, T.; Waditee-Sirisattha, R.; Vilaivan, T.; Praneenarat, T. Paper-based sensor from pyrrolidinyl peptide nucleic acid for the efficient detection of Bacillus cereus. Analytical and Bioanalytical Chemistry 2021, 413, 6661-6669.